Phil. Trans. R. Soc. Lond. A **314**, 229–310 (1985) [229]
Printed in Great Britain

THE TAUPO ERUPTION, NEW ZEALAND
II. THE TAUPO IGNIMBRITE

By C. J. N. WILSON†
Geology Department, Imperial College, London SW7 2BP, U.K.

(*Communicated by G. P. L. Walker, F.R.S.* – *Received* 21 *September* 1983 – *revised* 23 *May* 1984)

[Plates 1–8]

CONTENTS

† Present address: Geology Department, Auckland University, Private Bag, Auckland, New Zealand.

The *ca.* 30 km^3 Taupo ignimbrite was erupted as a climax to the *ca.* AD 186 Taupo eruption in the central North Island of New Zealand. It was erupted as a single vent-generated flow unit over a time period of *ca.* 400 s and was emplaced very rapidly (locally at more than 250–300 m s^{-1}) and violently. The parent flow reached 80 ± 10 km from source in all directions, crossed all but one of the mountains within its range and only stopped when it ran out of material.

The ignimbrite is divisible into layers 1 and 2, and a distant facies which combines features of both layers. Layer 1 was generated as a result of strong fluidization in the flow head, caused by air ingestion, and consists of two main facies. Layer 1(P) is a pumiceous, mildly to strongly fines-depleted unit, generated by the expulsion of material from the flow front, and termed the jetted deposits. The overlying layer 1(H) is a thinner, crystal- and lithic-rich, fines-depleted unit, generated by the sedimentation of coarse/dense constituents segregated out by strong fluidization within the flow head and termed the ground layer. Layer 2 consists of two facies with similar compositions but contrasting morphologies; during emplacement, material left behind by the flow body partially drained into depressions to form the valley-ponded ignimbrite, leaving the veneer deposit as a thin, landscape mantling layer on interfluves. The distant facies occurs in some outermost hilly areas of the ignimbrite where the flow velocity remained high but its volume had shrunk through deposition so that air ingestion fluidization affected the whole flow.

The ignimbrite shows great lateral variations. Each facies, or variants therein, exhibits systematic degrees of development with varying distances from vent. Near vent, the flow consisted of a series of batches of material which by *ca.* 25 km had coalesced into a single wavy flow and by *ca.* 40 km into a single wave. Out to *ca.* 13 km, the flow was rather dilute and highly turbulent as it deflated from the collapsing eruption column. Beyond this distance it was fairly concentrated, being less than 100% expanded over its non-fluidized compacted state, and had acquired a fluidization-induced stable density stratification, which strongly suppressed turbulence in the flow body. Deflation from the eruption column was largely complete by *ca.* 13 km but influenced the flow as far as 20–25 km from vent.

Grainsize and compositional parameters measured in the ignimbrite show lateral variations which equal or exceed the entire spectrum of published ignimbrite data. The flow had deflated and coalesced from the eruption column by *ca.* 20 km from vent. Beyond this distance most lateral variations are modelled by considering the flow to be a giant fluidized bed. As the flow moved, material was deposited from its base, and hence predictable vertical variations in the model fluidized bed are comparable with lateral variations in the ignimbrite. The agreement is excellent, and, in particular, discontinuities in the nature of the ignimbrite at 55–60 km from vent suggest that the more distal ignimbrite represents a vast segregation layer generated above the moving flow. Differences between the model and variations of some parameters reflect the influence of kinetic processes, such as shearing and local fluidization, that operated regardless of the bulk flow composition. The strong

fluidization in the flow is a result of the high flow velocities (promoting air ingestion), not vice versa as is often accepted.

Contrasts in the natures of layers 1 and 2 imply that the first material erupted contained significantly coarser, and a higher content of, lithics than the bulk of the flow. During emplacement, this earlier material was depleted by deposition and diluted by material introduced from the flow body. Systematic regional variations also occur in the ignimbrite: for example, it contains lower crystal:lithic ratios and higher density pumice in a northeasterly sector, and vice versa to the southwest. Ignimbrite found in mountainous areas shows changes consistent with its derivation from the upper, more mobile and pumiceous top of the flow.

Fluidization processes generated structures and facies in the ignimbrite on various scales. Individual segregation bodies found at any exposure show features mimicking those of the ground layer, i.e. fines depletion and crystal- and lithic-enrichment. Fluidization-induced grading visible at individual exposures accounts for the great range of grading styles seen in the valley-ponded ignimbrite, and strong fluidization has locally generated an upper fines- and pumice- rich segregation layer (here termed layer 2c). On the largest scale, fluidization was primarily responsible for the generation of the layer 1 deposits, and for the grainsize and compositional zonation within the flow that produced the lateral variations in the ignimbrite. Ingested and heated air is inferred to have been the most important gas source for fluidization within the flow, although several other gas sources were locally dominant.

It is clear that the thickness, grainsize and composition of the ignimbrite at any point are not simply related to values of these parameters in either the originally erupted material or the parent flow, and that, except for its density, the dimensions and composition of the parent flow cannot be directly inferred from the ignimbrite.

1. Introduction

In the preceding Paper I (Wilson & Walker 1985) the Taupo ignimbrite was set in context within the Taupo eruption; here a detailed account of the ignimbrite is presented. The Taupo ignimbrite is separated genetically and stratigraphically from the other ignimbrite deposits of the Taupo eruption (Paper I). It was generated in a single short-lived episode which formed the eruption climax, and it is of interest for several reasons.

First, it is very young, fresh, entirely non-welded and reasonably well preserved. Also, being thin and widespread, its full thickness is exposed over large areas, allowing detailed sampling.

Second, although the ignimbrite is a single vent-generated flow unit, it contains a great range of facies and varieties, some of which have not previously been recognized. There is great scope to examine processes generating the various facies seen in ignimbrites, and to examine how these processes vary in effect as the flow is formed and moves away from vent to its outermost limits.

Third, from the distribution of the ignimbrite, it is evident that the parent flow was very violent. The facies in and characteristics of this deposit can be compared with those of more 'conventional' ignimbrites to see how violence affects the emplacement mechanics of large pyroclastic flows. In particular, evidence is available to assess the role of turbulence in the flow and to infer the degree of expansion of the flow.

Fourth, structures in the ignimbrite show that fluidization processes were important; the effects of these processes can be examined at various scales to test predictions of the fluidization behaviour of pyroclastic flows inferred from experimental studies.

The total volume of the ignimbrite (that lying on-land outside Lake Taupo and excluding layer 3) is about 30 km^3, equivalent to about 10 km^3 of magma plus 2.1 km^3 of lithic fragments

(table 1). Field and grainsize data in this paper are from Wilson (1981), supplemented by recent additional work. Several abbreviations and symbols are used here, as in earlier papers, to denote facies and parameters measured in the ignimbrite; these are listed at the end of this section.

TABLE 1. VOLUMES OF THE UNITS FORMING THE TAUPO IGNIMBRITE

unit	volume, *in situ* km³	volume, magma km³	volume, lithics km³
distant facies	0.3	10	negligible
layer 2 VPI	15		
layer 2 IVD	10		
layer 1(H): ground layer	1.1		2.1[a]
layer 1(P): jetted deposits	4.1		
total	30.5		

[a] The lithic volume comprises 1.6 km³ which is the lithic content of the bulk of the erupted material (see figure 57), together with 0.5 km³ which represents additional very coarse lithics in the first erupted material.

As in Paper I, all distances from vent are measured from the geometric centre of the Horomatangi Reefs in Lake Taupo, all heights above vent from the modern level of Lake Taupo (357 m above sea level) and all grid references given to the nearest 100 yards† in the New Zealand map grid.

Notation

c.c.f. crystal concentration factor
c.m.f. coarse ($\geqslant 4$ mm):medium (2 mm to $\frac{1}{4}$ mm):fine ($\leqslant \frac{1}{8}$ mm)
FDI fines-depleted ignimbrite (Walker *et al.* 1980*a*)
IVD ignimbrite veneer deposit (Walker *et al.* 1981*b*)
p.c.l. pumice:crystal:lithic
PCZ pumice-concentration zone (Wilson & Walker 1982)
VPI valley-ponded ignimbrite (Walker *et al.* 1981*b*)
L_m average length of the five largest lithic clasts at any locality
P_m average length of the five largest pumice clasts at any locality

2. LABORATORY TECHNIQUES

Samples were sieved at one-phi (ϕ) intervals, where $\phi = -\log_2$ (grainsize/mm), down to 63 μm. The < 63 μm material in 104 samples was analysed by using pipette methods, down to 4 μm. The raw pipette data were converted to a closer approximation to true percentages by mass by using data from splits of each sample which were sieved on a 31 μm mesh. A given size class is denoted by the mesh size of the sieve that retains it (or the equivalent mesh size for the pipette-analysed fraction).

This study departs from previous practice in that the Folk & Ward (1957) parameters M_z and σ_I,

$$M_z = \tfrac{1}{3}(\phi_{84}+\phi_{50}+\phi_{16}),$$
$$\sigma_I = \tfrac{1}{4}(\phi_{84}-\phi_{16}) + (\phi_{95}-\phi_5)/6.6,$$

† 1 yard ≈ 91 cm.

are used in place of Md_ϕ and σ_ϕ (Inman 1952). This change was made for two reasons: first, M_z and σ_I were used to characterize samples used in fluidization experiments (Wilson 1984) and, second, the extensive use of pipetting techniques allows M_z and σ_I to be calculated with acceptable accuracy.

Most samples were separated down to and including the $\frac{1}{4}$ mm fraction into their three main components: pumice (vesiculated juvenile material), lithics (foreign rock fragments plus minor non-vesticulated juvenile material) and crystals (derived from the magma), using hand-picking or grain-counting methods, or both. Previous workers (e.g. Walker 1972) referred the content of free crystals in a sample by a crystal-enrichment factor to the inferred original-magmatic crystal content, taken as the percentage by mass of crystals in large pumice clasts. Thirteen samples of coarse pumice from the Taupo ignimbrite have been crushed and their crystals separated to yield crystal contents (percentages by mass) ranging from 2.9 to 5.1%, and averaging 3.5%, with all but two samples being between 3.1 and 3.8%. Here, account is taken also of the crystals contained within large pumice clasts in a sample. Pumices coarser than 4 mm are assumed to contain 3.5% by mass crystals and these crystals are added to the free-crystal content. The total crystal content of the sample (recalculated so that the contents of pumice plus crystals total 100%) is then divided by the 3.5% inferred magmatic content to give a crystal-concentration factor (c.c.f.).

The pumice bulk-density in various size fractions was obtained by pouring the sample into a measuring cylinder and tapping gently to obtain a consistent volume (including intergrain voids), which was then divided into the sample mass. Pumice clast-densities were measured in a few samples by using an immersion technique to measure individual clast volumes (see Wilson (1981) for details).

3. Field distribution and emplacement velocities

The overall distribution of the ignimbrite shows that the parent flow was little influenced by the often-rugged topography (figure 1). Apart from a limited area southwest of Ruapehu, the outer limit of the ignimbrite is at 80 ± 10 km from vent, regardless of the intervening relief, and the ignimbrite covers about 20000 km^2, an area which is among the largest documented for any ignimbrite, despite its modest volume.

The relationship between the relief and the distance travelled is complex. North and northnortheast of the vent the flow crossed a subdued landscape but travelled only 70–75 km, whereas eastsoutheast of vent it crossed the entire axial greywacke ranges to reach 80–85 km from source. Southsouthwest of vent however, Ruapehu, which rises over 2400 m above vent level, evidently blocked or diverted the distal part of the flow, and northnorthwest of vent, a significant volume of the flow was trapped in a remnant of the pre-eruption Lake Taupo (Paper I, §3).

Within 60–65 km of vent the flow appears to have traversed the landscape remarkably uniformly, even in the axial ranges where the local relief exceeds 700 m. In these and other mountainous areas the ignimbrite has often been removed by erosion, but in many localities (e.g. where the bedrock is greywacke) its former existence is revealed by residual rhyolite lava or pumice clasts, or both, in the surficial regolith. Even around its margin the ignimbrite still outcrops over a local height range of several hundred metres, showing that the flow must have been travelling at high speed right to its outer limits (figure 2). The flow deposited a layer over

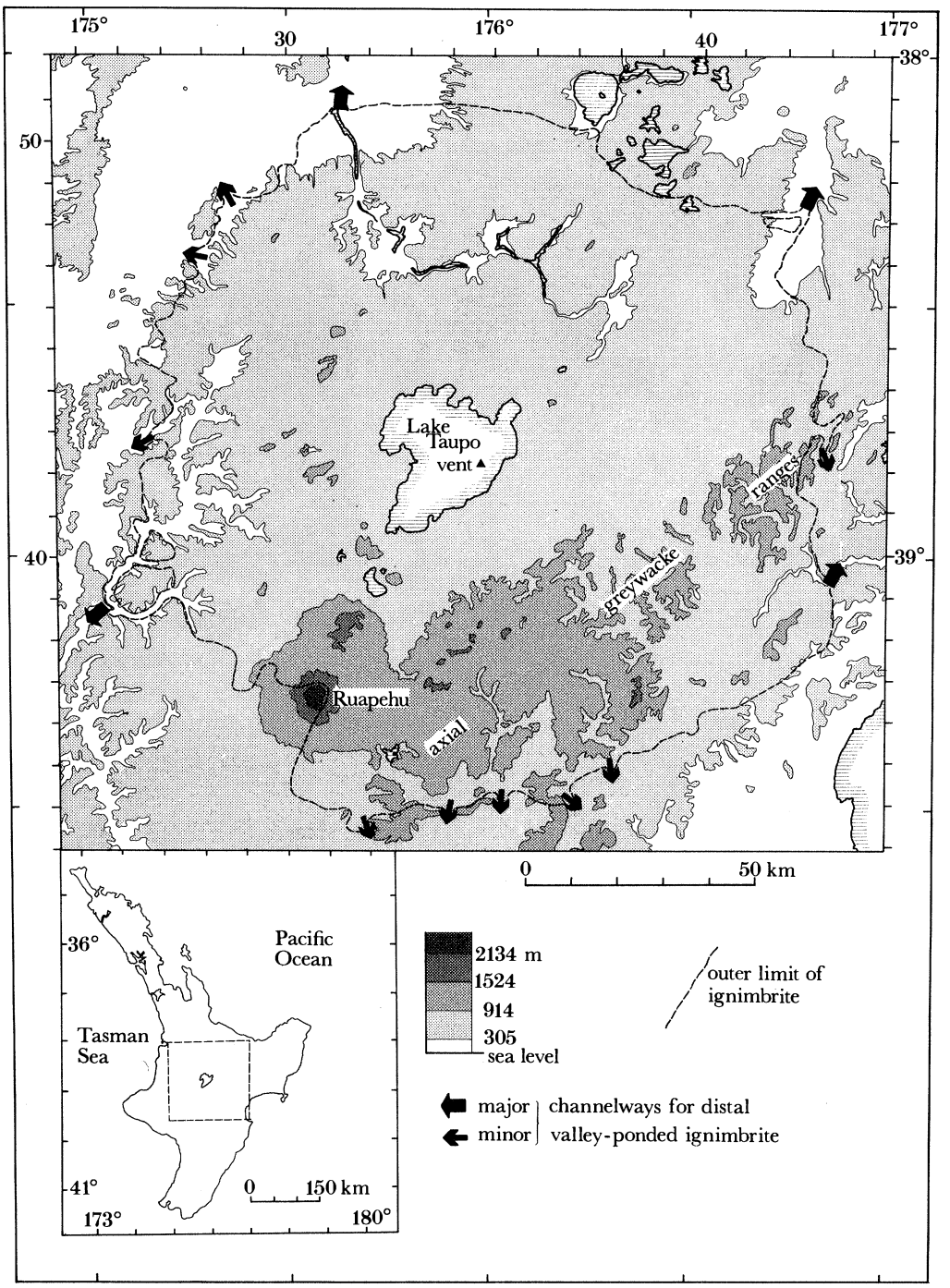

FIGURE 1. Map of the area covered by the Taupo ignimbrite, showing the topography of the area traversed by the parent flow. Ticks and numbers on the inner margin refer to 10000 yard grid squares as used on the N.Z.M.S. 1, 1:63,360 topographic maps.

the entire area traversed, and the outer limits of the ignimbrite are where the flow ran out of material rather than merely slowed to a halt. Beyond 60–65 km from vent the ignimbrite becomes patchy and is largely confined to valleys, although parts of the flow were capable of climbing over 700 m. No ignimbrite outcrops have yet been found over 90 km from vent, but voluminous mudflow deposits extend for tens of kilometres further down the main valleys (Paper I).

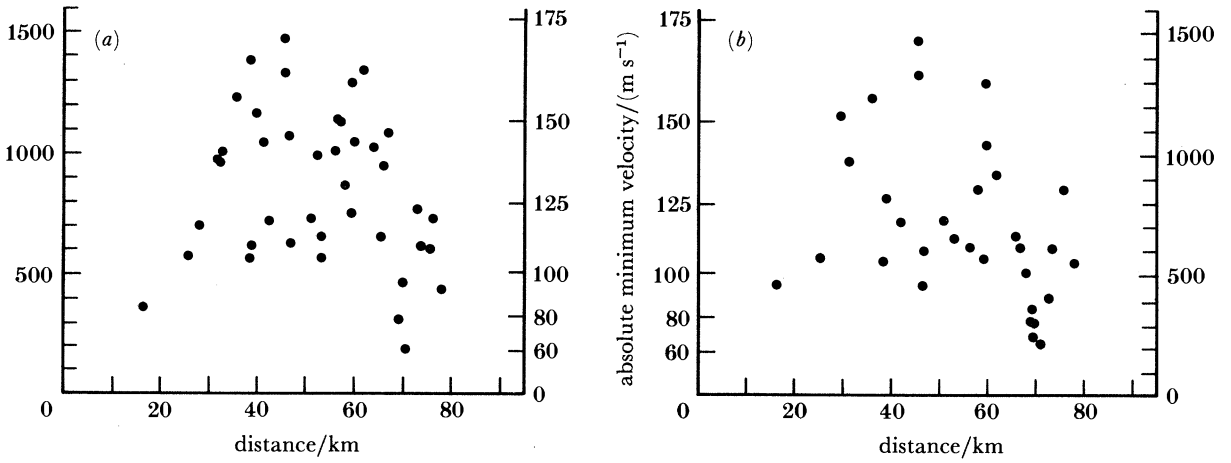

FIGURE 2. Heights of mountains climbed and the inferred absolute minimum velocities required by the Taupo flow, against the distance from vent. Heights are relative to (*a*) the inferred vent level, and (*b*) the local base level (see text).

The heights of obstacles climbed by the flow are used to estimate its velocity at various points, from the equation linking potential energy to kinetic energy (Sparks 1976) either with respect to the vent level (reflecting the overall kinetic energy budget of the flow) or by using the local relief (which more accurately measures the local flow velocity). Both methods yield absolute minimum velocity estimates in excess of 150 m s^{-1} (figure 2) and it is likely that the flow exceeded 250–300 m s^{-1} near vent and sustained velocities locally in excess of 150 m s^{-1} to within a few kilometres of its outer limit. Other aspects of the violence of the Taupo flow are discussed in Wilson & Walker (1981).

4. Field relations, field data and laboratory data

The ignimbrite is described in terms of the layering scheme introduced by Sparks *et al.* (1973), as modified in Wilson & Walker (1982), which considers an ignimbrite to consist of layers 1, 2 and 3, and a distant facies. Layer 1 consists of deposits which are inferred to have been generated by processes operating in, or in advance of, the pyroclastic flow head. Layer 2 is inferred to represent, or be deposited from, the body of the flow, while layer 3 is an airfall ash thought to be deposited by the dilute ash cloud present above the moving flow (Sparks & Walker 1977). The distant facies is newly recognized in the outermost reaches of the Taupo ignimbrite, replacing layers 1 and 2; it is inferred to represent the deposit where the flow retained a high velocity but was running out of material (Wilson & Walker 1982).

(*a*) *Layer* 1

(i) *Field relations*

Layer 1 occurs throughout most of the ignimbrite area, although there are many short breaks in its continuity, and it is only absent from interfluves in the most distal outcrops where it and layer 2 are replaced by the distant facies. Two lithofacies, layers 1(P) and 1(H) are recognized (Wilson & Walker 1982). They show different morphologies in exposures (figure 3) and are separated by an erosive contact.

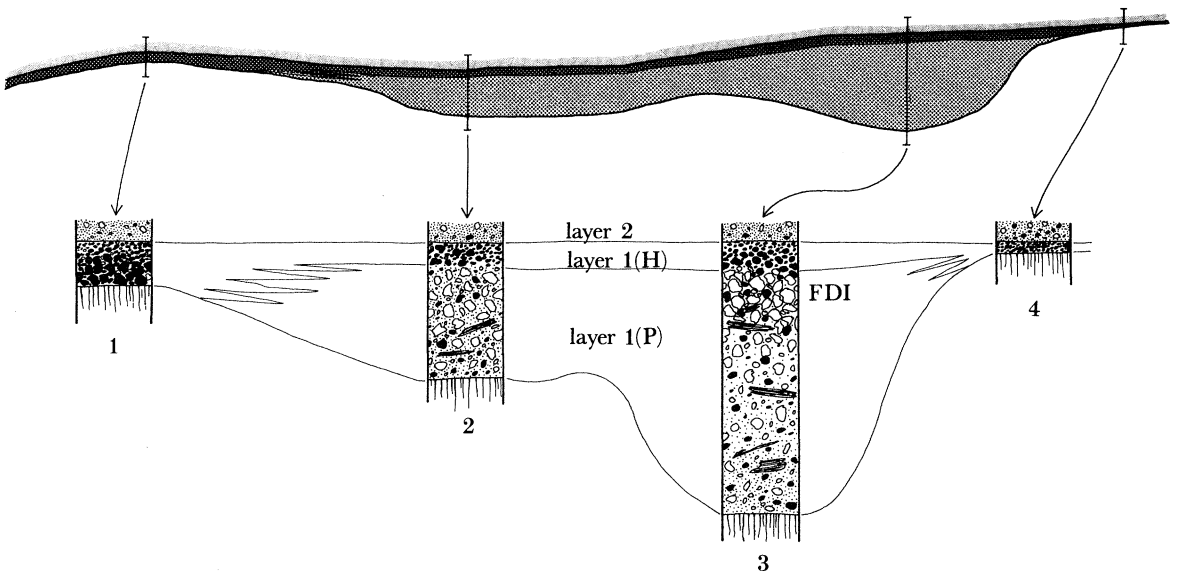

FIGURE 3. Schematic cross sections showing field relationships of layers 1(P) and 1(H). The upper section illustrates the relative thicknesses and lateral continuity of the layers, and the lower sections show: 1, typical, lithic-rich, normally graded layer 1(H); 2, layer 1(P) overlain by layer 1(H), the two having similar L_m sizes but different compositions; 3, thicker, nearer-vent layer 1(P) in which the fines content decreases upwards to give FDI; 4, thin, fine-grained layer 1(H) forming the entire thickness of layer 1 where the other deposits were removed by intraflow erosion.

Layer 1(*P*). Layer 1(P) forms the lowest deposit of the ignimbrite. It varies greatly in thickness from a few centimetres up to more than 8 m, being commoner and thicker in topographic depressions, although it has been observed on slopes of up to 28–30°. It is normally two to twenty times as thick as the associated layer 1(H). It is dominantly pumiceous, commonly containing a fine-grained matrix rich in fluidization segregation bodies (parts of the deposit where crystals and lithics are enriched and fine material has been removed by high gas flow rates; see Wilson (1980, 1984)), and has similar-sized lithics to layer 1(H). Often its fines content (in this paper 'fines' are arbitrarily defined as material less than $\frac{1}{4}$ mm) decreases upwards, at one extreme forming fines-depleted ignimbrite (FDI; Walker *et al.* 1980*a*). Three other distinctive but quantitatively minor layer 1(P) varieties also occur; there are informally labelled varieties a, b and c (see below). Layer 1(P) is separated from layer 1(H) by an erosive contact which may be sharp or sheared, the latter situation resulting in minor quantities of material intermediate in nature between the two facies.

All the varieties of layer 1(P), that is, FDI, 'normal' layer 1(P) and varieties a, b and c, show

a characteristic appearance (figure 4, plates 1 and 2) and distribution about the vent (figures 5 and 6). Within 12–15 km of vent, layer 1(P) is absent. As sections are examined at increasing distances from vent, layer 1(P) first appears as a pumiceous fines-depleted top over a lithic-rich, fines-depleted base (figure 4*a*) at exposures 13–26 km from vent, while, beyond 16 km, normal and FDI-bearing layer 1(P) deposits are found.

Walker *et al.* (1980*a*) documented exposures of FDI out to 45 km from vent but it is now known that the outer limit of FDI is somewhat irregular, and reaches 50 km northwest from vent (figure 6). It is absent from a broad area east and northeast of vent where layer 1(P) shows little or no upward fines-depletion (figure 4*b*), this being the sector where the vegetation had been buried by airfall deposits before the Taupo ignimbrite was emplaced. From this an important connection was inferred between the occurrence of vegetation and the formation of FDI (Walker *et al.* 1980*a*). Beyond the outer limits of FDI proper, layer 1(P) commonly shows some upward fines-depletion but more often has a uniform content of fine material, especially in the most distal exposures.

The three minor varieties of layer 1(P) occur over more limited areas (figure 6):

Variety a. Above the modern tree-line (1200–1350 m above sea level) layer 1(P) is distinctly bimodal, consisting of abundant coarse pumice clasts in a fine-grained crystal and lithic bearing matrix (figure 4*d*). Coarse lithics occur in minor amounts, while carbonized vegetation fragments are common. The large pumices are noticeably very light and are often well rounded.

Variety b. In two areas close to Lake Taupo, layer 1(P) has a fines-rich vesicular matrix which shows no upward fines-depletion (figure 4*e*). The unit lacks carbonized vegetation, but has numerous elongate holes, up to 20 cm diameter, which are usually lined with a thin layer of pumiceous ash in which bark impressions are preserved.

Variety c. At only two distal localities (3294 4794 and 2641 4069) layer 1(P) is strongly bimodal, consisting of common coarse, very light and well rounded pumices in a very fine-grained pumiceous matrix. Sparse fragments of carbonized vegetation are the only other visible component.

All exposures of layer 1(P), except varieties b and c, contain abundant fluidization segregation bodies (Wilson 1980). Both pods and pipes are abundant, but the latter almost always originate from included carbonized branches and logs. Small pipes are contained within layer 1(P), but larger examples may penetrate through into layer 2. In addition, many coarse lithics and pumices in the fines-bearing layer 1(P) deposits (except varieties b and c) are separated from the matrix by a thin fines-free sheath of lithics and crystals so that they can be cleanly detached from the deposit with no adhering matrix. All gradations are found between such individual clasts and large segregation bodies which contain coarse clasts.

Layer 1(H). Layer 1(H) overlies layer 1(P). It is thinner but more continuous than the latter,

Description of plate 1

Figure 4. Layer 1(P) (excluding FDI, which is illustrated in Walker *et al.* 1980*a*). (*a*) Near-vent, wholly fines-depleted, compositionally zoned layer 1(P): R, Rotongaio phreatoplinian ash; L, lithic-rich base; P, pumice-rich top; H, layer 1(H); 2, layer 2 (veneer deposit). Locality at 3488 4078, 14 km from vent. (*b*) To the east of vent where layer 1(P) overlies thick co-eruptive airfall deposits: T, Taupo plinian pumice: P, layer 1(P): H, layer 1(H). Locality at 3971 4053, 49 km from vent. (*c*) A distal exposure at the base of a *ca.* 40 m thick valley pond where layer 1(P) is thin and layer 1(H) absent. Locality at 3681 3464, 72 km from vent. (*d*) At high altitudes, where variety a of layer 1(P) occurs, overlain by a poorly preserved layer 2 (veneer deposit). Locality at 3357 3820, 38 km from vent. (*e*) Layer 1(P), variety b, overlain by a thin layer 1(H) and layer 2: S, underlying soil. Locality at 3356 4061, 18 km from vent.

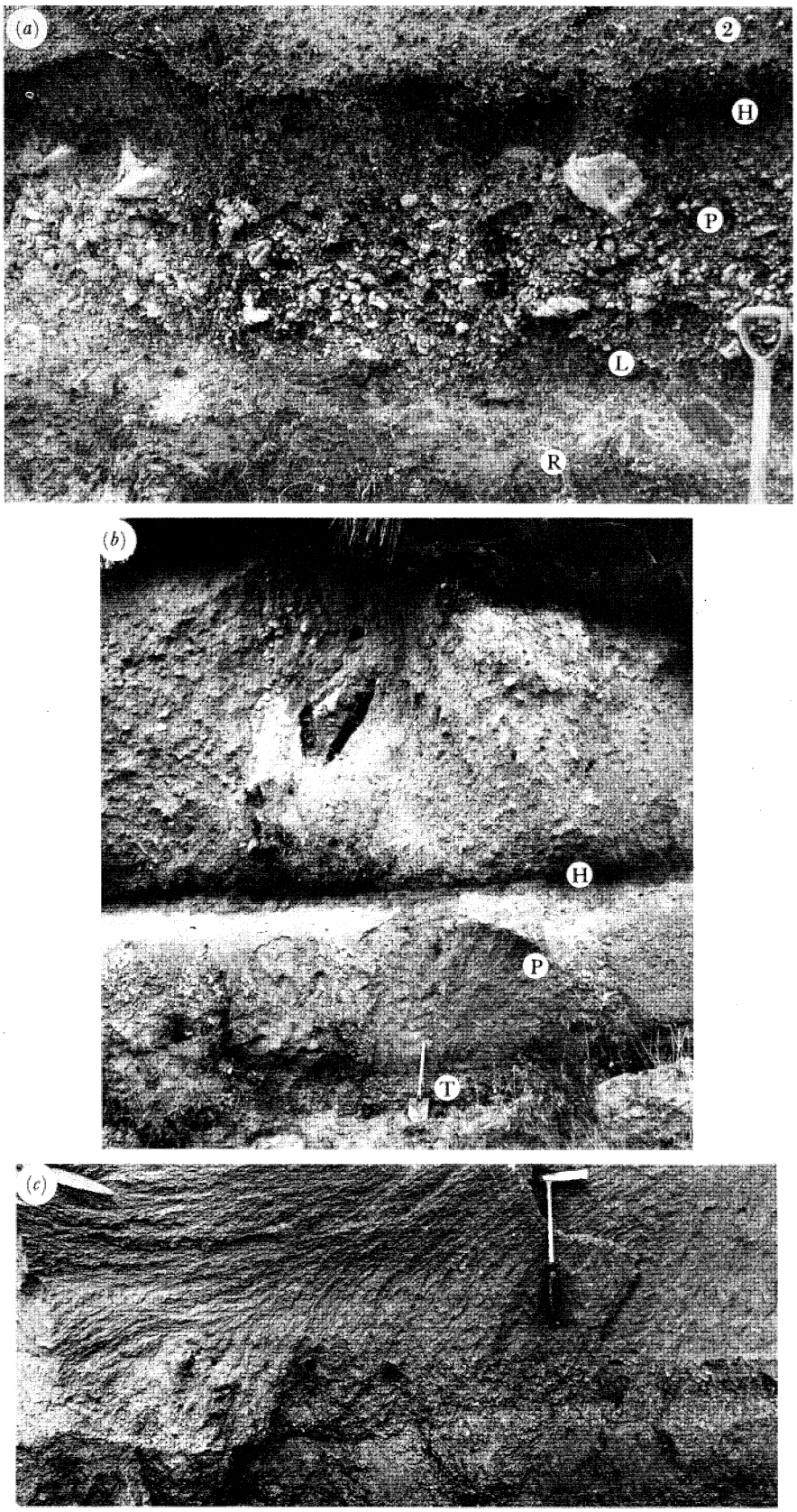

FIGURE 4 (*a*)–(*c*). For description see opposite.

(*Facing p.* 238)

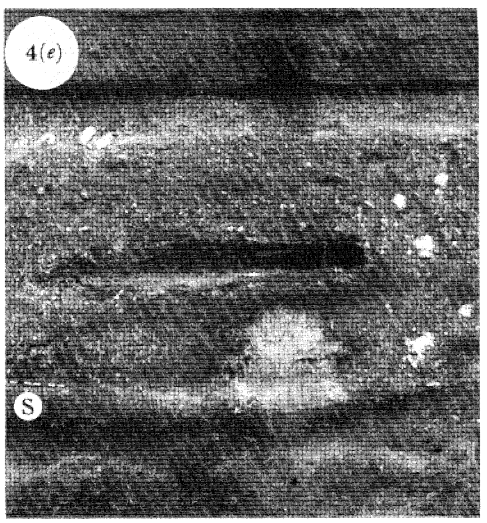

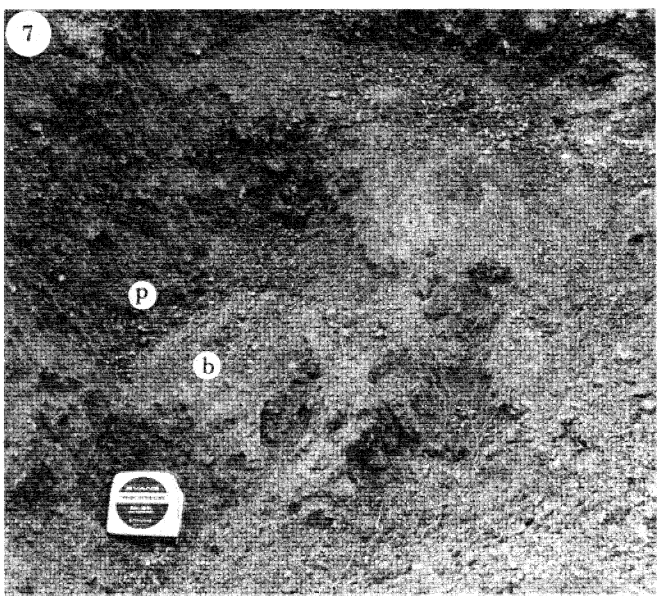

FIGURE 4 (*d*), (*e*). For description see p. 238.

FIGURE 7. The matrix of the near-vent layer 1(H), showing the fines-bearing (b) and fines-poor (p) 'phases'. Locality at 3493 4353, 12 km from vent.

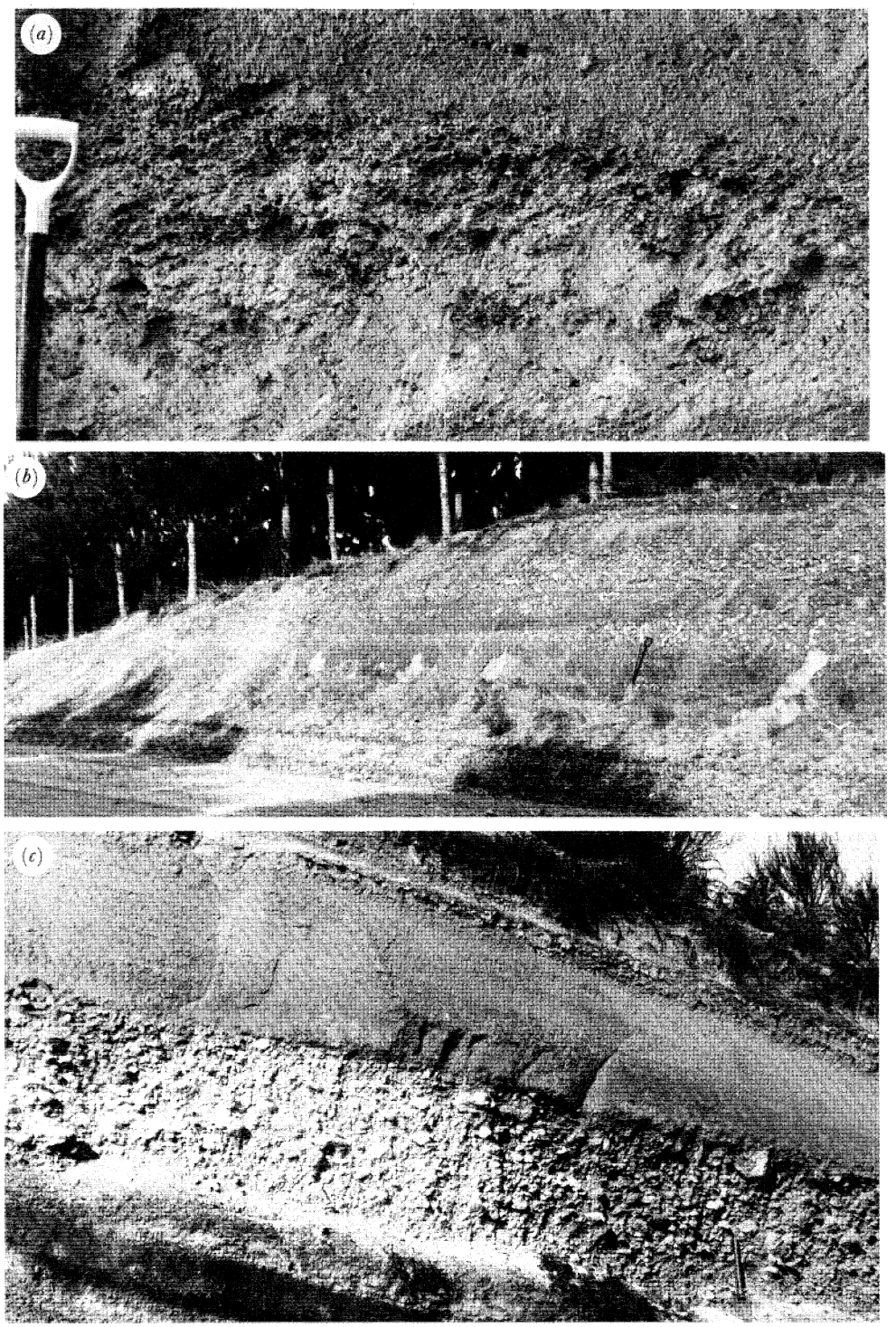

FIGURE 29 (*a*)–(*c*). Structures in the IVD (see text for discussion). (*a*) Detail of a lithic-rich lens within the IVD at the locality illustrated in (*e*). (*b*) Coarse-scale stratification. The flow travelled from left to right, closely parallel to the length of the exposure. Locality at **3619 4113**, **17** km from vent. (*c*) Fine-scale stratification in the IVD overlying coarse FDI. Locality at **3478 4050**, **16** km from vent. (*d*) Lee-side structure in the near-vent IVD where lee-side lenses are absent (cf. Walker *et al.* 1981*b*, figure 6(*b*)). The IVD overlies the Rotongaio phreatoplinian ash (R). The flow travelled from left to right, closely parallel to the length of the exposure. Locality at **3547 4163**, **10** km from vent. (*e*) Partial cross-section through a dune-like structure in the IVD, developed on a flat underlying surface. The flow travelled from left to right at a shallow angle to the length of the exposure. Locality at **3460 4120**, **9** km from vent. (*f*) Low-angle foreset bedding in the IVD developed on a flat underlying surface. The flow travelled from left to right, roughly parallel to the length of the exposure. Locality at **3489 4122**, **10** km from vent.

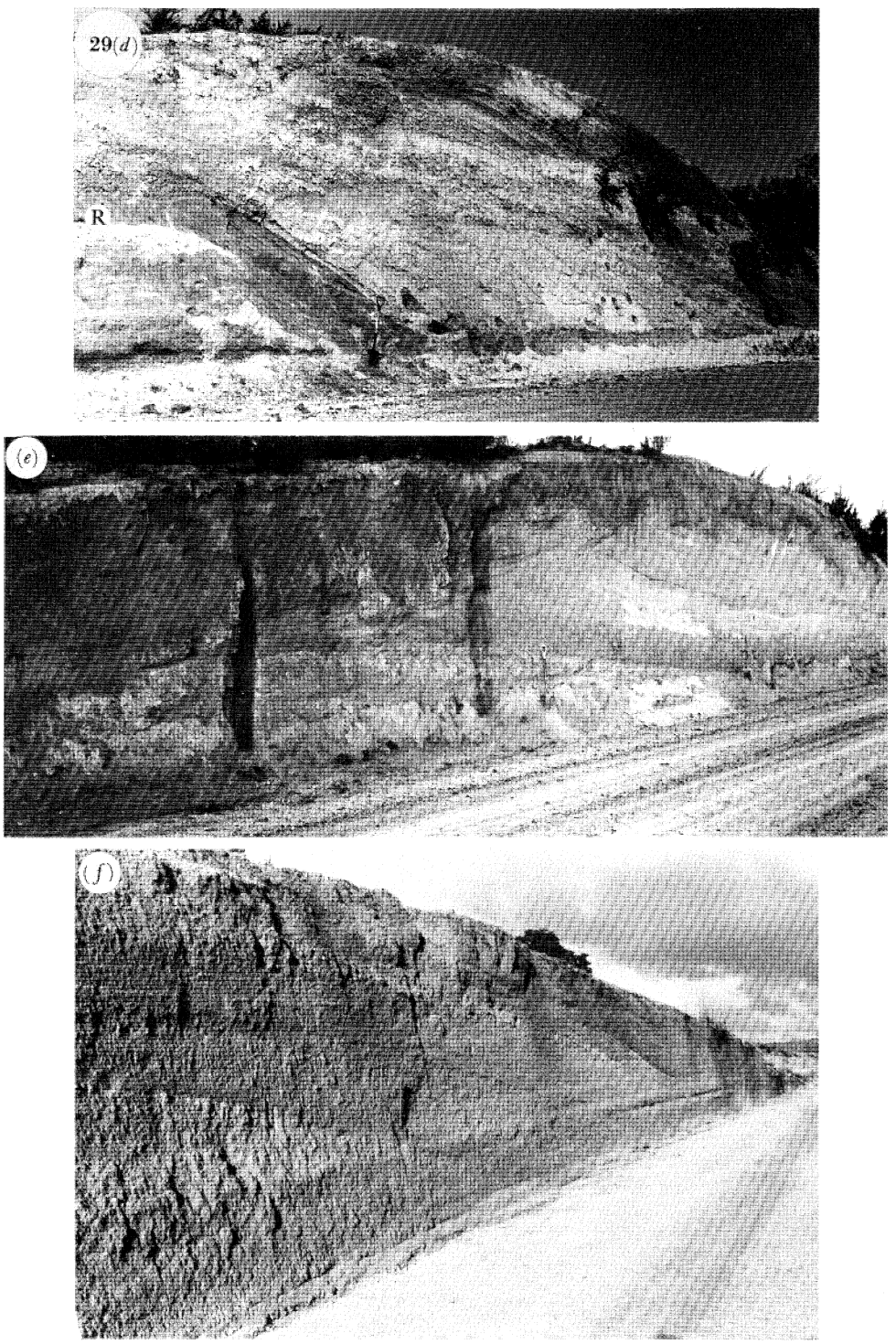

FIGURE 29 $(d)-(f)$. For description see plate 3.

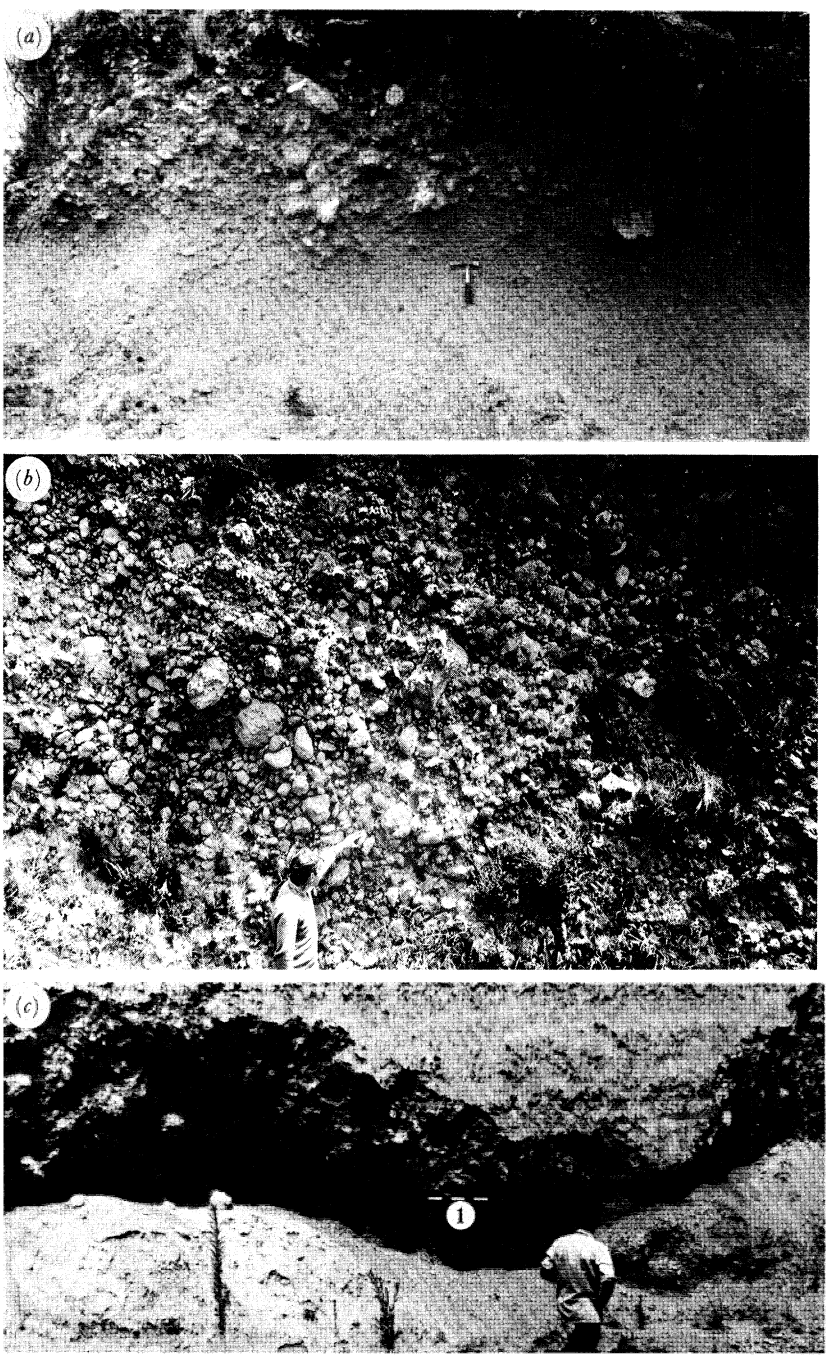

FIGURE 32. Pumice grading in the VPI (see text for discussion). (*a*) View of a type-3 VPI section showing an upper, clearly demarcated PCZ. Locality at 3843 4292, 36 km from vent. (*b*) Detail of coarse partially clast-supported PCZ. Locality at 3838 4139, 35 km from vent. (*c*) Base of a coarse PCZ unit which directly overlies layer 1(1) with only a poorly developed layer 2a intervening. Locality at 3454 4626, 37 km from vent.

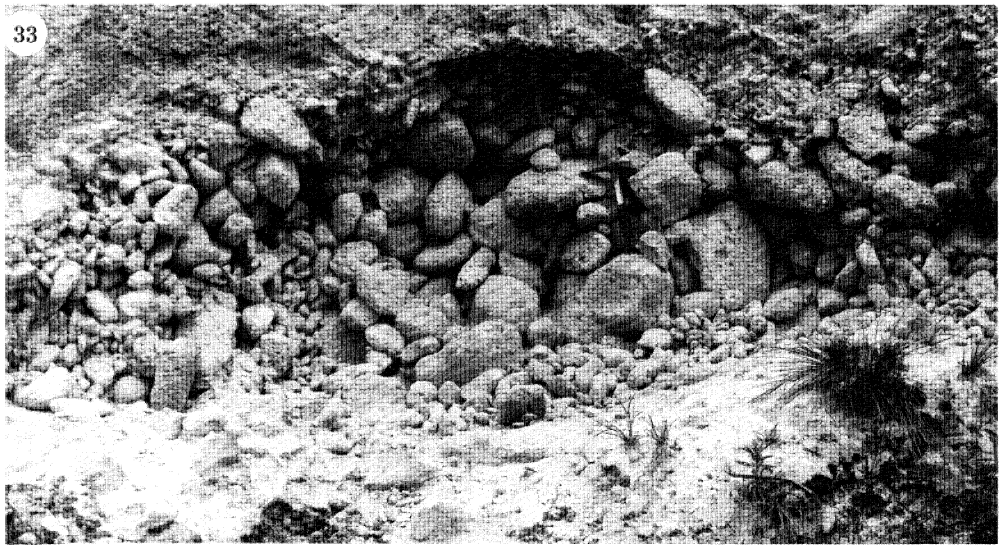

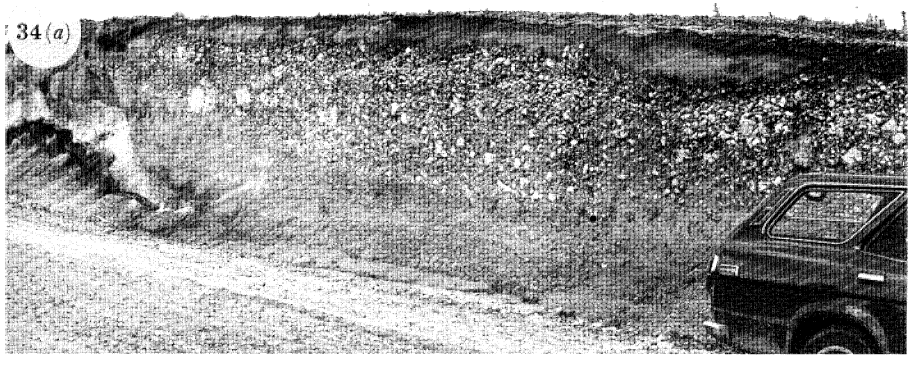

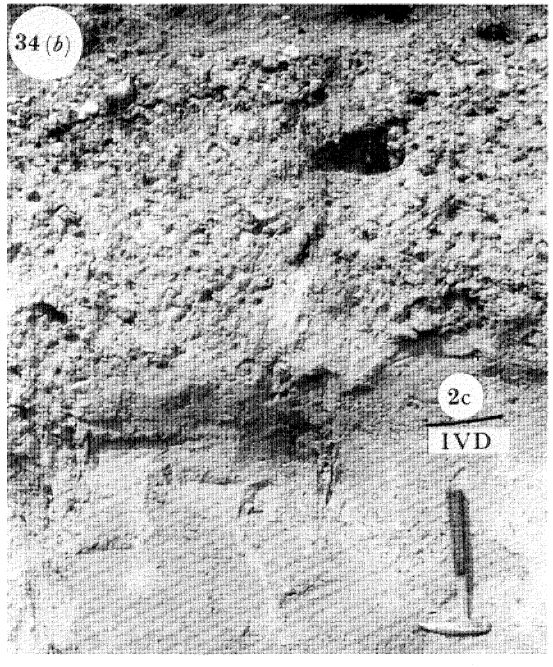

FIGURE 33. Pumiceous, matrix-absent lens in the VPI (see §4 (*b*) (i)). Locality at **3998 3991**, 54 km from vent.

FIGURE 34. (*a*) Fine-grained layer 2c overlying a coarse, type 3 VPI unit, the latter passing laterally into a stratified IVD. Locality at **3612 4080**, 19 km from vent. (*b*) Layer 2c, coarse-pumice-rich and strongly bimodal in its upper part, overlying the IVD; the boundary between them is fixed from the truncation of segregation pipes in the lower unit (see figure 35). Locality at **3243 3767**, 46 km from vent.

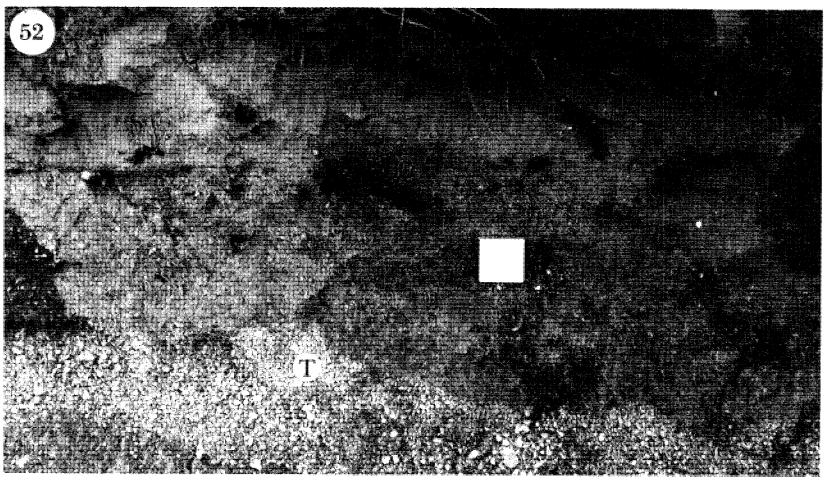

FIGURE 52. The distant facies overlying the Taupo plinian pumice (T). The tape case is 5 cm square. Locality at 4143 4672, 75 km from vent.

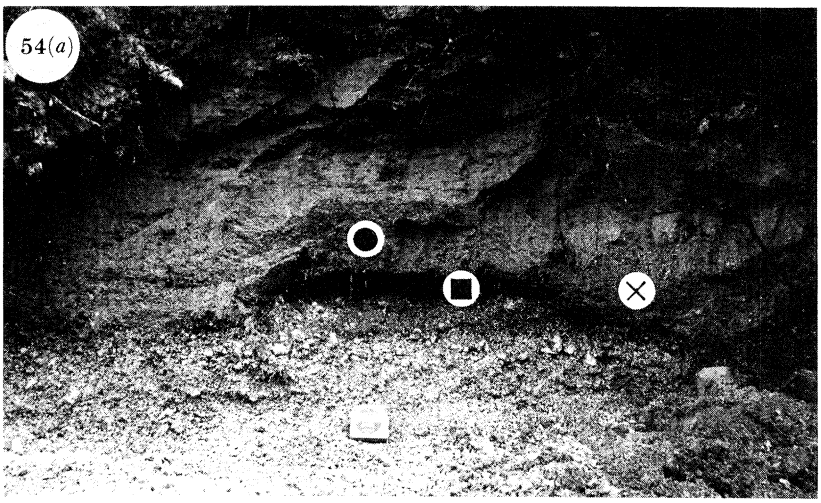

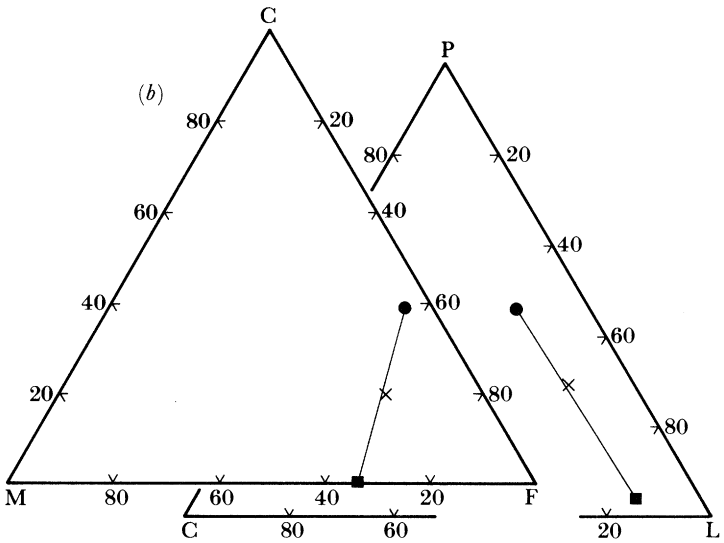

FIGURE 54. Erosion of layer 1 to produce a compositional zonation in the IVD. (*a*) Photograph of the IVD which has partly eroded the ground layer and underlying Taupo plinian pumice; symbols represent where the samples shown in (*b*) were collected. (*b*) C.m.f. and p.c.l. data (% by mass) from the IVD (●), ground layer (■), and the mixed material between the two (×). Locality at 3697 4346, 24 km from vent.

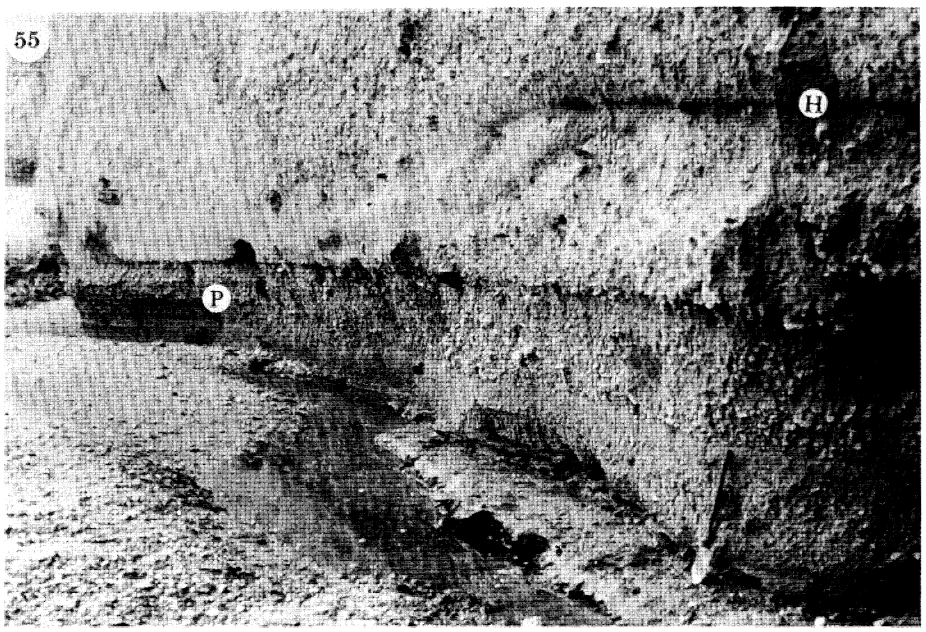

FIGURE 55. Role of a basal permeable layer in controlling the development of layer 2a. On the right, the VPI overlies a thin ground layer (H) with a poorly developed layer 2a; on the left, the ground layer has been removed and a clearly developed layer 2a overlies fines-bearing jetted deposits (P). The shovel rests on the pre-eruption palaeosol. Locality at 3612 3867, 35 km from vent.

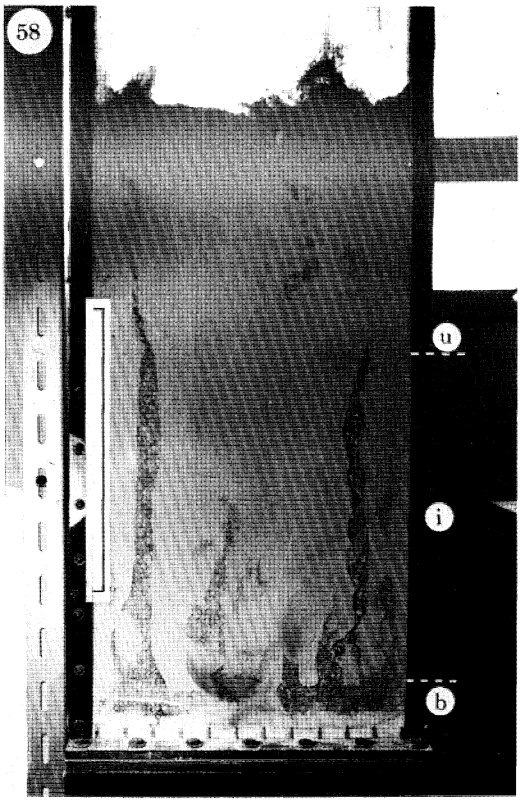

FIGURE 58. Fluidized ignimbrite sample (Wilson 1980, figure 4), showing the basal (b), intermediate (i) and upper (u) portions of the bed (see text for discussion). Scale bar is 25 cm.

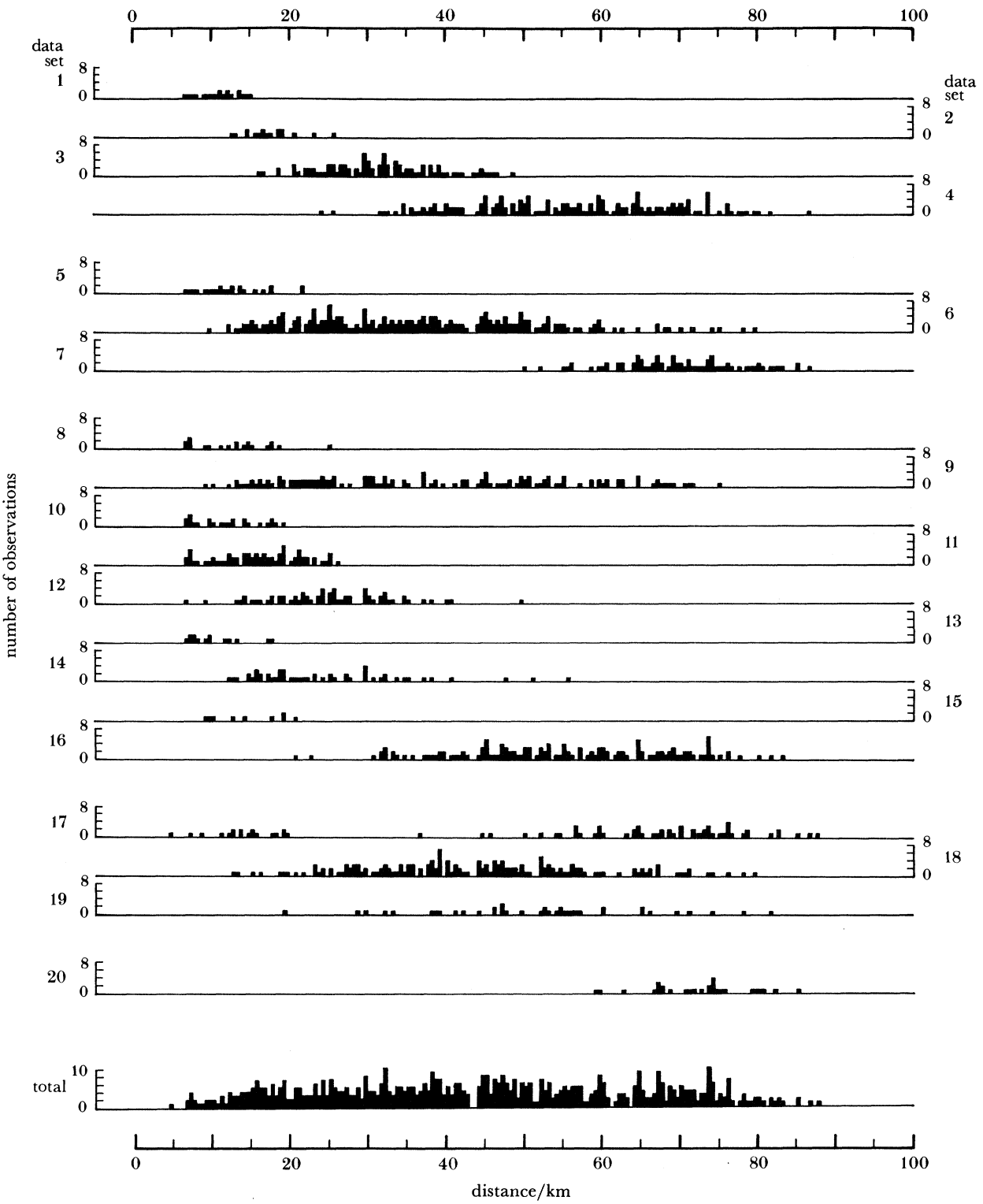

FIGURE 5. Histograms showing the distance from vent of localities where the following features were observed in the ignimbrite; 1, Layer 1(P) absent and replaced by 1(H); 2, wholly fines-depleted, compositionally zoned layer 1(P); 3, fines-bearing layer 1(P) zoned upwards into FDI; 4, layer 1(P) with little or no upwards fines-content zonation; 5, fines-bearing 'two-phase' layer 1(H); 6, typical layer 1(H); 7, layer 1(H) absent. 8–16, Data from the ignimbrite veneer deposit (see §4(*b*)(i)); 8, lithic-rich lenses present; 9, compositional zonation present; 10, compositional zonation absent (for localities less than 40 km from source only); 11, coarser-scale stratification present; 12, finer-scale stratification present; 13, lee-side lenses absent from favourable localities near vent; 14, lee-side lenses present; 15, bedforms found in the veneer deposit where the underlying surface was level; 16, no grainsize stratification in the veneer deposit. 17, Valley-ponded ignimbrite shows type 1 grading; 18, valley-ponded ignimbrite shows type-2 or -3 grading; 19, layer 2c present; 20, distant facies present.

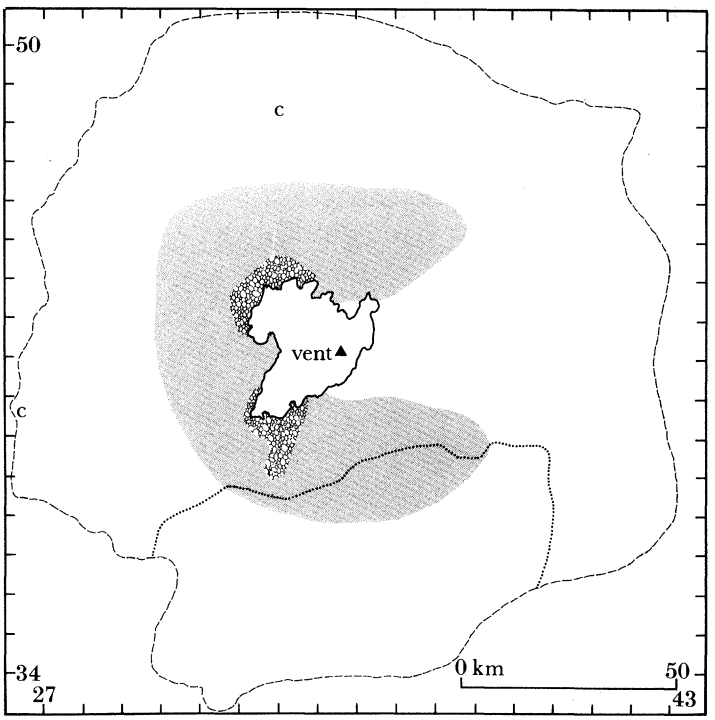

FIGURE 6. Map of outcrop areas of layer 1(P) varieties: FDI occurs within the shaded area, variety a south of the dotted line (cf. figure 1), variety b in two areas marked by the 'bubble' texture and variety c at the two localities marked by 'c'. 'Normal' layer 1(P) occurs over the remaining area of the ignimbrite. Here, and also in figures 11, 28, 30, 38, 40 and 67, the dashed perimeter marks the approximate outer limit of the ignimbrite and the marginal ticks and numbers refer to 10000 yard grid squares used on the N.Z.M.S. 1, 1:63360 topographic maps.

and has been observed on contact surfaces inclined at up to 60–70°. Apart from near-vent localities (figure 5) it is extremely poor in fines and rich in crystals and lithics. Its upper and lower contacts are erosive, and are commonly sheared to generate materials of intermediate grainsizes and compositions. It is described and illustrated by Walker *et al.* (1981*a*).

Normally layer 1(H) is coarsest at or just above its base, while its upper part, immediately below layer 2, may be rather fine grained. A similarly fine-grained layer 1(H) underlies layer 2 in situations where the other layer 1 deposits appear to have been removed by intraflow erosion associated with the emplacement of layer 2. In many near-vent localities (figure 5) the matrix of layer 1(H) contains minor amounts of pumiceous ash and consists of two 'phases': pods and irregular patches of fines-poor material in a fines-bearing matrix (figure 7, plate 2). Elsewhere, segregation structures are not seen within layer 1(H).

(ii) *Field data*

The maximum thicknesses of both layer 1 facies at any exposure decrease with distance from vent (figure 8). Less than *ca.* 30 km from vent, layer 1(P) tends to be rather thin, and field observations suggest that this is due to severe erosion during the emplacement of the flow.

Assuming that the average thickness of each facies is one third of the maximum at any given distance (figure 8) and that each layer covers half of the total area of the ignimbrite, and neglecting material less than 14 km from vent (i.e. the radius of a circle equal in area to Lake

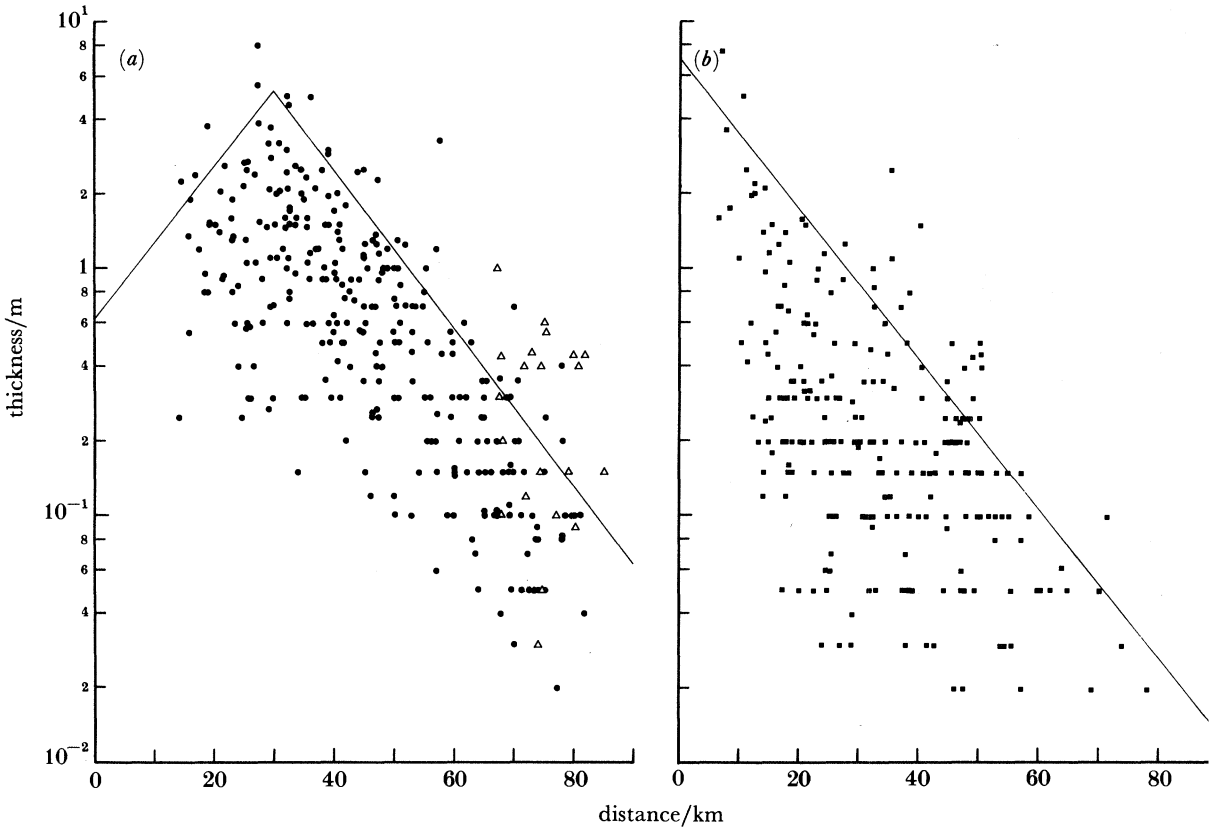

FIGURE 8. Thicknesses of (*a*) layers 1(P) (•) and (*b*) 1(H) (▪), against the distance from vent. In (*a*), ▵ denote data from the distant facies (see §4(*c*)). The lines are hand-fitted maximum-thickness trends, defined by:

layer 1(P), $D < 30$ km, thickness $= 0.62 \exp(+0.07D)$;
layer 1(P), $D \geqslant 30$ km, thickness $= 47 \exp(-0.074D)$;
layer 1(H), thickness $= 7.0 \exp(-0.07D)$,

where thickness is in metres and D the distance from vent in kilometres.

Taupo) and beyond 70 km from vent, the volumes of the facies are estimated as 4.1 km^3 for layer 1(P) and 1.1 km^3 for layer 1(H).

In figure 9, L_m data for each facies are plotted against the distance from vent. The facies have nearly identical L_m sizes at any distance, only differing in the coarser lithics found in the nearest-vent layer 1(H). The relative L_m sizes in layers 1 and 2 vary greatly from about an order of magnitude difference near vent to a factor of two or less in distal areas (figure 10). Layer 1 L_m data are plotted on a map in figure 11; note the two area of lower L_m values around Lake Taupo, which roughly coincide with the outcrop areas of variety b of layer 1(P) (figure 6). Layer 1(P) P_m sizes decrease steadily away from vent (figure 12) but more slowly than the L_m sizes.

(iii) *Laboratory data*

Representative sieve and component data from the different facies and varieties of layer 1 are given in figure 13.

On a coarse:medium:fine (c.m.f.) plot of the coarse ($\geqslant 4$ mm), medium (2 mm$-\frac{1}{4}$ mm) and fine ($\leqslant \frac{1}{8}$ mm) material in the samples, layers 1(P) and 1(H) form two overlapping data

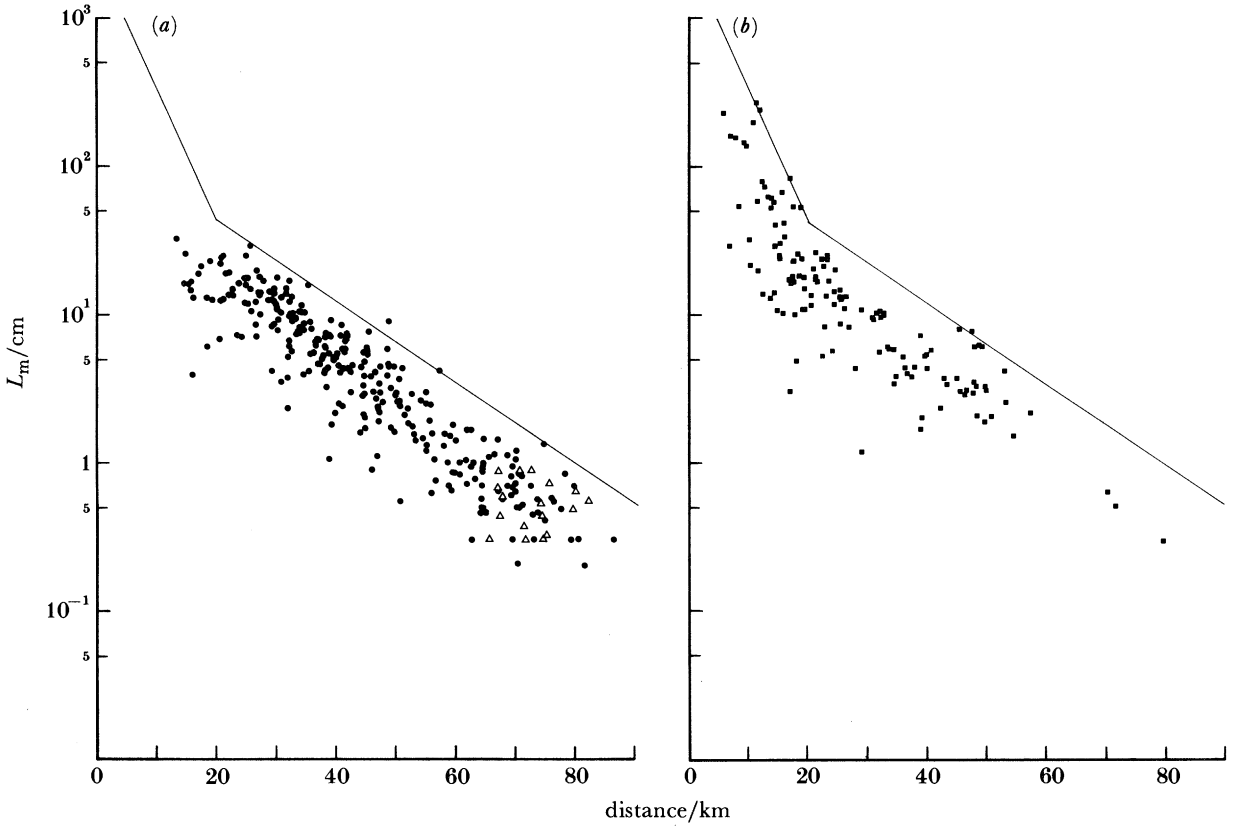

FIGURE 9. L_m sizes for (*a*) layer 1(P) and the distant facies, and (*b*) layer 1(H), against the distance from vent. Symbols are as in figure 8. The lines are hand-fitted maxima, defined by:

$$\text{distances} < 20 \text{ km}, \; L_m = 2800 \exp(-0.205D);$$
$$\text{distances} \geqslant 20 \text{ km}, \; l_m = 150 \exp(-0.063D),$$

where L_m is in centimetres.

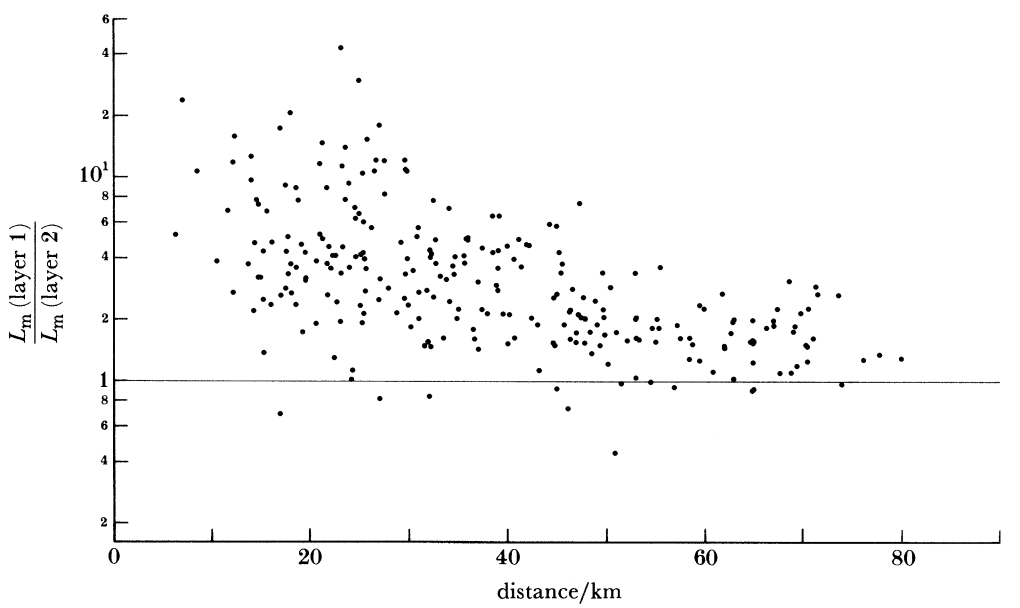

FIGURE 10. Relative L_m sizes in layers 1 and 2 at the same locality, against the distance from vent.

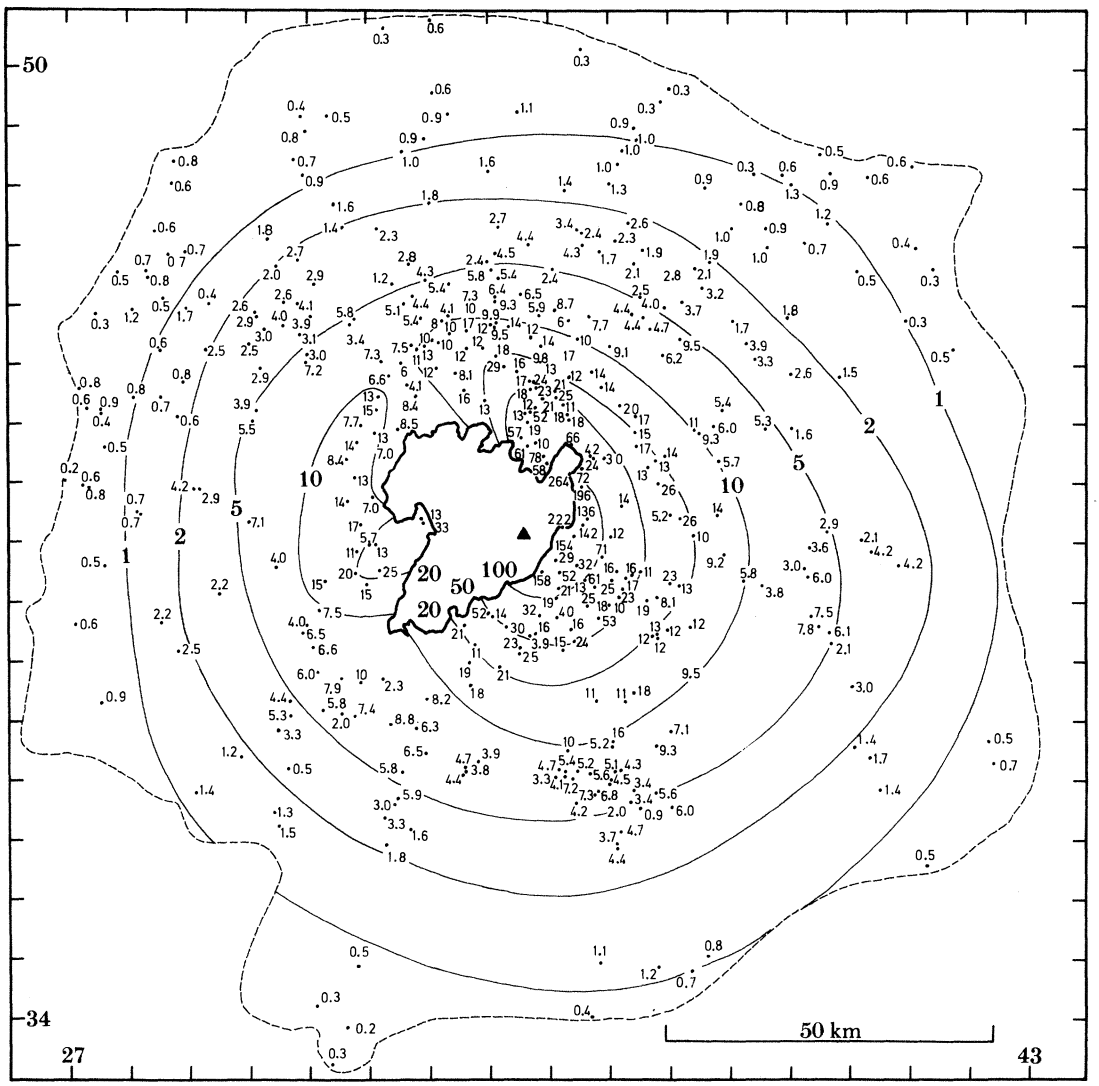

FIGURE 11. Map of the combined L_m data from layers 1(P), 1(H) and the distant facies. Values and isopleths are in centimetres.

sets (figure 14). Most layer 1(P) samples are rich in fine material, whereas most layer 1(H) samples are fines-poor, the overlap being caused by the loss of fines from layer 1(P) to generate the pumice-rich but fines-poor FDI, and the presence of fines in layer 1(H) samples from near-vent outcrops and the sheared zone between layers 1(P) and (H). If these factors are eliminated, then the two main facies have completely separate grainsize characteristics which diverge with increasing distance from vent, layer 1(P) becoming fines-richer and layer 1(H) remaining fines-poor (figure 15). Layer 1(P), excepting variety b, is always fines-depleted with respect to layer 2 (figure 16). Pipette-analysis data are plotted as (< 63 μm)/(< 10 μm) ratios against distance from vent in figure 17. There is no significant difference in the ratios for the nearest-vent layers 1(P), 1(H) and 2 samples, but differences between the ratios for layers 1(P) and 2 increase outwards from vent. However, variety c of layer 1(P) has a very low ratio, which is similar to those in layer 2.

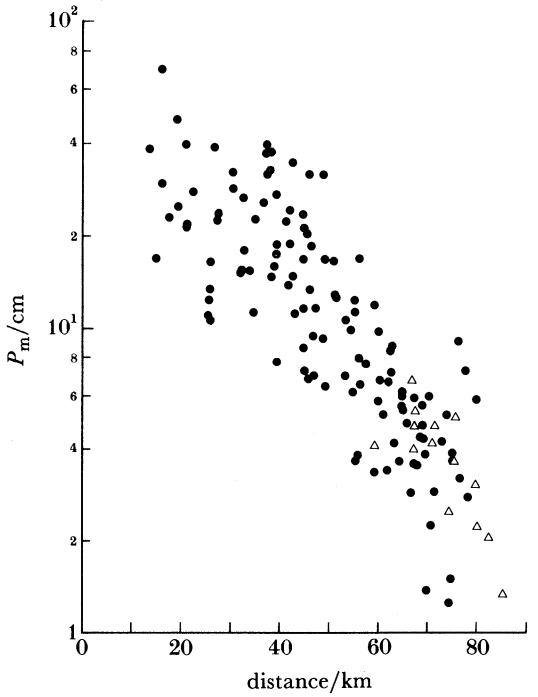

FIGURE 12. P_m sizes in layer 1(P) (•) and the distant facies (△), against the distance from vent.

The layer 1 samples show great variations in M_z and σ_I (figure 18). Generally, layer 1(H) is much better sorted than layer 1(P), while FDI is coarser but no more poorly sorted than the remainder of layer 1(P). Apart from FDI and varieties b and c, σ_I varies by less than 1ϕ for a given M_z-value in layer 1(P). All the M_z and σ_I data show systematic changes with distance from vent. In layer 1(P), M_z (figure 19*a*) decreases steadily by 6–7ϕ while σ_I (figure 19*b*) remains uniformly high out to about 40 km and then declines to reach minimum values of about 2 in distal areas. Layer 1(H) shows a general decrease in M_z away from vent (figure 19*c*) such that it is always 0–1.5ϕ coarser than layer 1(P), while σ_I decreases from 2–3 near vent to reach uniform values between 1.2 and 1.8 beyond 20–30 km (figure 19*d*).

The contents of crystals plus lithics in layer 1 samples show a strongly bimodal distribution, the modes corresponding to layers 1(P) and 1(H) (Wilson & Walker 1982, figure 1). On a p.c.l. (pumice–crystal–lithic) plot, the two facies form largely separate data sets (figure 20). Within layer 1(P), FDI and variety a are noticeably richer and poorer in crystals plus lithics,

FIGURE 13. Representative grainsize and compositional data from layers 1(P) and 1(H). The top part of the diagram is simplified from figure 5 and shows the ranges at which the various units are found; the numbers denote the relevant sections and their distances from vent. The sections are: 1, Fines-bearing layer 1(H); locality at 3493 4353, 12 km from vent (see figure 7). 2, Wholly fines-depleted, compositionally zoned layer 1(P); locality at 3209 4201, 23 km from vent. 3, Layer 1(P) zoned into FDI, with an overlying typical layer 1(H); locality at 3647 4419, 25 km from vent. 4, Layer 1(P) from the area east of vent where FDI is not developed; locality at 3938 4078, 46 km from vent. 5, Variety a of layer 1(P); locality at 3602 3798, 41 km from vent. 6, Variety b of layer 1(P), with an overlying layer 1(H); locality at 3356 4061, 18 km from vent (see figure 4*e*). 7, Variety c of layer 1(P); locality at 2636 4074, 77 km from vent. 8, Distal layer 1(P); locality at 3681 3464, 72 km from vent. For each histogram, the horizontal axis is the size fraction in terms of ϕ and the vertical axis is composition in % by mass; stippling, pumice; solid black, lithics; diagonal hatching, crystals; unornamented, not separated.

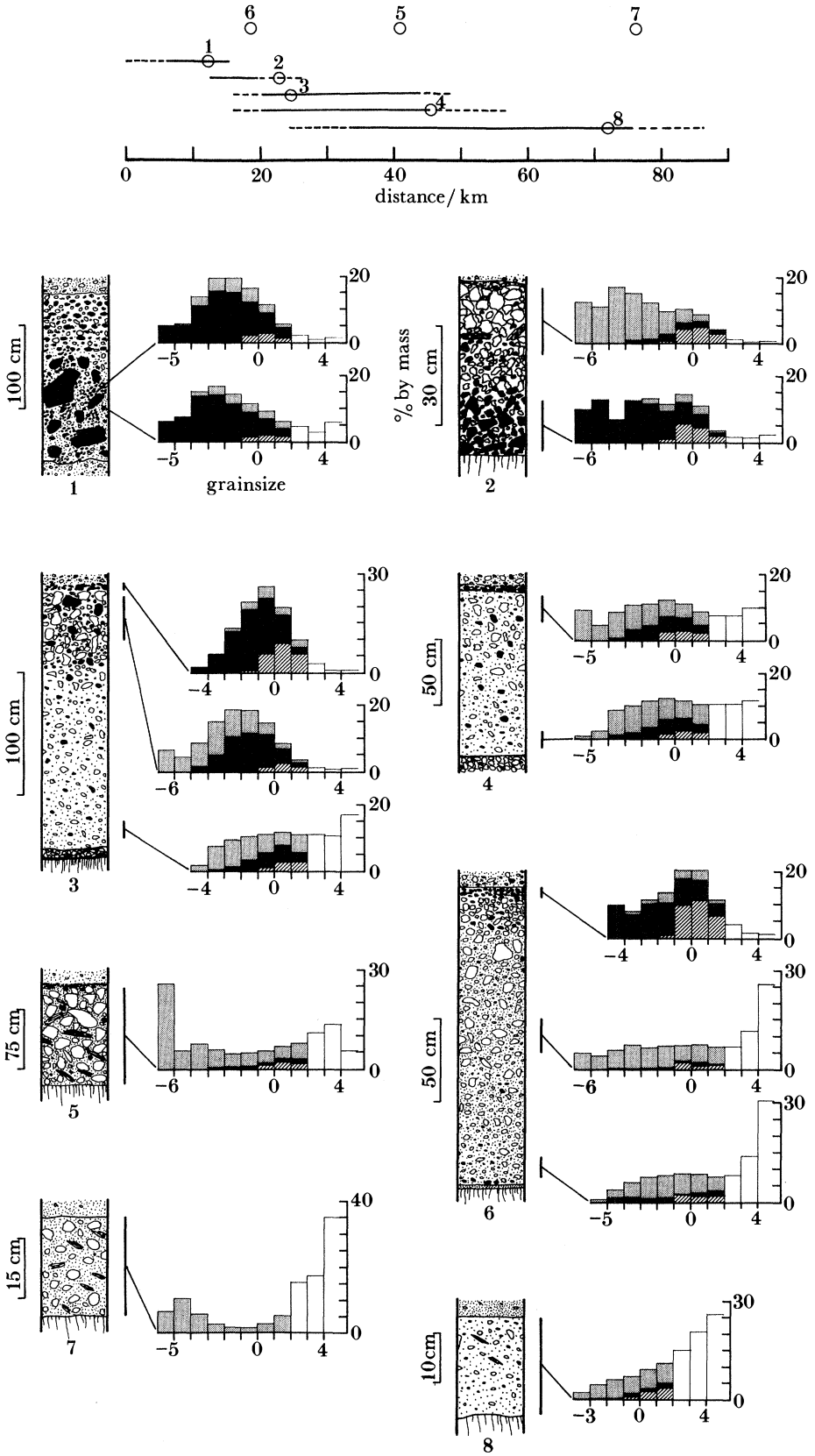

FIGURE 13. For description see opposite.

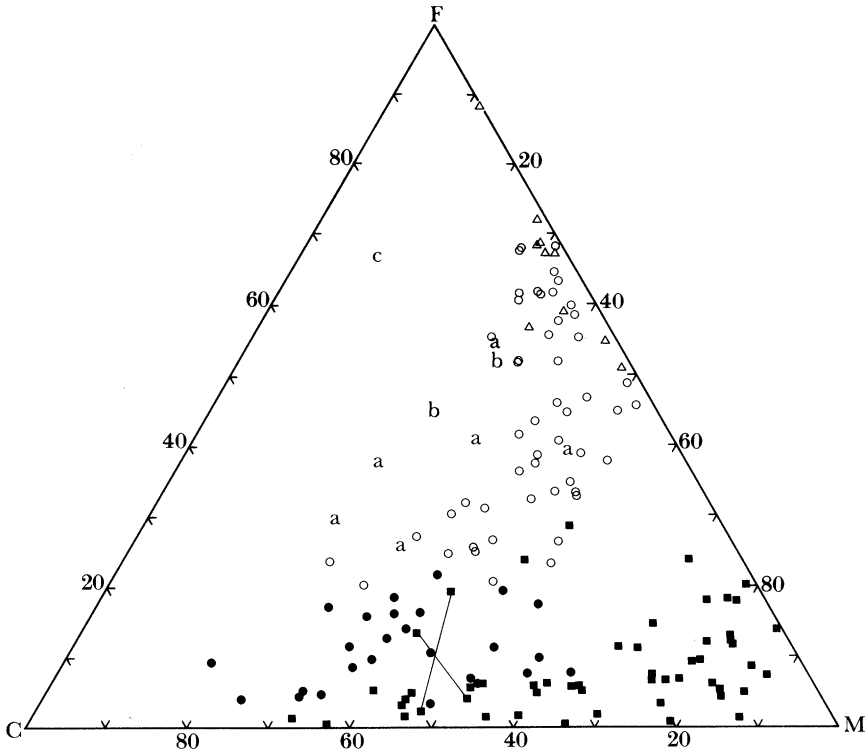

FIGURE 14. A c.m.f. diagram showing the proportions (% by mass) of $\geqslant 4$ mm (C), 2–$\frac{1}{4}$ mm (M) and $\leqslant \frac{1}{8}$ mm (F) material in the layer 1 deposits and distant facies. ●, FDI; ○, layer 1(P), excepting varieties a, b and c, which are denoted by the relevant letter; △, distant facies; ■, layer 1(H). Tie lines connect samples from the fines-bearing and fines-poor 'phases' of the near-vent layer 1(H) matrix (cf. figures 7 and 13).

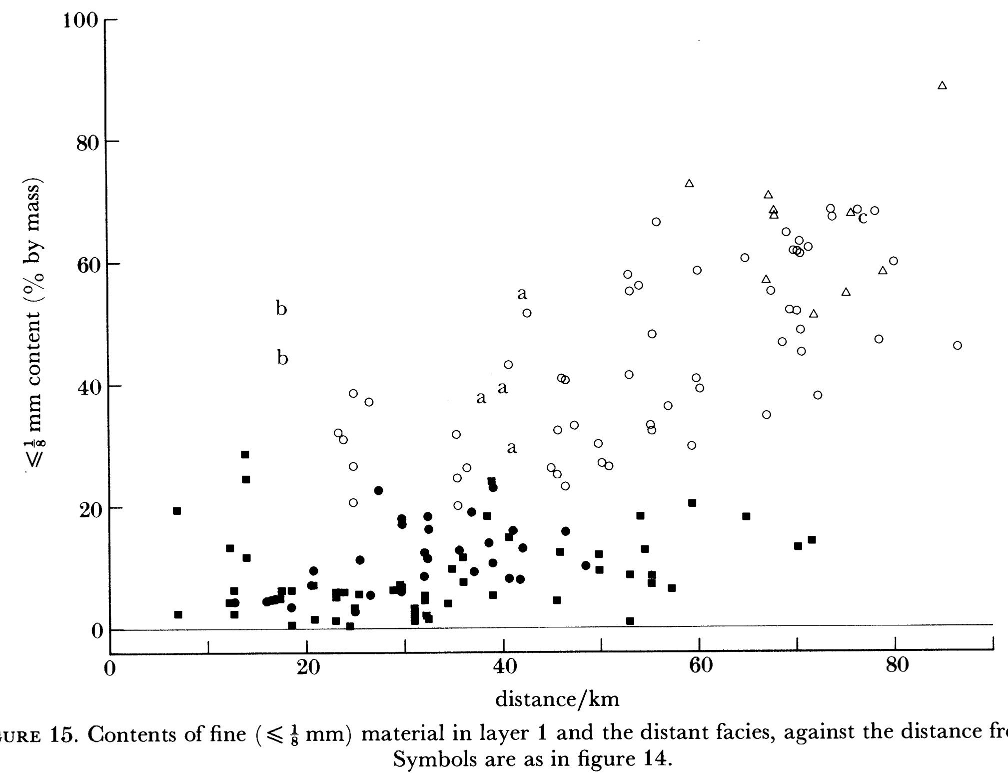

FIGURE 15. Contents of fine ($\leqslant \frac{1}{8}$ mm) material in layer 1 and the distant facies, against the distance from vent. Symbols are as in figure 14.

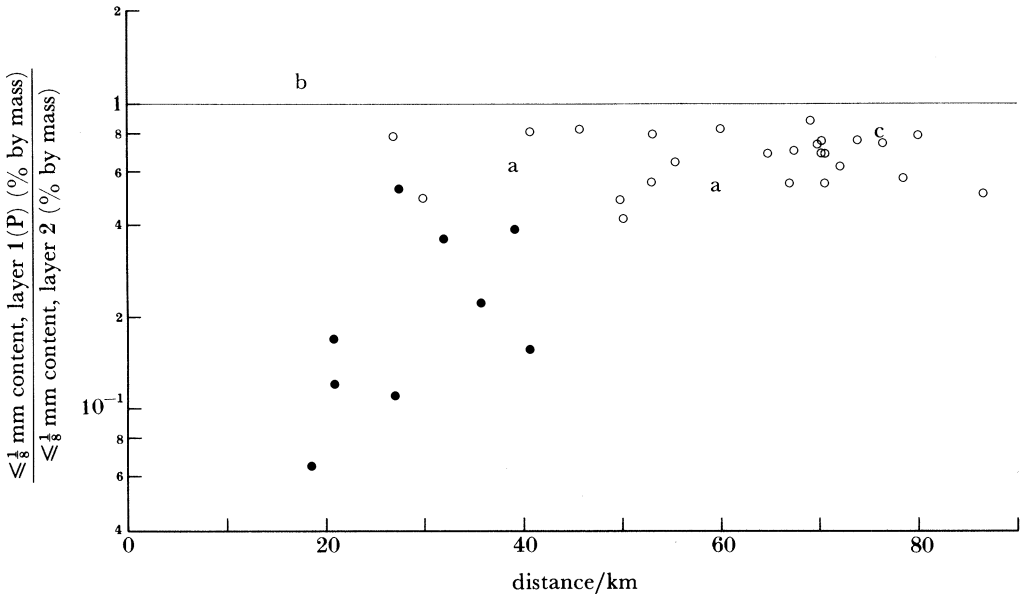

FIGURE 16. Relative contents of fine material in layers 1(P) and 2 at the same locality, against the distance from vent. Symbols are as in figure 14.

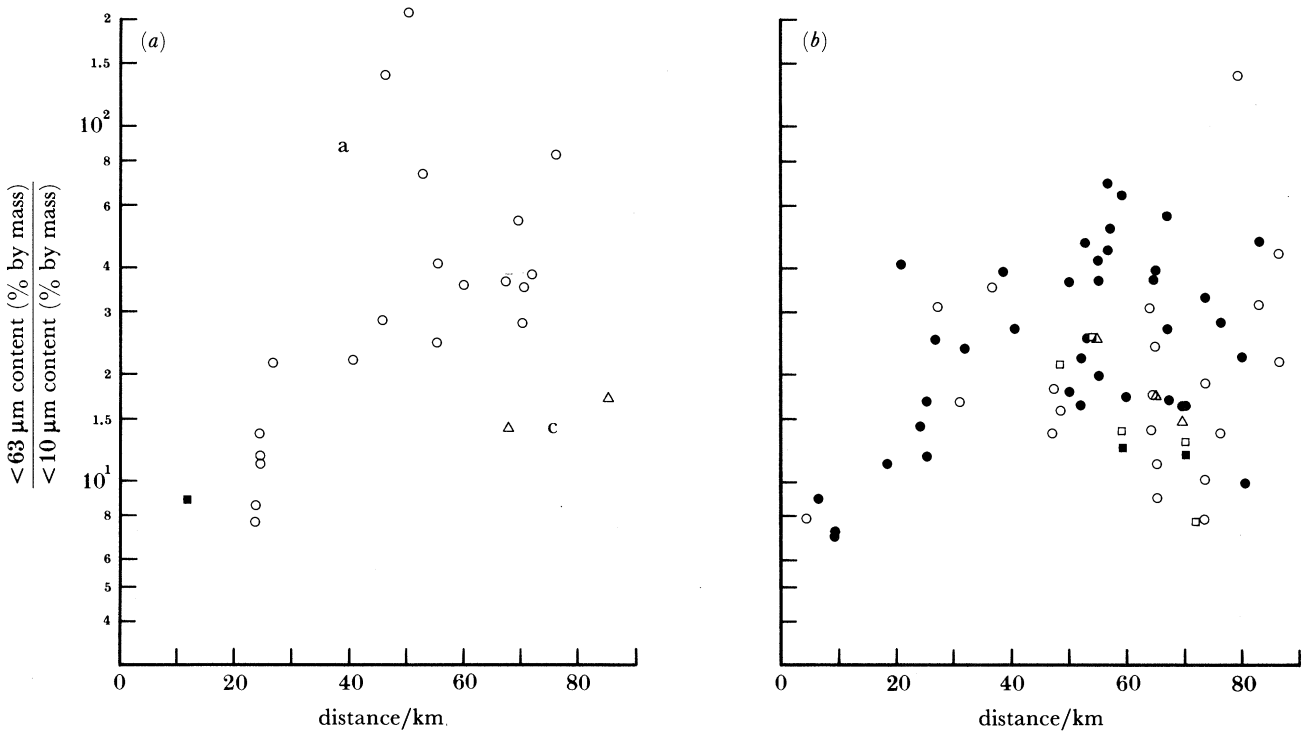

FIGURE 17. Ratios of < 63 μm to < 10 μm contents in (*a*) layer 1 and the distant facies, and (*b*) layer 2, against the distance from vent. Symbols for layer 1 and the distant facies are as in figure 14. Symbols for layer 2 are: ●, veneer deposit; other symbols, valley-ponded ignimbrite, namely ■, layer 2a; ○, layer 2b; □, pumice-concentration zone; △, layer 2c (see §4(*b*)).

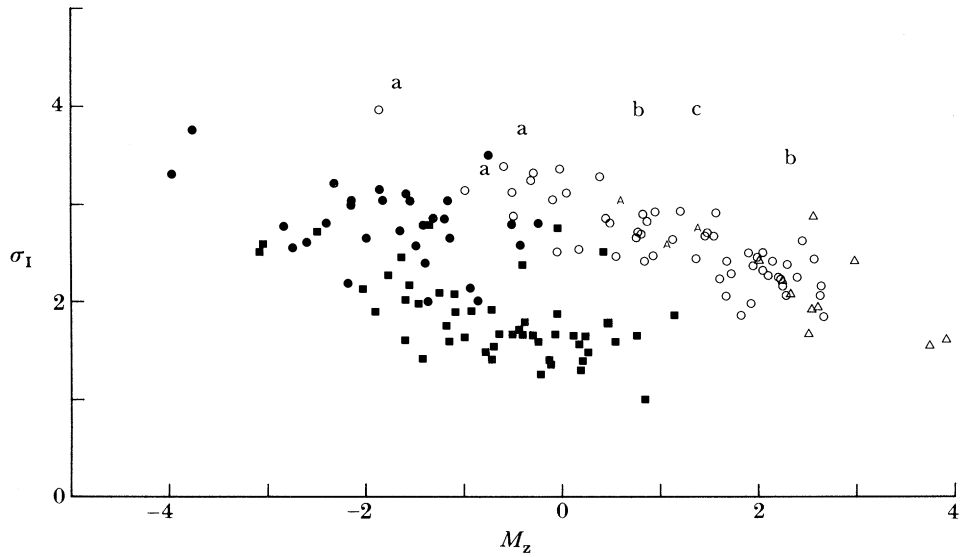

FIGURE 18. M_z against σ_I for layer 1 and the distant facies. Symbols are as in figure 14.

respectively, while variety c is almost pure pumice. The crystal-plus-lithic content of layer 1(P) decreases away from vent, whereas layer 1(H) remains rich in these components (figure 21). With few exceptions (notably varieties b and c), layer 1(P) is enriched in crystals and lithics with respect to layer 2 (figure 22).

All but a few layer 1 samples are crystal-enriched relative to the inferred magmatic content (figure 23). Within layer 1(P), the highest c.c.fs are in FDI and the lowest in variety c. In a plot of c.c.f. against distance from vent, two diverging trends are seen (figure 24); in layer 1(P) c.c.fs decrease outwards, whereas in layer 1(H) they increase, rapidly out to 20–30 km and more slowly thereafter, remaining high even in distal areas. The relative proportions of crystals and lithics show wide variations in layer 1, despite the fact that if their abundances were being controlled by fluidization processes then they would be expected to behave similarly (Wilson 1984). When plotted against the distance from vent (figure 25), the crystal:lithic ratios increase markedly, though with much scatter, especially in layer 1(P).

Pumice bulk-densities tend to be higher in layer 1(H) than in layer 1(P). Plotted against the distance from vent (figure 26), the values decrease in layer 1(P) but remain uniformly high in layer 1(H), both data sets having much scatter.

(*b*) *Layer* 2

(i) *Field relations*

Layer 2 forms most of the exposed ignimbrite (table 1), as two distinctive facies (figure 27), an ignimbrite veneer deposit and the valley-ponded ignimbrite, except on very distal hilly interfluves where the distant facies occurs.

Both layer 2 facies show considerable colour variations. Mostly, both are pale grey to white, or are stained to a pale brown by the distillation products from the pyrolysis of incorporated vegetation. Less commonly, the ignimbrite is pervasively coloured to shades in the sequence pale grey, pale orange, salmon pink, brick red to reddish purple, though only rarely is the sequence taken to completion. Normally, the base and top of layer 2 are pale grey or orange,

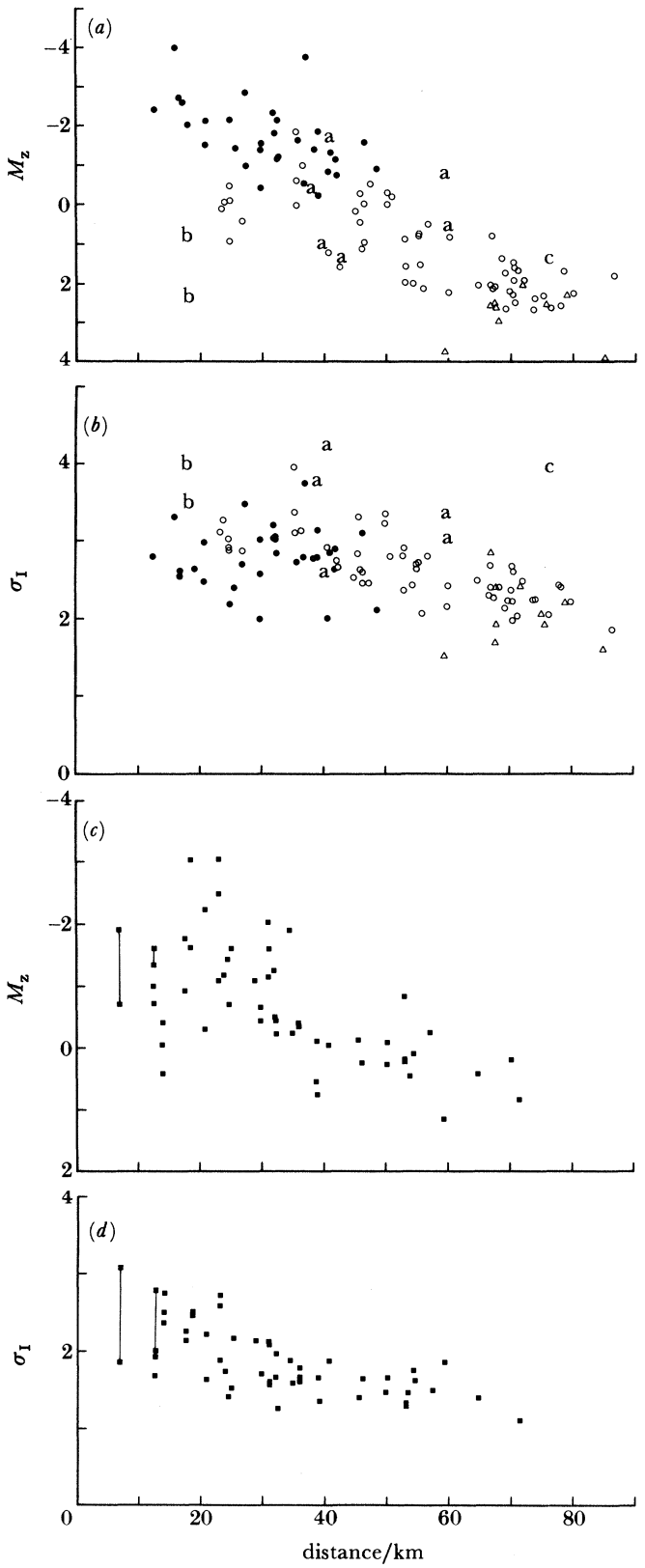

FIGURE 19. M_z and σ_I data for layer 1(P) and the distant facies (*a*), (*b*), and layer 1(H) (*c*), (*d*), against the distance from vent. Symbols are as in figure 14. Tie lines in (*c*) and (*d*) connect samples from the fines-bearing and fines-poor 'phases' in the matrix of the near-vent layer 1(H) (figure 7).

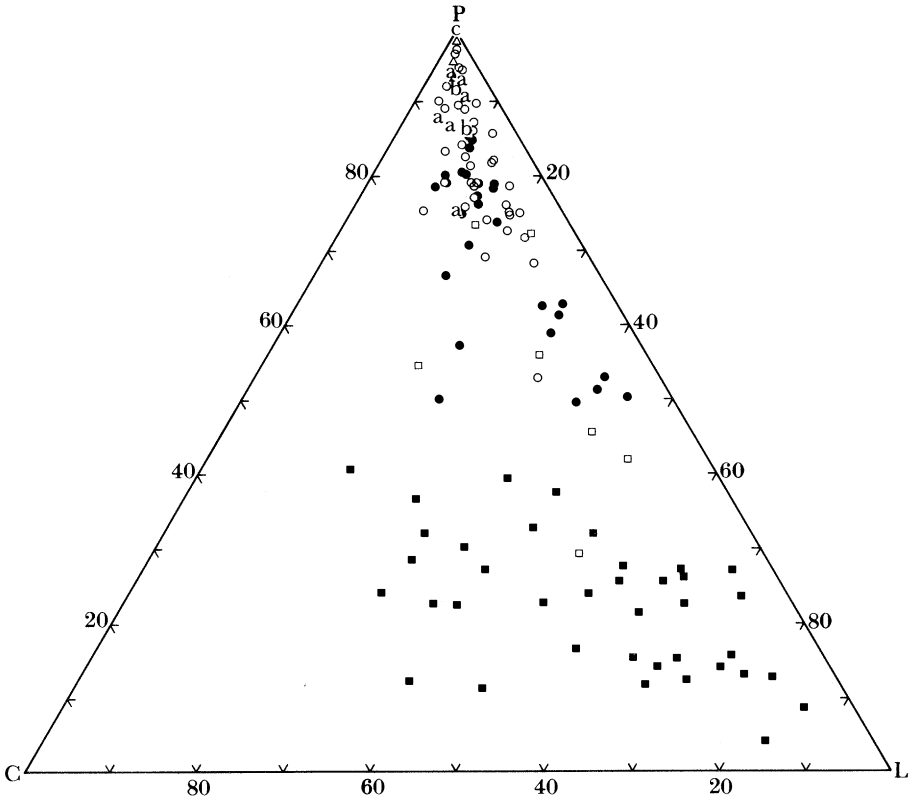

FIGURE 20. A p.c.l. diagram showing the contents (% by mass) of pumice (P), crystals (C) and lithics (L) in layer 1. Symbols are as in figure 14 except that material from the sheared zone between layers 1(P) and 1(H) is denoted by open squares.

and the 'highest' colour is developed in the top third of the layer. These colours are attributed to thermal oxidation. They are well developed only in certain areas of the ignimbrite outcrop (figure 28).

The ignimbrite veneer deposit (IVD). The main features of the IVD are described by Walker *et al.* (1980*b*, 1981*b*); some further aspects of the deposit and additional data are discussed and illustrated here (figure 29, plates 3 and 4). On a gross scale, the IVD is a landscape-mantling layer, but on the single-exposure scale it tends to smooth over the finer details of the underlying surface. Closer to vent, elevations in the underlying surface less than about 10 m apart are poorly reproduced on the upper surface of the deposit because of the preferential erosion of layer 1 over high points and the tendency of the IVD to thicken into hollows, whereas in distal exposures the IVD is usually thin enough to parallel all but the smallest features (less than about 1 m apart) in the underlying surface.

The distribution of the IVD and structures within it are shown in figures 5 and 30. The IVD is often discontinuous beyond 60–65 km from vent except in the north sector, where it persists almost to the outer limits of the ignimbrite. Valley ponds beyond the limits of continuous IVD are often flanked by narrow outcrops of rather thick IVD on the valley sides. Within 60–65 km of vent, the IVD persists to heights of more than 1000 m above vent level, but is often absent from high ground. Its absence there is considered to be due to erosion rather than non-deposition because its laterally equivalent valley-ponded ignimbrite is known from heights of more than

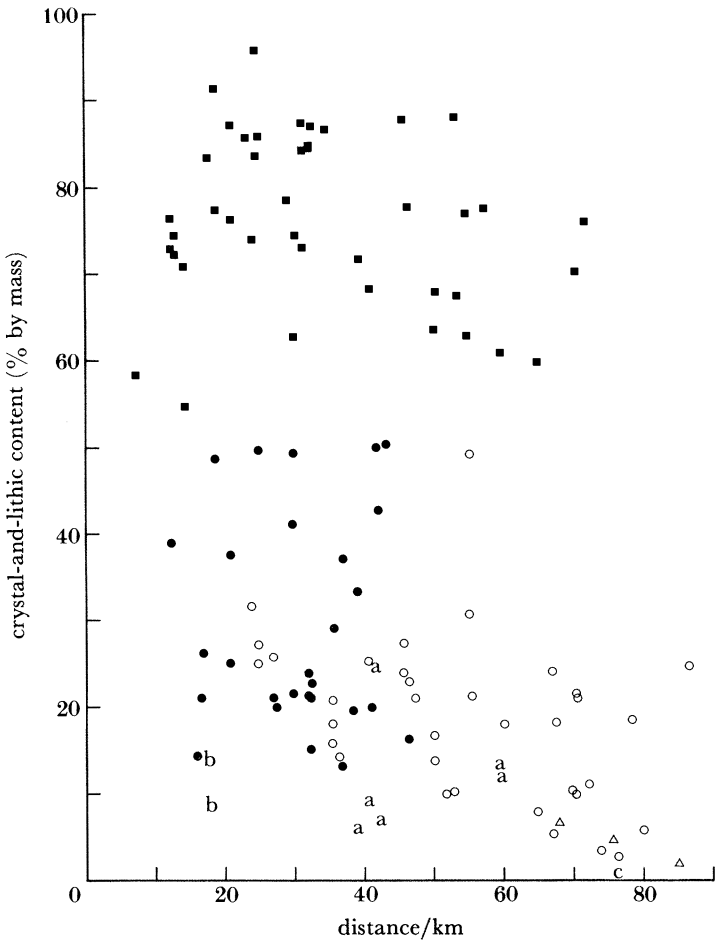

FIGURE 21. Contents of crystals and lithics in layer 1, against the distance from vent. Symbols are as in figure 14.

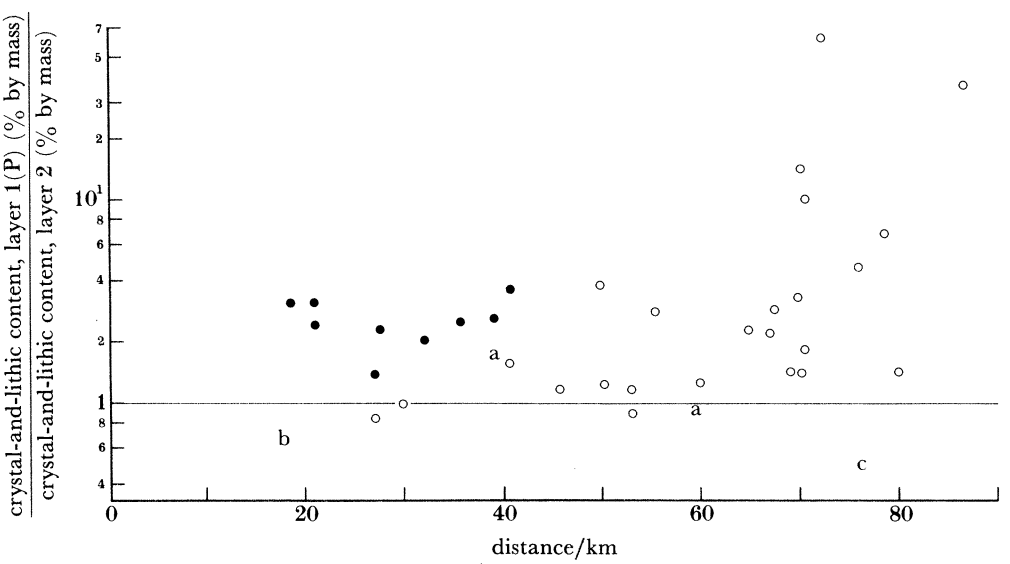

FIGURE 22. Relative contents of crystals and lithics in layers 1(P) and 2 at the same locality, against the distance from vent. Symbols are as in figure 14.

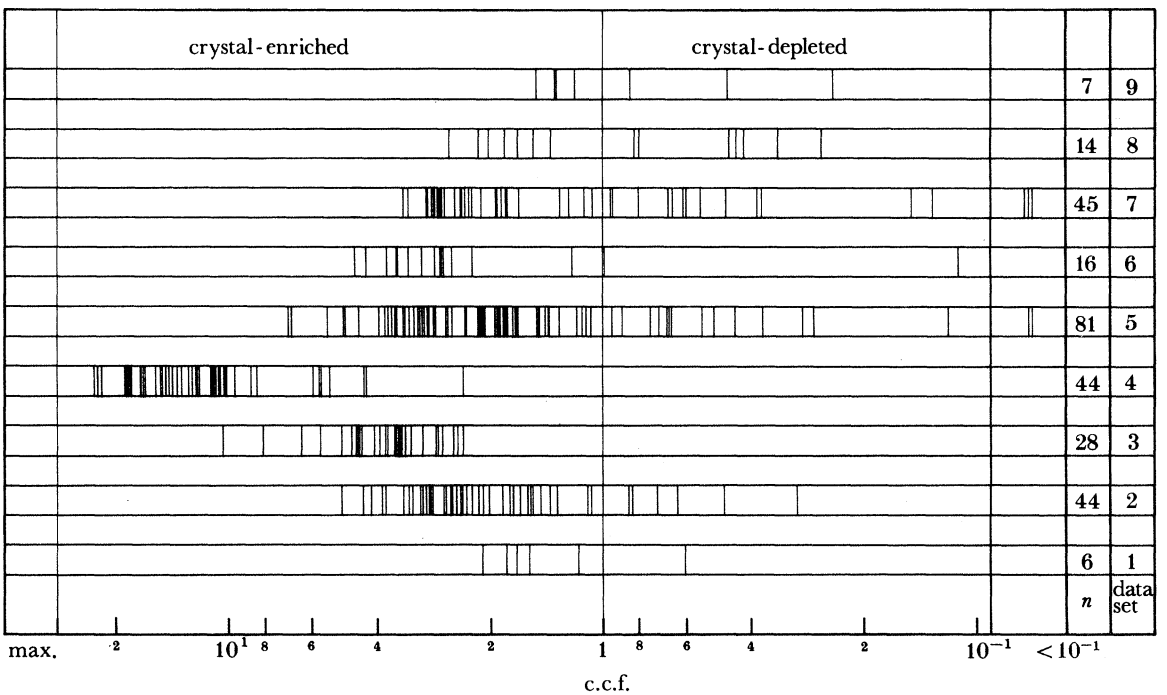

FIGURE 23. C.c.fs for the early ignimbrite flow units (data set 1; see Paper I, §2), and the Taupo ignimbrite; 2, all layer 1(P) varieties, except FDI, plus the distant facies; 3, FDI; 4, layer 1(H); 5, the ignimbrite veneer deposit; 6, layer 2a; 7, layer 2b; 8, the pumice-concentration zone; 9, layer 2c. The maximum c.c.f. is 28.6, which would denote a deposit wholly free of pumice; *n* denotes the number of samples.

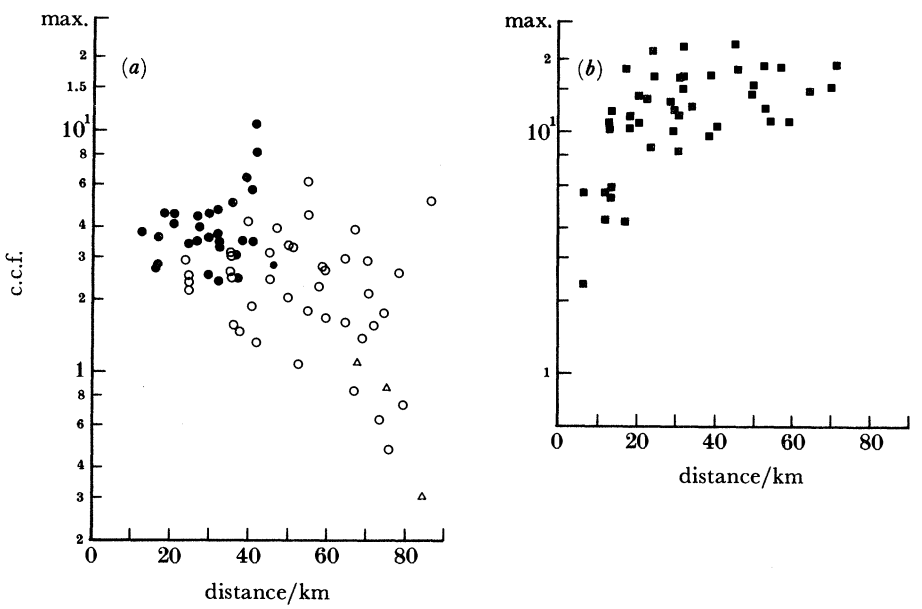

FIGURE 24. C.c.fs for (*a*) layer 1(P) and the distant facies and (*b*) layer 1(H), against the distance from vent. Symbols are as in figure 14, except that varieties a, b and c of layer 1(P) are not separately denoted.

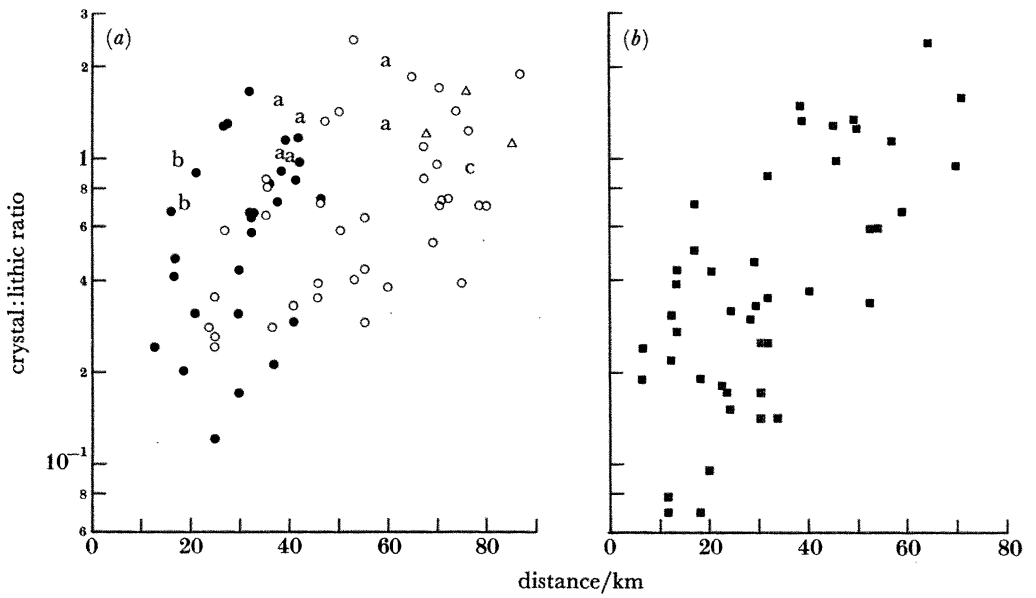

FIGURE 25. Crystal:lithic ratios in (*a*) layer 1(P) and the distant facies and (*b*) layer 1(H), against the distance from vent. Symbols are as in figure 14.

1300 m above vent and from valleys otherwise detached from source (which presumably, as at lower altitudes, were once connected by an IVD to source), and because of the presence previously mentioned of rhyolite lava lithics in the regolith. Because of its fine-grained and loose nature, and the slowness with which vegetation could re-establish itself, the IVD had a poor survival potential.

The IVD often contains fluidization segregation bodies, which within about 40 km of vent occur in five situations:

First, as small (less than about 5 cm across) scattered pods, widespread but never abundant, which tend to occur towards the base of the layer.

Second, where all but a few residual pockets of layer 1 deposits have been eroded off during flow emplacement, small segregation pods sometimes occur immediately above these pockets.

Third, on the upstream side of obstacles, where sub-vertical segregation pipes occasionally appear and increase in abundance upwards.

Fourth, in thick accumulations on the lee-side of obstacles, where sub-vertical pipes are sometimes seen.

Fifth, around and above carbonized vegetation, both as fines-free, crystal- and lithic-rich sheaths around individual carbon fragments and as pipes emanating from them.

Beyond *ca.* 40 km from vent segregation bodies are only found in association with carbonized vegetation. At its most extreme, the IVD locally contains more than 10% by volume carbon and is generally crystal- and lithic-enriched and rather fines-depleted.

A great variety of bedforms and structures are developed in the IVD (figures 5 and 29). Three aspects are considered here:

Compositional layering and zonation. At some exposures less than 25 km from vent, rare flat-lying lithic-rich lenses up to a few metres long and a few tens of centimetres thick are found (figure 29*a*). Larger examples have a pumiceous fines-rich matrix which contains

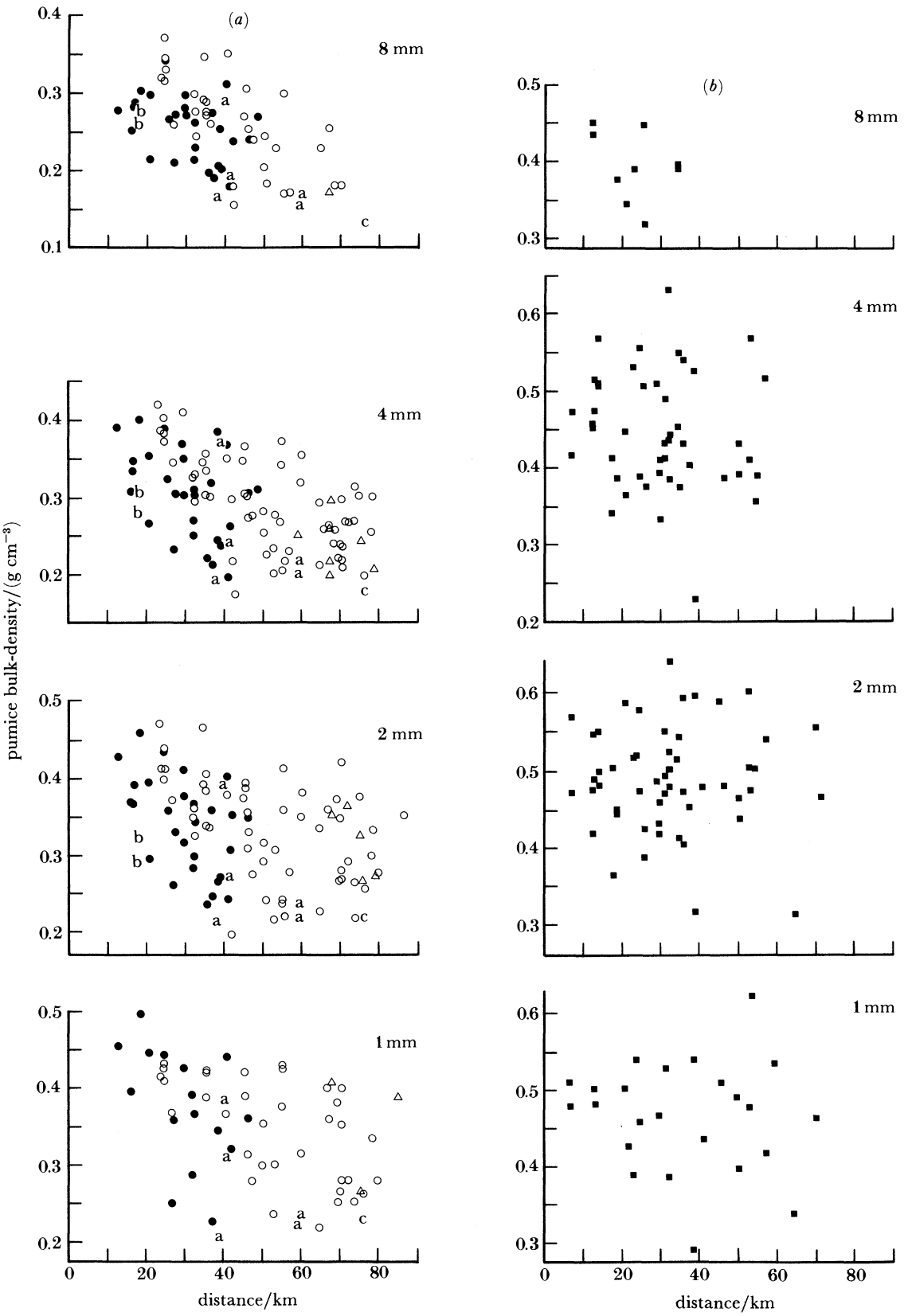

FIGURE 26. Pumice bulk-densities in various size fractions of (*a*) layer 1(P) and the distant facies and (*b*) layer 1(H), against the distance from vent. Symbols are as in figure 14.

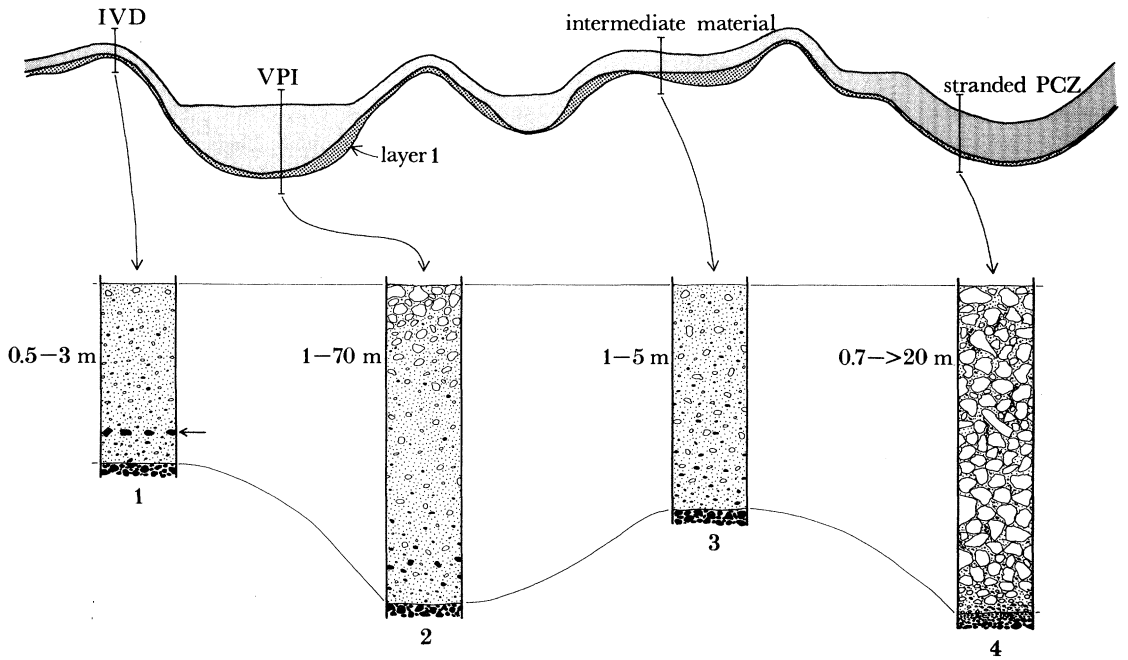

FIGURE 27. Schematic sections illustrating relationships between the ignimbrite veneer deposit (IVD) and valley-ponded ignimbrite (VPI). The sections show (see text for further discussion): 1, typical IVD, showing grainsize stratification, an overall compositional zonation towards a more pumiceous top and a one-clast-thick lithic-concentration zone (arrowed); 2, typical VPI showing poorly defined layer 2a, normal-lithic and reverse-pumice grading (the latter to give a pumice-concentration zone – PCZ); 3, material intermediate between the IVD and VPI found on flat-lying interfluves; 4, stranded PCZ material with a thin layer 2a (see Wilson & Walker 1982, figure 4).

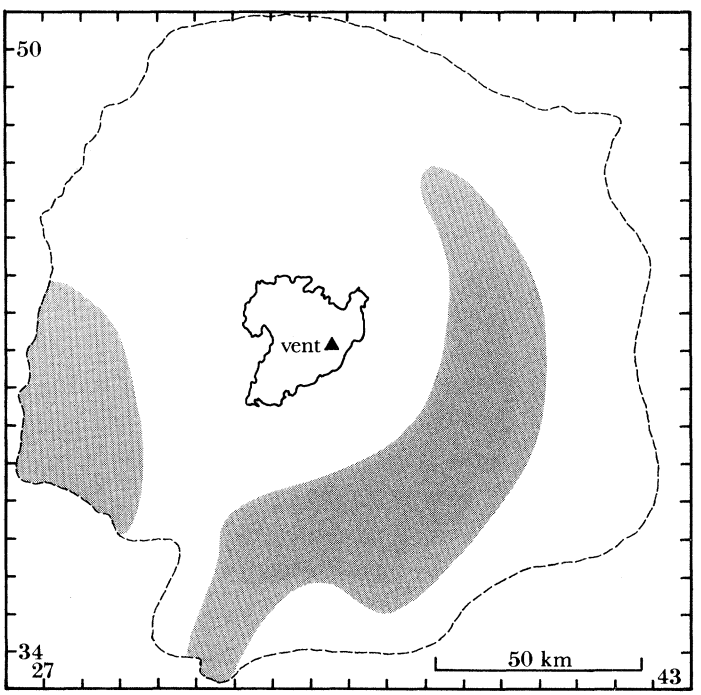

FIGURE 28. Map showing areas (shaded) where thermal alteration colours are best developed in layer 2 deposits.

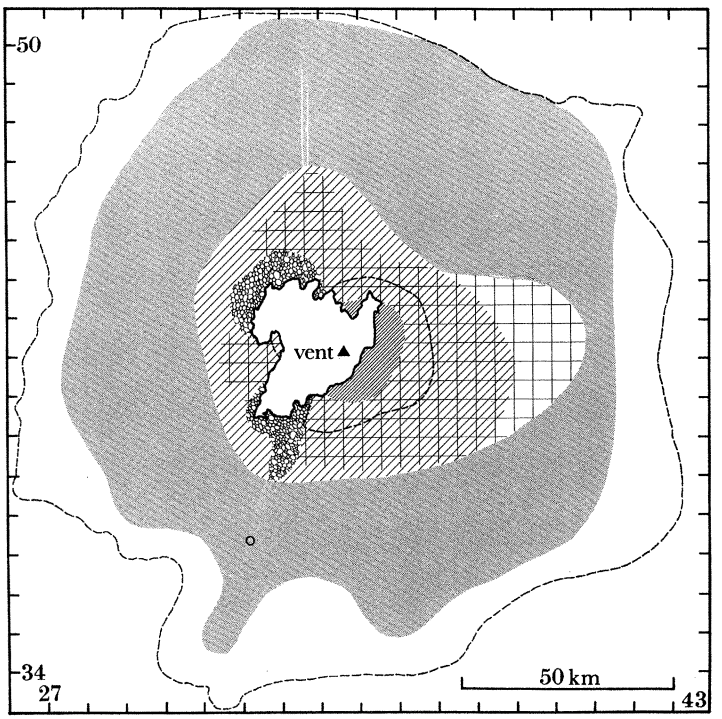

FIGURE 30. Map of the outcrop areas of effectively continuous IVD (shading) and the structures within it. The diagonal hatching denotes where a grainsize stratification occurs; within this area, the dashed line marks the outer limit of the coarser, nearer-vent style (§4 (*b*) (i)) and the denser hatching is where lee-side lenses are absent from the downstream side of obstacles. The cross hatching denotes areas where lee-side lenses are common. The open circle marks an isolated outcrop where the IVD is grainsize stratified (Walker *et al.* 1981*b*, figure 3*c*). The bubble ornamentation denotes where the IVD is vesicular and contains tree moulds (see Paper I, §3).

abundant segregation pods, while smaller examples are single fines-depleted, crystal- and lithic-rich lenses.

At most localities, except some closest (less than 19 km) and furthest from vent (figure 5, data sets 9 and 10), the IVD is compositionally zoned from a lithic-richer base to a pumice-richer top. This zonation occurs in two styles. In the first style, there is a general enrichment in lithics and crystals in the lower parts of the IVD, which is sometimes accompanied by a single-clast-thickness lithic-enrichment zone. This zone occurs 15–55 cm above the base of the IVD and consists of coarse lithics that are usually sheathed in a thin, fines-free coating of crystals and lithics. Where this first style of zonation is well developed, layer 1 is usually absent or poorly developed, and the IVD may directly overlie the pre-ignimbrite deposits with a strongly erosive contact. In the second style, the zonation is only marked by an upward decrease in the visible lithic content, accompanied by an enrichment in crystals and lithics in the basal few centimetres of the IVD (see, for example, Walker *et al.* 1981*b*, figure 8).

The IVD generally becomes finer grained upwards, but occasionally the top few tens of centimetres of the unit contain variable amounts of coarse pumice. Only very rarely does the IVD pass upwards into the valley-ponded ignimbrite (see, for example, Walker *et al.* 1981*b*, figure 3*c*); they are almost always lateral equivalents.

Grainsize stratification. At many localities less than 40 km from vent, plus one at about 50 km (Walker *et al.* 1981*b*, figure 3*c*), the IVD shows some kind of internal layering. Two

kinds are present (figure 29*b*, *c*). The first consists of fluctuations in the coarse pumice content, which produce a stratification obvious even on freshly cut exposures, whereas the second results from subtle fluctuations in the overall grainsize which are only visible on weathered surfaces. The first is seen in sections only out to 25 km from vent, while the second persists to greater distances (figure 30). When both kinds occur together, the first forms fewer but thicker layers (*ca.* 10 cm–1 m), whereas the second comprises more numerous thinner bands (*ca.* 1–10 cm). Individual layers can be traced for tens of metres along an exposure but they cannot be correlated between exposures. The number of layers decreases with the IVD thickness away from vent (figure 31).

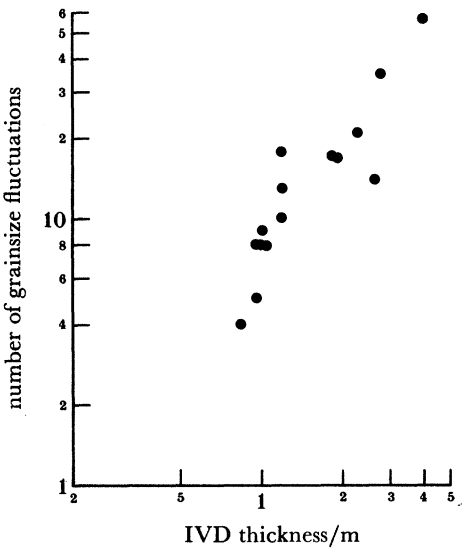

FIGURE 31. Plot of the number of grainsize fluctuations seen in the stratified IVD, against the IVD thickness.

Bedforms: topography-induced. On a local scale, the ignimbrite was emplaced over innumerable small obstacles, which have affected the deposition of material from the flow. The IVD thickness is greater on the upstream and downstream sides and less over the crests of obstacles, thus reducing their expression on the surface of the deposit. On the upstream side, the IVD tends to be coarser and often shows degassing structures, but no bedforms apart from rare internal shear planes. Out to at most about 55 km from vent, the downstream IVD shows a foreset bedding, the style of which varies with distance from vent (figures 29 and 30).

Closest to source (to a maximum of 18 km from vent) the deposition angle of the foreset beds decreases steadily upwards, from the slope angle of the obstacle to a minimum which may be less than 5°. When the obstacle slopes at less than about 10°, the layering in the IVD tends to parallel the underlying ground surface. The foreset beds are defined by the coarser-scale grainsize stratification (see above) and by thin bimodal stringers of typically 3–10 cm pumices in a fines-rich matrix. There is no appreciable grainsize or compositional change in the deposit when passing from the upstream to the downstream side.

At greater distances from vent (*ca.* 12 km to a maximum of 55 km) the foreset beds consist of interbedded finer material and lee-side lenses (Walker *et al.* 1981*b*, figure 6). Where a coarse-scale stratification is present in the IVD, each lee-side lens appears to thin up-vent into and be equivalent to a single coarse-scale layer. With steep-sided obstacles, the deposition angle of the foreset beds decreases upwards until a minimum angle of 10–15° is reached. With more

gently sloping obstacles, the lee-side lenses appear as shallow-dipping (less than 10°) lenses within an IVD that otherwise mantles the surface. The area covered by lee-side lens accumulations can sometimes exceed 10^4 m^2, and the lee-side lenses can evenly mantle the smaller-scale topography in the lee of the major obstacle. In some proximal localities the lee-side lenses contain a few lithics; otherwise they are wholly pumiceous, while the associated IVD is depleted in coarse lithics for a greater distance behind the obstacle than that to which lee-side lenses are observed. In addition, layer 1 deposits tend to be poorly developed or absent below the lee-side accumulations.

Further than 20–50 km from vent, which distance appears to depend on the position about the vent (figure 30), lee-side lenses are very rare.

Bedforms: self-induced. In some near-vent areas, the IVD surface is undulating and appears to form dune-like structures (figure 29*e*), but erosion prevents detailed measurements of their lateral dimensions. At some exposures less than 21 km from vent, bedforms are seen within the IVD even where the flow travelled across level ground. Two styles of bedform are seen, a low-angle (less than 15°) foreset bedding (figure 29*f*) and a complex lensoid bedding, which may occur together (see, for example, Walker *et al.* 1981 *b*, figure 6*a*). The first closely resembles the foreset bedding described above, except that the obstacle involved is merely earlier material deposited by the flow. The second consists of lensoids which are shown in sections normal as well as parallel to the inferred flow direction. Many lensoids may be seen at one exposure, but usually less than five of them overlap at any point.

The self-induced bedforms change in nature away from vent in the same way as the topography-induced bedforms; less than about 14 km from vent, the bedforms are defined by the coarser-scale stratification and bimodal stringers, whereas from 14 to 21 km lee-side lenses may occur.

The valley-ponded ignimbrite (VPI). The VPI forms a flat-topped terrace in nearly all the valleys and depressions out to 70–90 km from vent. Individual valley ponds vary widely in size, from a few square metres to more than 100 km^2, and in thickness from less than 1 m to about 70 m. The top surface of a valley pond is usually planar, rarely gently undulating, and, where unobstructed, it slopes at a similar gradient to the pre-ignimbrite valley. In many places though, constrictions have dammed the flow to form a step-like succession of terraces. Most valley ponds are a single flow unit but some show more than one flow unit, often owing to the subdivision of layer 2b (Wilson *et al.* in prep.) but also because of the presence of layer 2c, which is described for the first time in this paper.

The transition from the VPI into the IVD is marked by several features. First, the sub-horizontal upper surface of the valley pond changes to being sub-parallel to the pre-ignimbrite surface in the IVD. Second, the content and size of visible pumices decrease from the VPI into the IVD, until greater than 5–10 cm pumices are rare in the latter. However, the content and L_m sizes of lithics in the IVD and VPI are very similar. Third, at localities less than 40 km from vent, a grainsize stratification (see earlier) often becomes visible at the margins of the valley pond and improves in definition into the IVD. Where the local slope is less than 5° the IVD-to-VPI transition takes tens to hundreds of metres (and may not reach completion), while where the angle is less than 20° it may occur in less than 2 m. Extensive areas of flat-lying interfluves may be covered by material which drapes the surface like an IVD, but which has VPI grainsize characteristics and passes into a true IVD only on steeper slopes (figure 27).

Layer 2a. In the VPI, a layer 2a is usually but not invariably present and is often poorly defined. It varies from a vague upward increase in maximum clast size to a sharply defined, reversely graded layer from 5 to 100 cm thick. Sometimes there is an overall reverse grading within layer 2 and no separate layer 2a can be defined. Where layer 2a is definable, its basal contact is often erosive and layer 1 is poorly developed or absent.

Layer 2a is rich in fines and contains common lithics similar in size to those in the adjacent IVD. These coarse lithics may sometimes occur as a one-clast-thickness concentration zone like that in the IVD (see above), which is found within layer 2a unlike the lithic-concentration zone sometimes found at the boundary between layers 2a and 2b (Sparks *et al.* 1973; Sparks 1976), which may also be present.

Layer 2b and the pumice concentration zone. Layer 2b usually forms more than 70% of the thickness of the VPI. It is commonly marked by a coarse-tail grading, where large pumices are concentrated at the top and large lithics at the base of layer 2b (Sparks 1976). Sections showing the best-developed coarse-tail grading (flow types 2 and 3 of Wilson (1980)) are found from 15 to 60 km from vent (figure 5), while many VPI sections less than 20 km and more than 55 km from vent show no coarse-tail grading (flow type 1 of Wilson (1980)). In the proximal type 1 sections, a separate layer 2a cannot be defined, and the maximum clast sizes increase into the valley pond over distances of several metres from the sides as well as the base of the deposit.

In layer 2b, an upward enrichment in large pumices is often spectacular, whereas a corresponding downward enrichment in large lithics is much less well developed. In some cases it is possible to infer from the presence of distinctive local lithologies that the coarse lithics concentrated at the base of layer 2b were derived by erosion from layer 1. The upward enrichment in pumice ranges from a vaguely defined increase in the largest pumice sizes to a sharply defined pumice-concentration zone (PCZ) resting on a fine grained layer 2b (figure 32*a*, plate 5). The PCZ contains the coarsest pumices in the ignimbrite (figure 32*b*), set in a fine-grained matrix, which in some cases is almost purely pumiceous. The coarse pumices are usually just matrix supported, but in some cases the coarser blocks are in contact. In some areas where the topography is very irregular, the PCZ forms most of the thickness of layer 2 (figure 32*c*; Wilson & Walker 1982, figure 4). These thick PCZ outcrops sometimes occur adjacent to other valley ponds which are markedly finer grained and which lack any strong upward pumice enrichment.

At the top of layer 2b and occasionally also at the top of individual locally generated flow units within layer 2b, elongate flat-lying bodies and lenses sometimes occur (figure 33, plate 6). These are up to about 1 m thick and typically 2–3 m, occasionally up to 10 m, in length. Their three-dimensional form is uncertain. They consist of a matrix-absent assemblage of coarse, light, very well rounded pumices, with no accompanying crystals, lithics or carbon. These bodies resemble the lee-side lenses in the IVD, but occur on the sub-horizontal top of the deposit, remote from obstructions, and clearly have a different origin. Similar features are seen above individual flow units in the pyroclastic flow deposits generated in the 1980 eruptions of Mount St Helens (author's unpublished data).

Layer 2c. At many localities, a deposit, termed layer 2c (figure 34, plate 6), overlies layer 2b, with an intervening discontinuity of some kind, this layer being present in addition to the several flow units sometimes seen within layer 2b (Wilson *et al.* 1985). This is treated as part of layer 2 and yet not the same as layer 2b for four reasons. First, layer 2c presents a marked

grainsize or compositional contrast, or both, to layer 2b. Second, its outcrop is distinctive; it is absent from hilly interfluves and only occurs above or marginal to the VPI (figure 35). Third, it forms isolated outcrops within valleys and is hence inferred to represent a locally generated, as opposed to vent-generated, unit. Fourth, the presence of heat-alteration colours, mentioned earlier, and the absence of reworking between this unit and the underlying material show that layer 2c is a primary deposit and not a secondary mudflow.

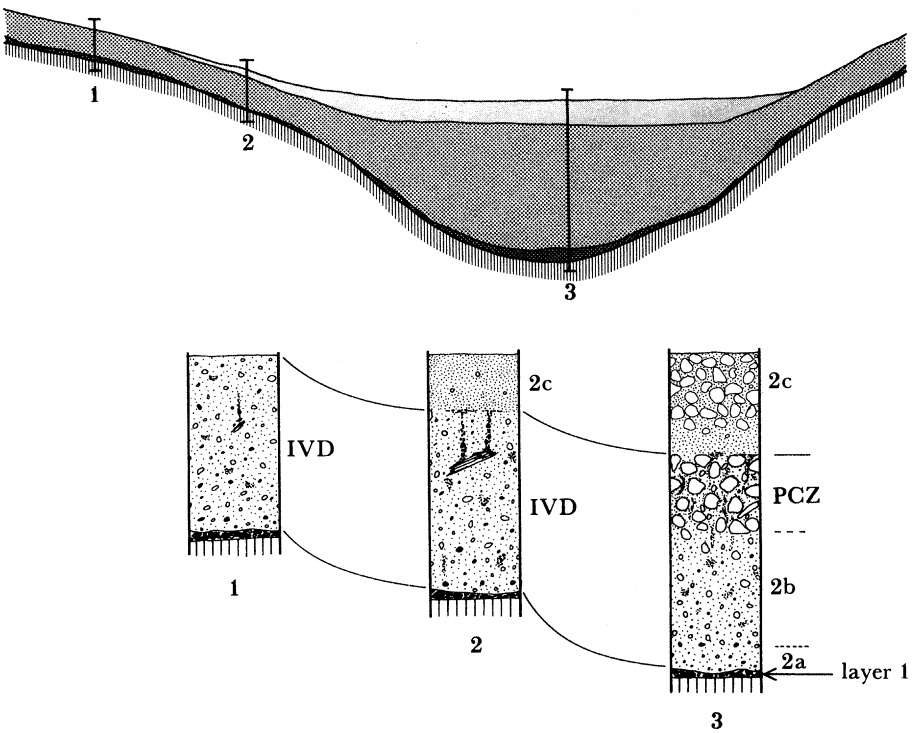

FIGURE 35. Schematic sections showing the outcrop nature of layer 2c, which is usually absent from above the IVD (section 1) and present only above the VPI (section 3), but may be present above gently sloping IVD outcrops immediately adjacent to valley ponds (section 2).

Layer 2c appears in two varieties, one fine grained and the other strongly bimodal with coarse, exceedingly light and very well-rounded pumices in a fine-grained matrix. Field evidence shows that the only difference between these varieties is the presence of the coarse-pumice mode and they interchange laterally. Both are rich in fines and pumice, visible crystals and lithics being very scarce. Occasionally a discontinuous, crystal- and lithic-rich, fines-poor layer underlies layer 2c, consisting of the sheared-out tops of segregation pipes in the underlying material.

Segregation bodies in the VPI. Segregation bodies are common in the VPI with two exceptions. First, they are completely absent from the near-vent type 1 sections. Second, in layer 2c and in the VPI more than 60 km from vent, segregation bodies almost always seem to emanate from carbonized vegetation or to have been generated by secondary gas sources. Pockets of fines-depleted material are common, locally abundant, at the base of layer 2a, and some of them are identical in appearance to the underlying layer 1(H). Within layer 2b, the presence of segregation bodies defines the type 3 sections (Wilson 1980), often accompanied by a sharply demarcated PCZ. Segregation pipes and pods are common within the PCZ matrix,

while most of the coarser pumices are sheathed in a thin, fines-free layer of crystals and lithics. Segregation structures associated with carbonized vegetation occur throughout the VPI, ranging from small pods to pipes which are up to 50 cm wide and tens of metres long. In some areas, the local carbon content may exceed 10% by volume, and patches of the VPI may become fines-depleted. The carbon fragments themselves are usually sheathed in a fines-free, crystal-and lithic-rich coating.

(ii) *Field data*

The IVD thickness decreases away from vent along moderately well defined trends (figure 36*a*). Assuming that the average thickness of the IVD is one half of the maximum at any given distance (figure 36*a*) and that the IVD covers the entire land area out to 60 km and half the area from 60 to 80 km from vent, neglecting material less than 14 km from vent and allowing 2000 km^2 for the area occupied by the valley ponds, yield a volume of 8.5 km^3. The extra thickness of IVD material on flat-lying interfluves would increase this to about 10 km^3.

The VPI is usually five to fifty times as thick as the adjacent IVD and it shows no systematic thickness variation away from vent (figure 36*b*). In any given valley, the thickness of the ignimbrite pond depends on a variety of factors, which are discussed in Wilson & Walker (1982). The volume of the VPI is difficult to assess, owing to the great number and range in size of the ponds. Assuming, from field observations, that the valley ponds cover 2000 km^2 and have an average depth of 5–10 m, gives their volume as 10–20 km^3; 15 km^3 is chosen in table 1 as a best estimate.

The IVD and VPI L_m sizes decrease away from vent at roughly similar rates (figure 37). The differences between the two are not considered significant and largely reflect the erosion of coarser lithics from layer 1. The combined L_m data are plotted on a map in figure 38. Rather low L_m values occur in the areas around Lake Taupo, and individual isopleths extend furthest to the east, as in layer 1 (figure 11).

The IVD P_m sizes decrease steadily away from vent, whereas the VPI P_m sizes remain uniform or increase slightly outwards to about 40 km, but then decrease, particularly beyond 60 km from vent (figure 39). Within the VPI, the smallest P_m sizes are in layer 2a, and the largest in the PCZ and the coarse-pumice bearing layer 2c. The P_m data for layers 2b and 2c are plotted on a map in figure 40. Note that there are only minor differences in P_m sizes between the nearest-vent IVD and VPI (figure 39), that the largest pumices are found in a broad band about 40 km from vent and that they are unevenly distributed about the vent (figure 40).

(iii) *Laboratory data*

The IVD and VPI form two overlapping data sets on a c.m.f. plot (figure 41). Apart from the nearest-vent material, most IVD samples contain less than 10% by mass coarse material, whereas many VPI samples are rich in coarse material, either lithics (layer 2a) or pumice (layers 2b and 2c). In the field, the PCZ at the top of layer 2b is noticeably bimodal, and the presence or absence of a separate coarse-pumice mode is used here as an arbitrary divider between PCZ and layer 2b samples, respectively; both together constitute layer 2b in the Sparks *et al.* (1973) layering scheme. The IVD and VPI share similar contents of fines, amounts in the latter being slightly lower owing to the presence of appreciable amounts of coarse material. With increasing distance from vent (figure 42), the IVD becomes gradually fines-richer, with

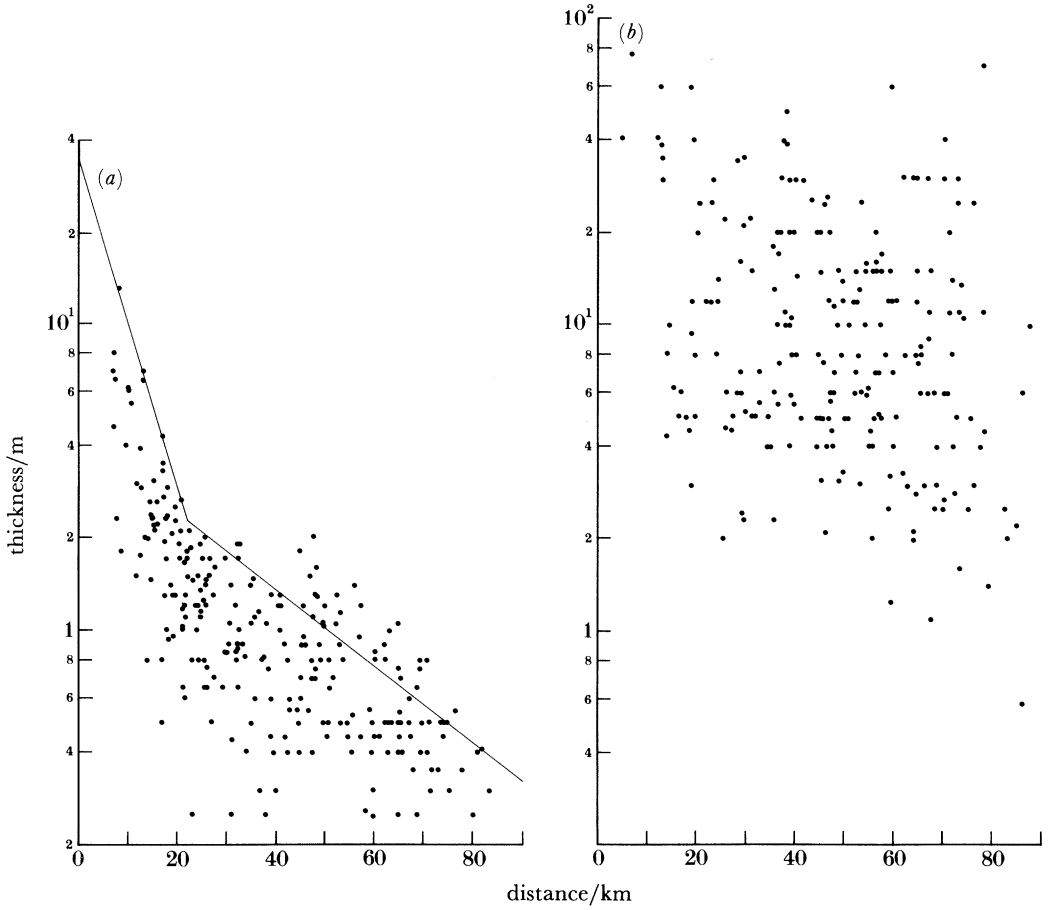

FIGURE 36. Thicknesses of (*a*) the IVD and (*b*) the VPI, against the distance from vent. Lines on the IVD data are hand-fitted maximum-thickness trends (unusually thick IVD sections which are found on flat-lying interfluves are ignored) given by:

$$\text{distances} < 22 \text{ km, thickness} = 34 \exp(-0.124D);$$
$$\text{distances} \geqslant 22 \text{ km, thickness} = 4.3 \exp(-0.029D),$$

where the thickness is in metres.

a poorly defined inflexion at 55–60 km, while layer 2b has an even content of fines out to about 55 km, which then jumps sharply by up to 30% by mass. The < 63 μm contents of both facies show similar changes with distance from vent (figure 43), decreasing slightly out to about 20 km, remaining steady to 50–60 km and thereafter rising. Pipette-analysis data are plotted in figure 17. Both layer 2 facies behave similarly, having low (< 63 μm)/(< 10 μm) ratios near vent, which then rise outwards as far as 40 km and thereafter vary greatly, sometimes reaching values similar to those found near vent.

The M_z and σ_I data form two overlapping sets (figure 44), although the IVD has a slightly smaller range of M_z values. The M_z data show complex variations with distance (figure 45*a*). Closest to vent, M_z is similar in both facies but thereafter differs; in the IVD it decreases out to *ca.* 20 km, remains steady from 20 km to 50–60 km and thereafter declines gradually. In the VPI, layer 2a shows M_z values which vary, with the amount of coarse lithic material incorporated from layer 1, between those of the IVD and layer 2b. Layer 2b has rather uniform M_z values out to 55–60 km, which then suddenly decrease by *ca.* 2ϕ and thereafter decline in

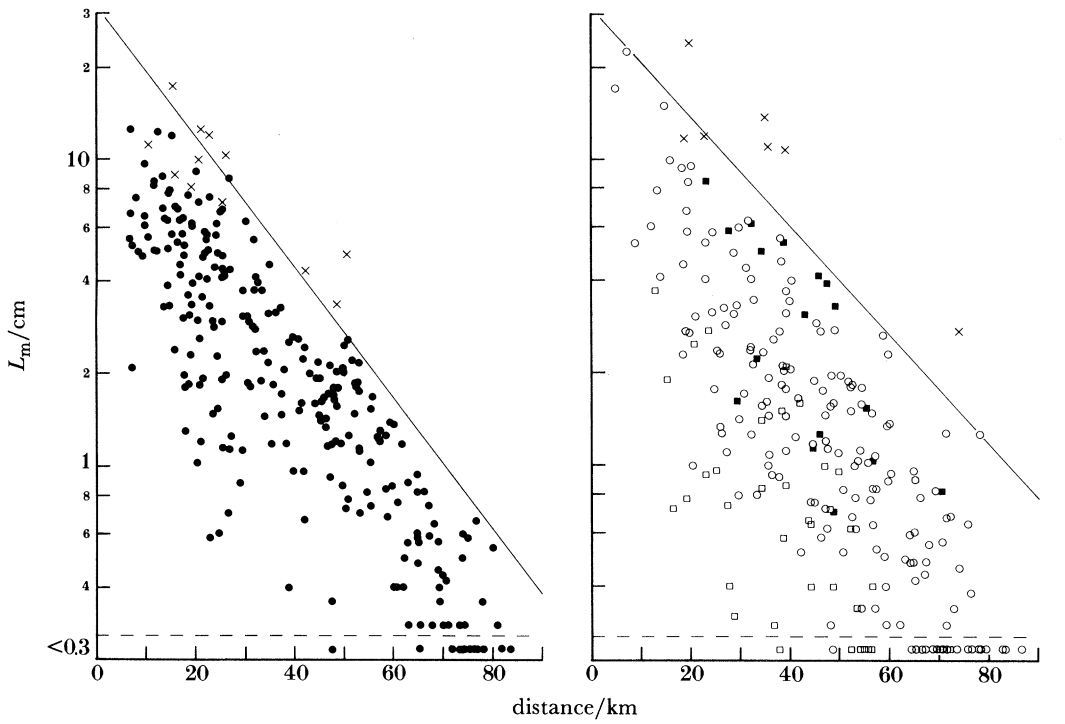

FIGURE 37. L_m sizes in (*a*) the IVD and (*b*) the VPI, against the distance from vent. ●, IVD; ■, layer 2a; ○, layer 2b; □, PCZ, and ×, IVD or layer 2a where coarse lithics appear to have been derived by erosion from layer 1. Lines are hand-fitted maxima (excluding data plotted as crosses) defined by:

$$\text{IVD: } L_m = 31 \exp(-0.050D);$$
$$\text{VPI: } L_m = 31 \exp(-0.041D),$$

where L_m is in centimetres.

parallel with the IVD. The finer variant of layer 2c is finer than layer 2b at less than 60 km from vent, but is very similar in more distal areas. The relationships and changes seen in σ_I are essentially identical to those for M_z (figure 45*b*); again, σ_I is similar in both layer 2 facies nearest to vent, and σ_I in layer 2b drops sharply at 55–60 km from vent.

The compositions of the layer 2 facies are essentially identical (figure 46), but plotted against the distance from vent a more complex pattern emerges (figure 47). In the IVD and layer 2a the crystal-plus-lithic contents rise to a broad maximum at 30–50 km and decline thereafter. Layer 2b shows uniform crystal-plus-lithic contents from very near vent (where they are similar to those in the IVD) out to 55–60 km where they drop abruptly by about a factor of three. The PCZ and layer 2c have uniformly lower crystal-plus-lithic contents at a given distance from vent than the rest of layer 2b. Differences in composition between the IVD and VPI are minor and non-systematic (figure 48*a*) and, in comparison with the compositional variations within the VPI itself (figure 48*b*), are not considered to be significant.

The c.c.f. values within layer 2 show great variations (figure 23), but the IVD and VPI cover similar ranges. The highest values in the IVD are at localities where carbonized vegetation is particularly abundant, and in the VPI in layer 2a (in some cases demonstrably a result of the incorporation of layer 1 material). The c.c.f. data for both layer 2 facies show identical trends with distance from vent (figure 49), rising from values of 1–2 nearest vent, to broad maxima between 30 and 50 km, and declining very steeply beyond 60 km. Crystal:lithic ratios in both layer 2 facies increase away from vent (figure 50) but with much scatter.

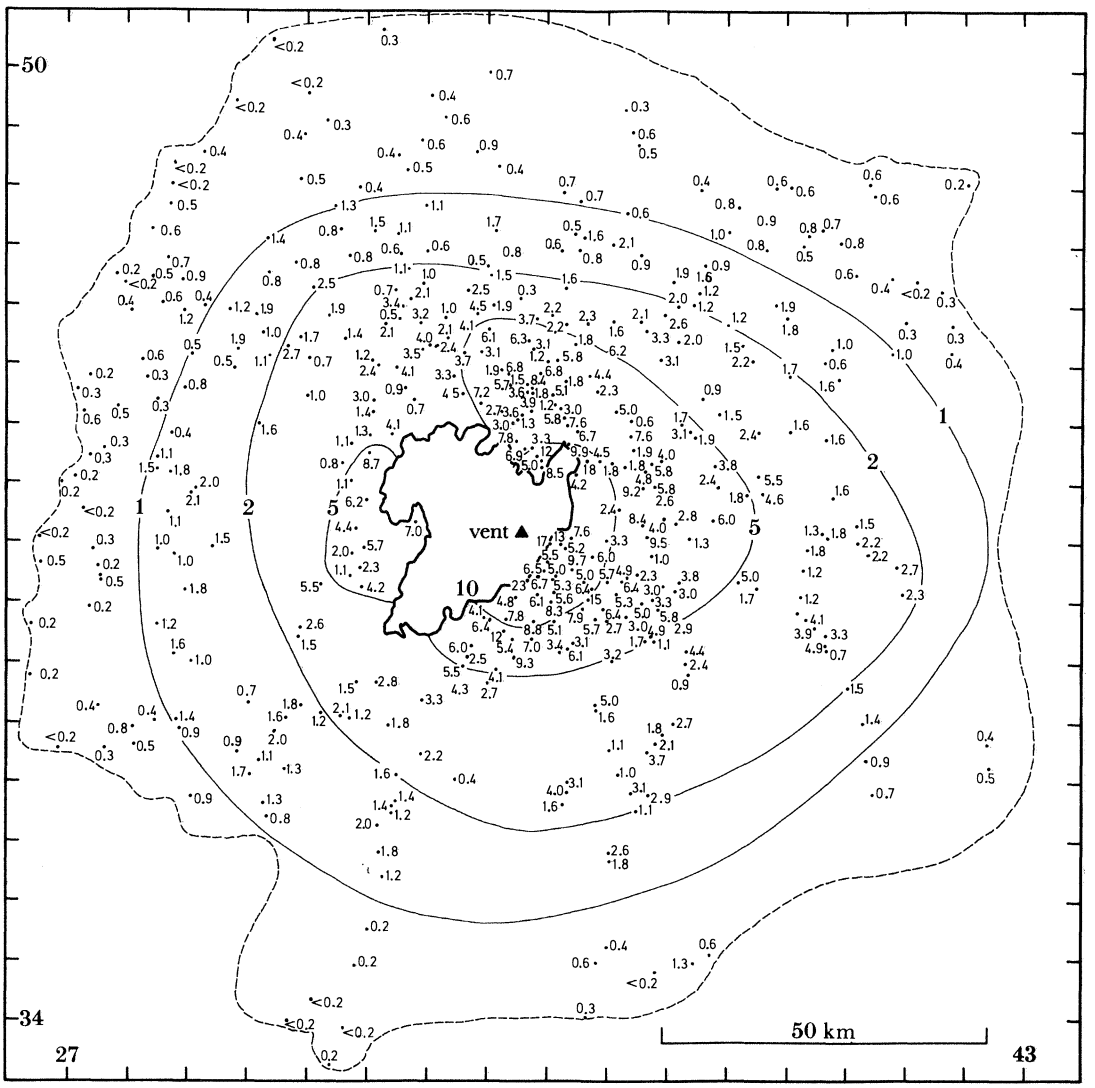

FIGURE 38. Map of the combined L_m data from layer 2. Values and isopleths are in centimetres.

Pumice bulk densities in layer 2 generally decrease away from vent (figure 51) but show great variations. Any systematic differences between pumice densities in the IVD and VPI are obscured by variations within each facies.

(*c*) *The distant facies*

The distant facies (figure 52, plate 7) replaces and is the lateral equivalent of both layer 1 and 2 on hilly interfluves in the outermost areas of the ignimbrite. It is occasionally found on hills rising a few hundred metres or more above the general landscape within, but near the outer margin of, the outcrop of 'normal' layer 1/layer 2-bearing ignimbrite. In the field, the distance facies grades from a coarser base, which contains pumices and lithics of a size appropriate to layer 1(P) and segregation bodies in a fines-rich matrix, to a much finer-grained, fines- and pumice-rich top. The base and top of the layer closely resemble layer 1(P) and the IVD as seen nearer to vent, but in this case there is no intervening discontinuity or layer 1(H).

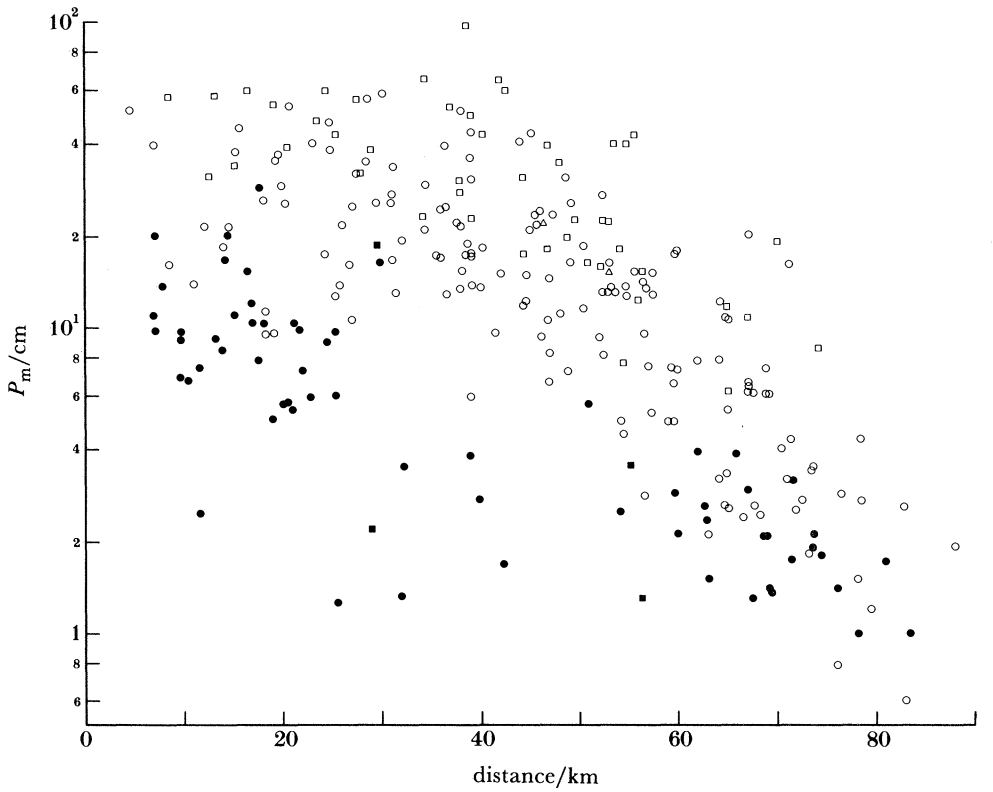

FIGURE 39. P_m sizes in layer 2, against the distance from vent: ●, IVD; ■, layer 2a; ○, layer 2b; □, PCZ; △, layer 2c (data only collected from the coarse-pumice-rich variety).

The distant facies is the same or of slightly greater thickness than layer 1(P) at a given distance from vent (figure 8) and has very similar L_m and P_m sizes (figures 9 and 12). It is slightly finer than most of layer 1(P) (figure 14) and has lower (< 63 μm)/(< 10 μm) ratios (figure 17). The M_z, σ_I and c.c.f. values and crystal:lithic ratios plot as extensions of the layer 1(P) data (figures 18, 19, 23, 24 and 25) and are different from those in the IVD. However, the crystal-plus-lithic contents of the distant facies (figures 20 and 21) are more like those of the IVD. Pumice bulk-density data are inconclusive (figure 26).

(*d*) *Layer* 3

Layer 3 is only very rarely seen above the ignimbrite in areas where the deposit was buried almost immediately after emplacement by, for example, mudflows or local faulting for the poor preservation of layer 3 has two obvious causes. First, much of the dilute cloud of the Taupo flow was swept eastwards and now forms a fine ash overlying the Taupo plinian pumice in areas beyond the limits of the ignimbrite (Paper I). Second, being the topmost layer of the eruption products, layer 3 would have been the first material to be eroded or altered to soil. Material of similar characteristics to a layer 3 ash infills clastic dykes in the ignimbrite (Paper I). All samples from buried layer 3 deposits overlying the ignimbrite and the clastic dykes are fine grained (M_z finer than $+3.5\phi$) and pumice rich (more than 97% by mass) (Wilson 1981).

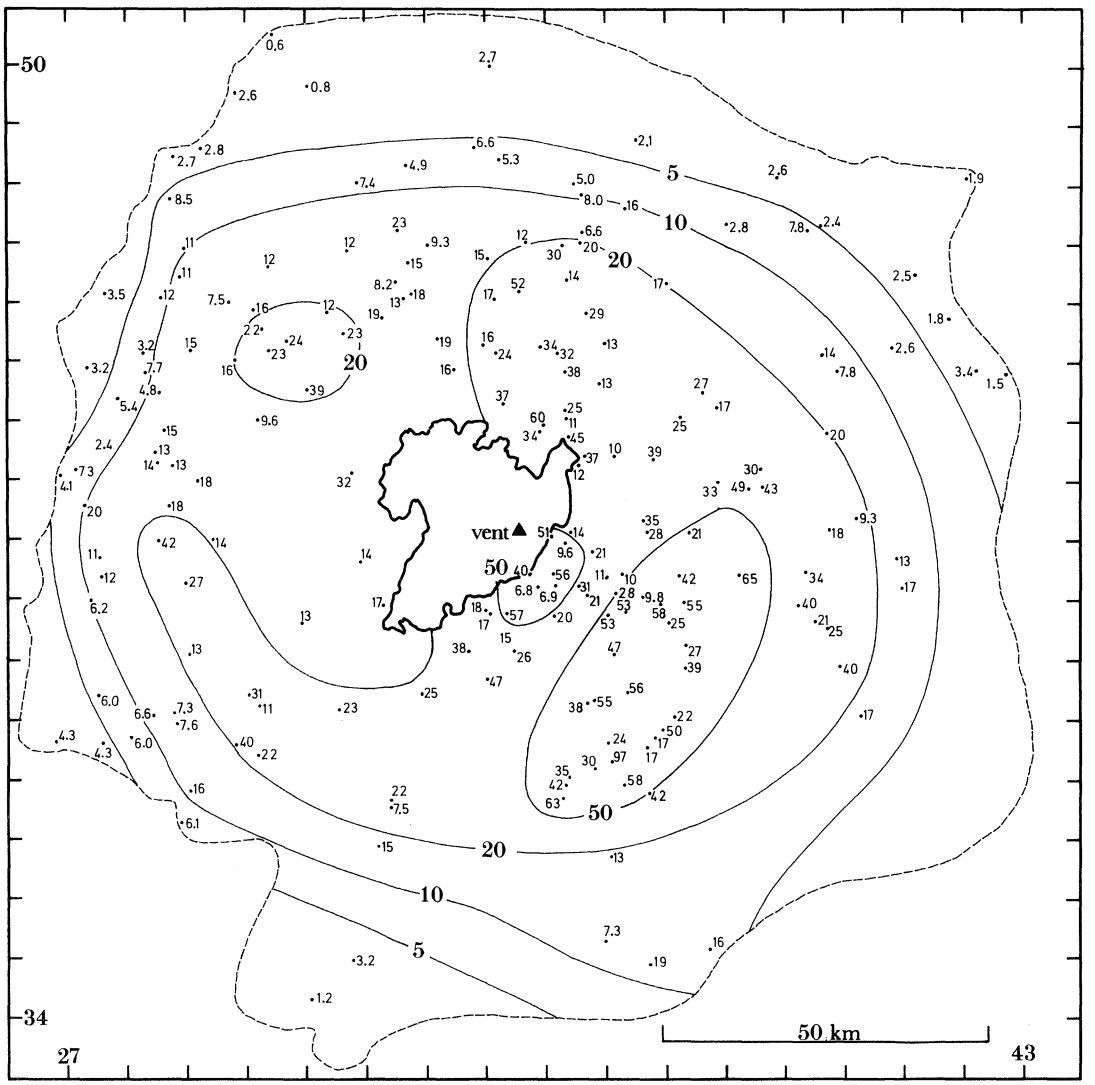

FIGURE 40. Map of the P_m data from layers 2b (including the PCZ) and 2c. Values and isopleths are in centimetres.

5. ORIGINS OF THE FACIES

With some exceptions, the origins of the facies are discussed in other papers and only summarized here, but particular aspects are detailed here.

(*a*) *Layer* 1

(i) *Layer* 1(*P*): *the jetted deposits*

Layer 1(P) is interpreted as material that was thrown forwards from the flow head by the explosive expansion of air ingested by the flow and is termed the jetted deposits (Wilson & Walker 1982). It is thought that a flow travelling at high speeds (figure 2) would ingest large quantities of air (see, for example, Wilson 1980), and that mixing with the hot, fines-rich turbulent flow would have resulted in the explosively violent expansion of this air. The jetted deposits are thought then to represent masses of the flow head which were flung off by the explosive air expansion and which travelled far enough in advance of the flow to be deposited

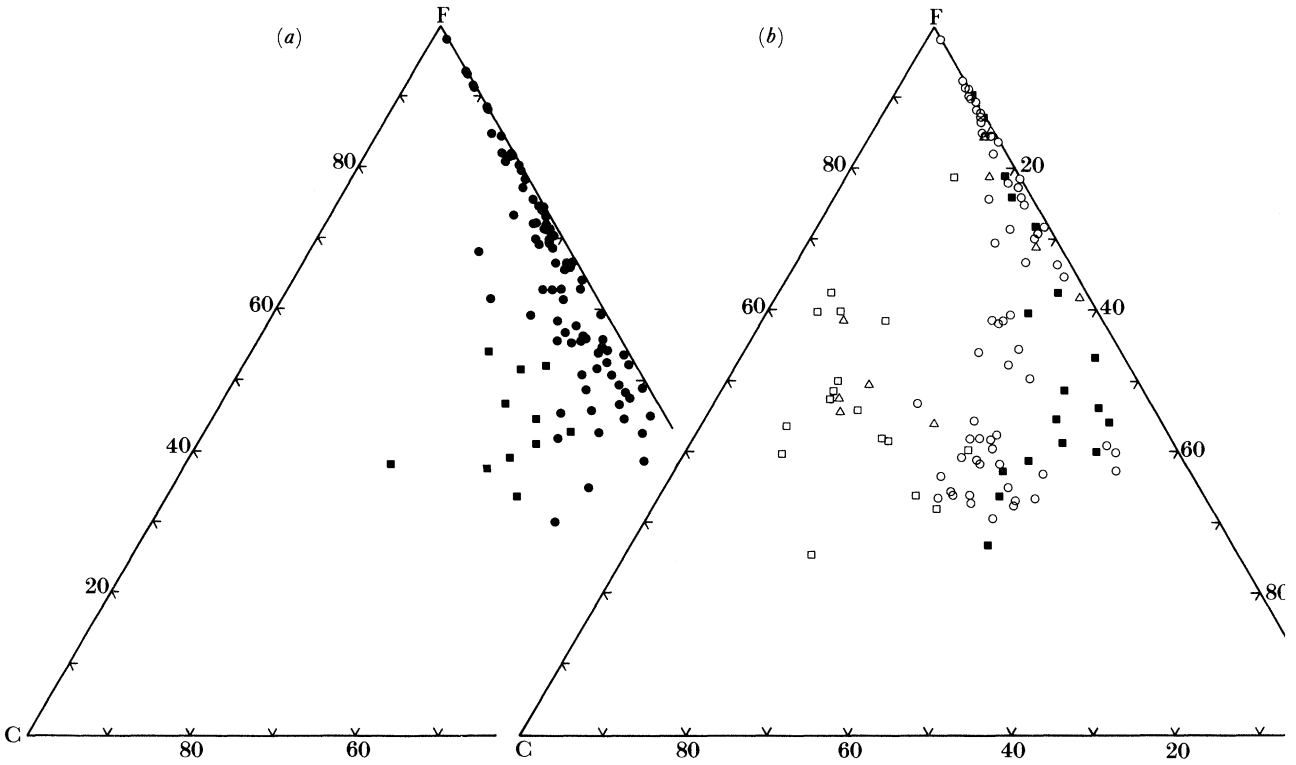

FIGURE 41. A c.m.f. diagram summarizing grainsize data from (*a*) the IVD and (*b*) the VPI. Symbols are as in figure 39, except that in part (*a*) samples from the nearest-vent (< 14 km) IVD are separately denoted by ■.

before being caught up by the rest of the flow. The varying degrees of fines depletion (figure 16) and crystal-plus-lithic enrichment (figure 22) seen in the jetted deposits are interpreted as the results of two fluidization events. The first of these is thought to have occurred within and in front of the flow head as the jetted material was ejected from the flow front and the second as the jetted material interacted with vegetation on the ground surface while coming to rest, but before burial by the rest of the flow. The absence of FDI from an area east of vent where the vegetation was buried by earlier airfall deposits suggests that the strongest fluidization was represented by the second of these two events (figure 53) (Walker *et al.* 1980*a*).

Varieties a, b and c are interpreted thus. From its outcrop area, variety a represents material that was jetted from the most energetic portion of the flow, which climbed the highest mountains. Its overall grainsize distribution resembles that of the layer 2 PCZ (see figures 14 and 41) and its composition that of the more distal jetted deposits; the significance of this is discussed later §8(*b*).

Variety b is though, from its carbon-free and vesicular nature to have been emplaced in a cold, wet state. This variety is interpreted to be the material jetted as the flow met remnants of the pre-eruption Lake Taupo (Paper I, §3). The marked fine mode in this unit (figures 13, 15 and 16) is interpreted to represent material generated by quenching.

Variety c has characteristics indistinguishable from those of distal layer 2b PCZ samples, and is thus interpreted to represent the same material. Note that some FDI samples also appear to have been derived from PCZ material at the top of the Taupo flow (Walker *et al.* 1980*a*). It is uncertain whether variety c was jetted from or merely 'caterpillar-tracked' over the flow

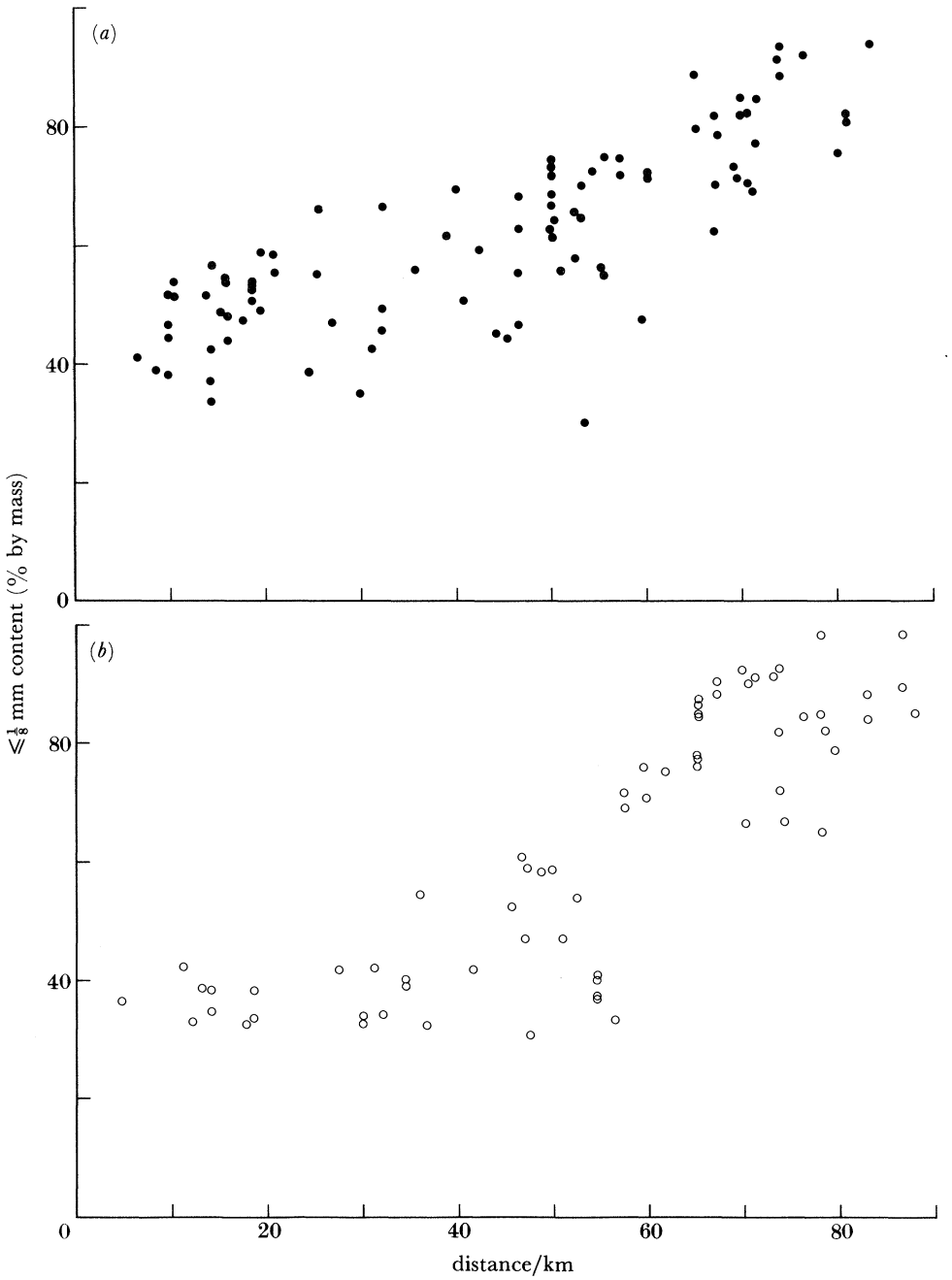

FIGURE 42. Contents of $\leqslant \frac{1}{8}$ mm fines in (*a*) the IVD and (*b*) layer 2b, against the distance from vent. In part (*b*), data from layers 2a, 2c and the PCZ are omitted owing to their fluctuation with local shearing and fluidization effects.

front; regardless of which mechanism operated, no detectable fines losses or crystal-plus-lithic enrichment occurred. Material identical to variety c occurs in at least two late Pleistocene ignimbrites in New Zealand and in an ignimbrite in the Miocene–Pliocene Deschutes Formation in central Oregon (author's unpublished data), and similar material is reported from the Bandelier Tuffs, New Mexico (J. V. Wright, personal communication) and the Cape Riva

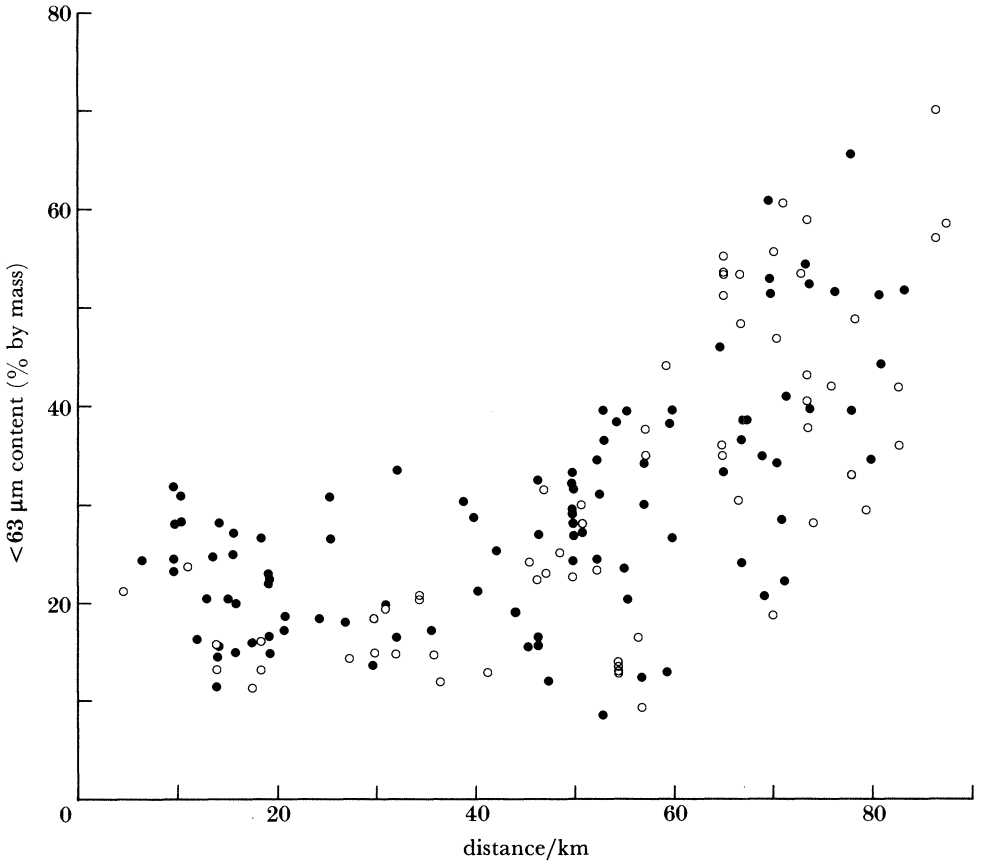

FIGURE 43. Contents of < 63 μm material in the IVD (●) and layer 2b (○) against the distance from vent. Data from layers 2a, 2c and the PCZ are omitted owing to their fluctuation with local shearing and fluidization effects.

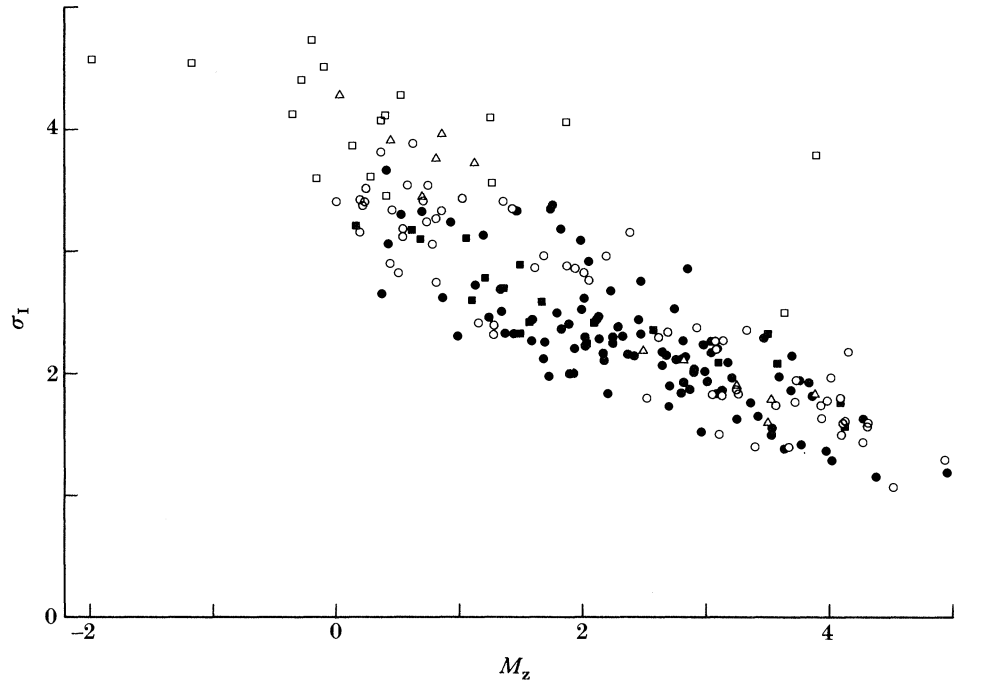

FIGURE 44. M_z against σ_I for layer 2. Symbols are as in figure 39.

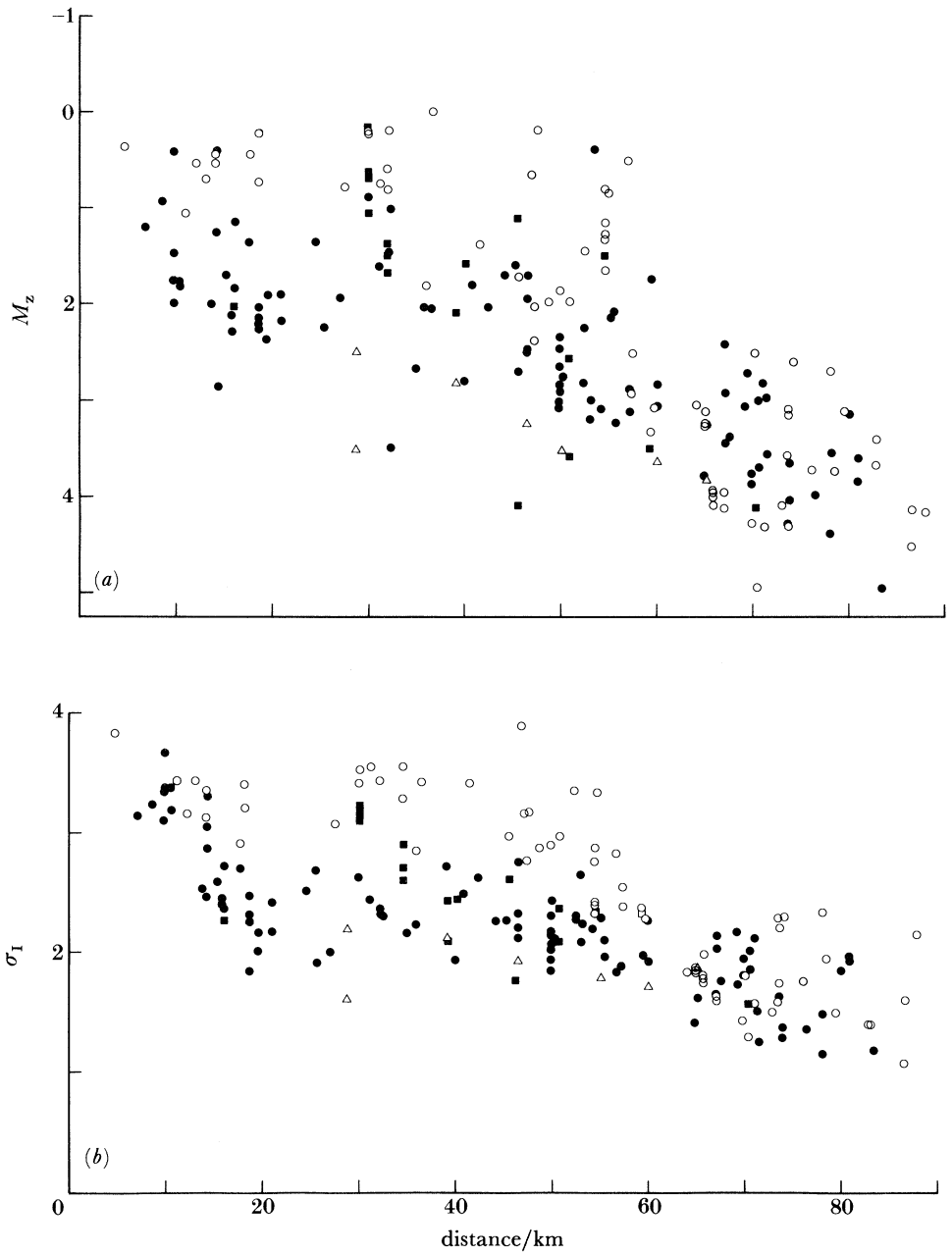

FIGURE 45. Variation of (*a*) M_z and (*b*) σ_I in layer 2 with distance from vent. Symbols are as in figure 39, but data from the PCZ and the coarse-pumice-rich variety of layer 2c are omitted, as M_z and σ_I these vary non-systematically owing to pumice floatation effects.

ignimbrite, Santorini (R. S. J. Sparks, personal communication). The stratigraphic position and composition of variety c (having a lower crystal-plus-lithic content and pumice bulk-density than the bulk of layer 2b, in contrast to other jetted deposits, and being strongly bimodal) make it distinctive and it may prove to be common. Although grouped here with the jetted deposits, its mode of origin requires further study.

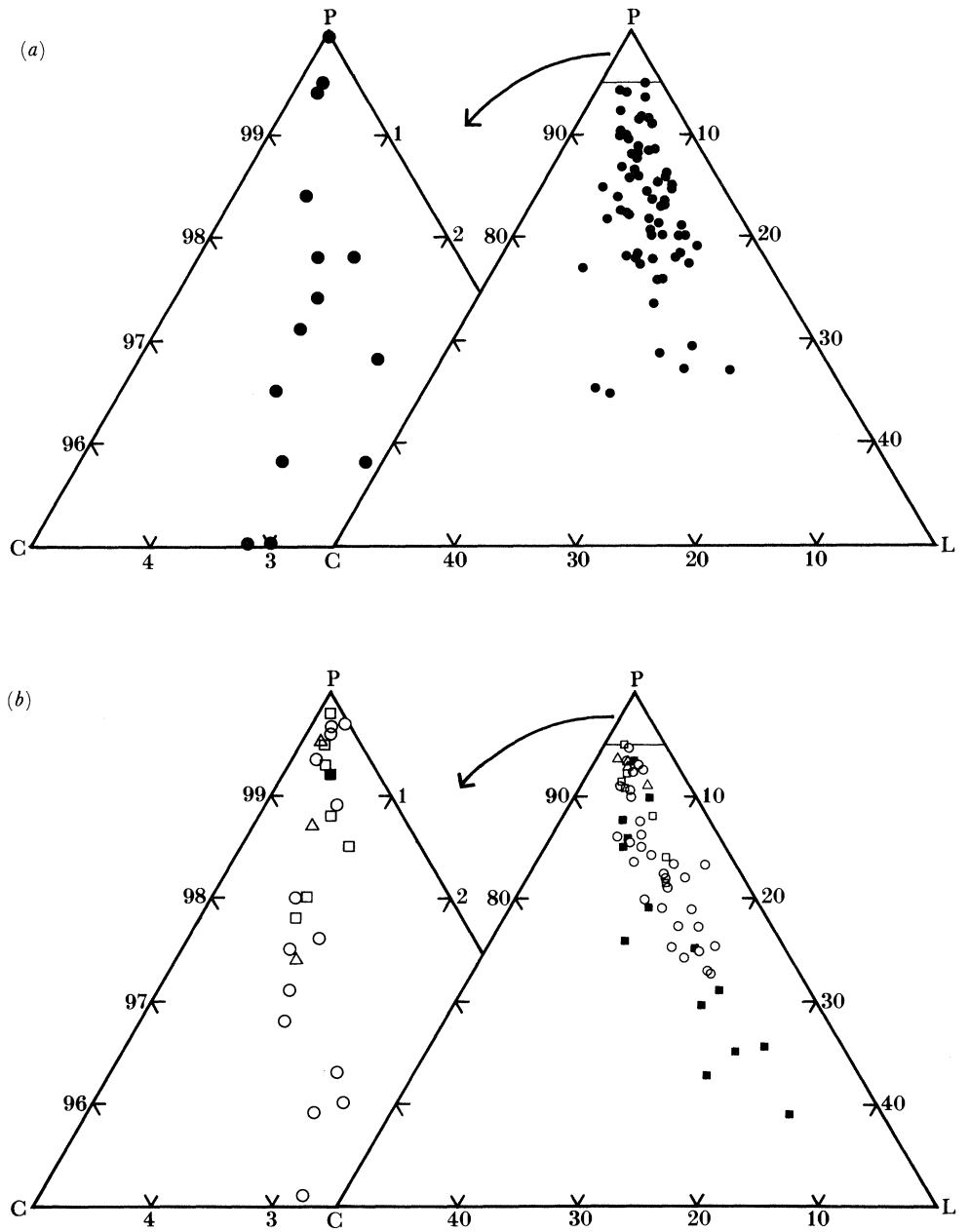

FIGURE 46. A p.c.l. diagram showing the contents (% by mass) of pumice, crystals and lithics in (*a*) the IVD and (*b*) the VPI. Symbols are as in figure 39.

(ii) *Layer* 1 (*H*): *the ground layer*

Layer 1(H) is interpreted as material segregated and sedimented out from the flow head owing to strong fluidization induced by air ingestion, and is genetically termed the ground layer (Walker *et al.* 1981*a*). Its relationship to the previously described ground-surge deposit (Sparks *et al.* 1973; Sparks & Walker 1973) is discussed in Wilson & Walker (1982).

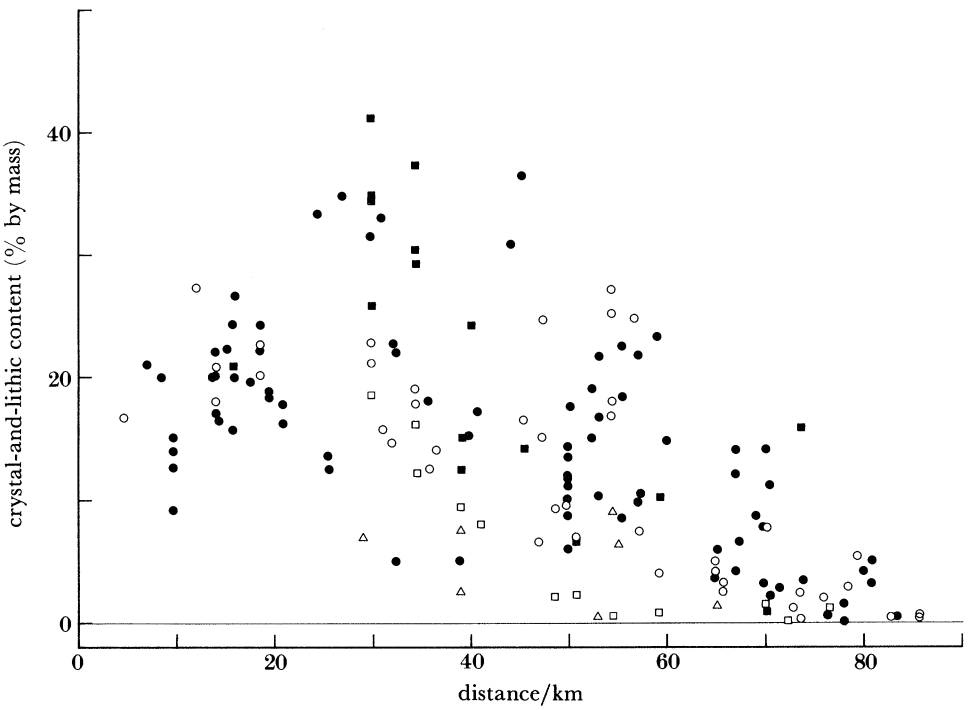

FIGURE 47. Contents of crystals and lithics in layer 2, against the distance from vent. Symbols are as in figure 39.

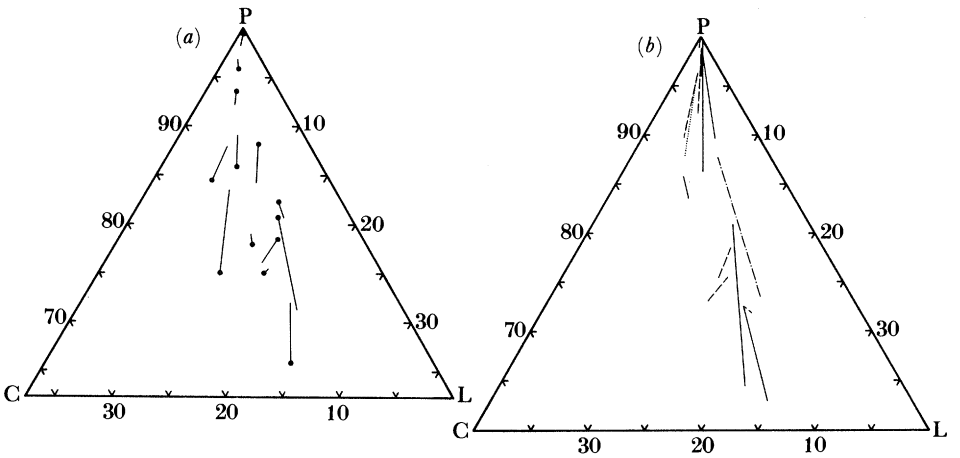

FIGURE 48. Two p.c.l. diagrams illustrating the compositional variations (*a*) between the IVD and layer 2b at the same or closely adjacent localities, and (*b*) within the VPI at any locality. The compositions are for the $\leqslant$ 2 mm fractions only, to reduce the effects of fluidization-induced coarse-pumice grading in the VPI. In (*a*), • denote the IVD composition. In (*b*), tie lines denote variations within: ——, layers 2a–2b (including the PCZ); ·····, layers 2a–2c; --------, layer 2b (including the PCZ); –·–·–·–·– layers 2b–2c. In all cases the lower sample is poorer in pumice.

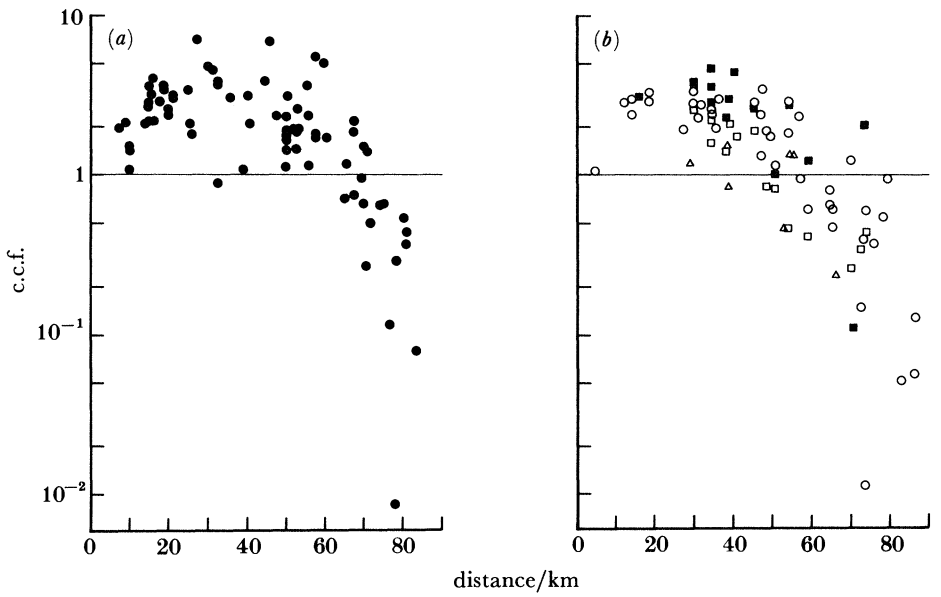

FIGURE 49. C.c.fs for (*a*) the IVD and (*b*) the VPI, against the distance from vent. Symbols are as in figure 39.

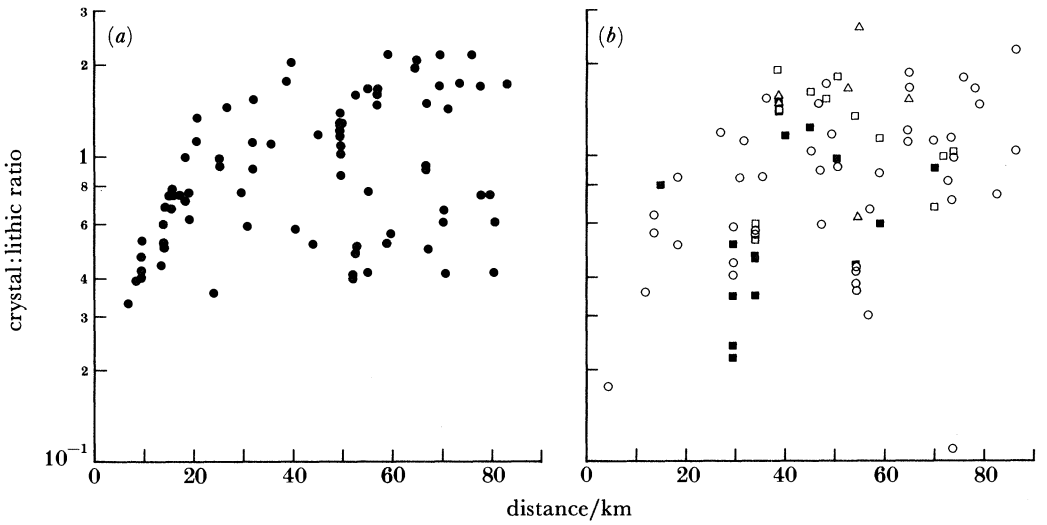

FIGURE 50. Crystal:lithic ratios in (*a*) the IVD and (*b*) the VPI, against the distance from vent. Symbols are as in figure 39.

(*b*) *Layer* 2

(i) *The IVD*

From its outcrop relationships with respect to the VPI, and its grainsize and compositional characteristics (notably its resemblance to layer 2a of the VPI), the IVD is interpreted as representing the basal and trailing parts of the flow, which were slowed by ground friction and left behind as the flow travelled across the landscape (Walker *et al.* 1981*b*; Wilson & Walker 1982).

Compositional layering and zonation. The lithic-rich lenses in the near-vent IVD, from their

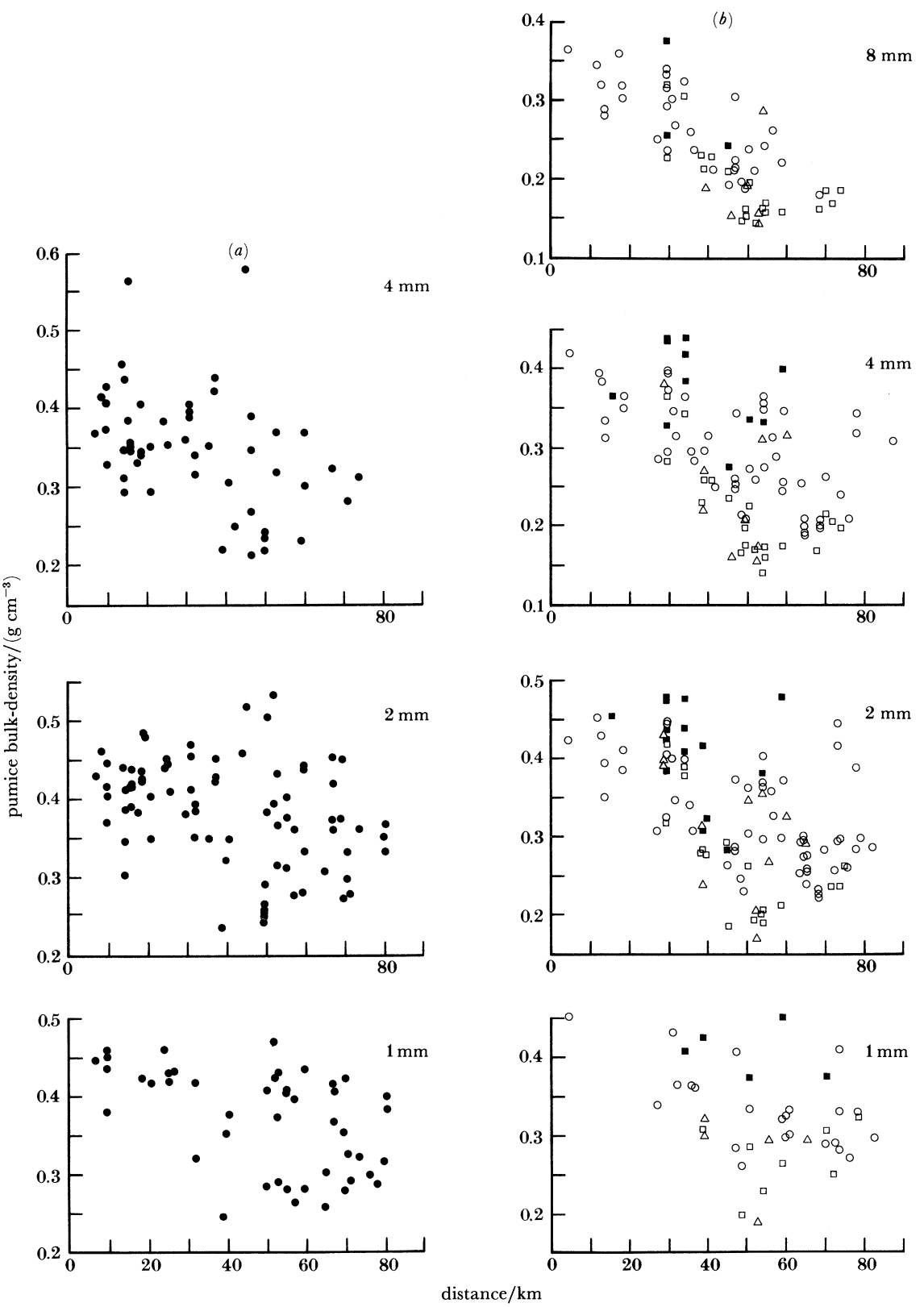

FIGURE 51. Pumice bulk-densities in various size fractions of (*a*) the IVD and (*b*) the VPI, against the distance from vent. Symbols are as in figure 39.

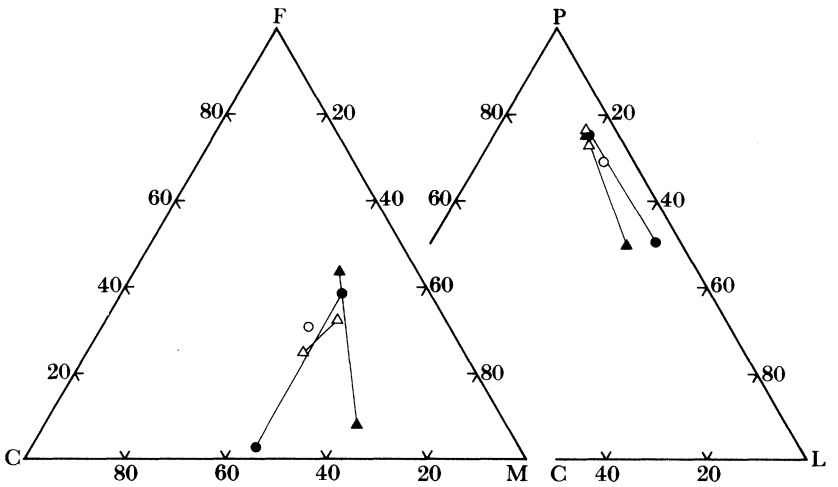

FIGURE 53. Comparison between the grainsize (c.m.f. triangle) and composition (p.c.l. triangle) of jetted deposits in areas where FDI does and does not occur (all figures are % by mass). Compositions were measured in the $\leqslant 2$ mm fractions only. ●, Fines- and pumice-richer basal and upper FDI samples from a locality at 3647 4419, 25 km from vent; ○, sample from locality at 3720 4243, 24 km from vent in the area where FDI is not developed; ▲, fines- and pumice-richer basal and upper FDI samples from a locality at 3021 4477, 46 km from vent; △, basal (fines- and pumice-richer) and upper samples from a locality at 3938 4078, 46 km from vent in the area where FDI is not developed. Note that differences between the basal samples are less than those between the basal and upper samples from FDI-bearing sections. This implies that the originally jetted material was roughly uniform in all areas about the vent, but that mixing with vegetation to generate FDI caused significant changes in grainsize and composition.

nature and similarity to the nearest-vent ground layer, are interpreted to represent material segregated out from the moving flow. Many of these lenses were actively segregating as they were emplaced and are thought to represent incipient ground layers deposited by individual batches of flow material moving away from vent (see next subsection).

The compositional zonation is interpreted to reflect the erosion of material from layer 1 and its upward movement into the base of the flow. The two styles of zoning described (see §4 (*b*) (i)) involve either all the components of layer 1 or only the larger lithics and minor amounts of crystals and lithics. The first style is best developed at points where layer 2 overlies a coarse, highly permeable layer such as the Taupo plinian pumice or FDI. Where the zoning is partly developed, the resulting layer 1/layer 2 mixture falls very close to an ideal mixing relationship between the end members (figure 54, plate 7). It is inferred that the permeable layer was trapped between the relatively impermeable moving flow and an underlying impermeable layer (the pre-eruption palaeosol or a phreatoplinian ash). It is then thought to have sheared under the influence of high pore-fluid pressures beneath the flow (Wilson 1981), allowing the erosion and incorporation of the layer 1 deposits. Where the second zoning style is found, and in the first style once the highly permeable deposit was removed, the flow was underlain by an impermeable base. Under such conditions, high pore-fluid pressures and high shear-strain rates are thought to have been confined to the flow itself, and only larger clasts were preferentially eroded from layer 1 and moved upward into layer 2 (Bagnold 1954; Sparks 1976). In support of this, the phreatoplinian ashes and underlying palaeosol show only minor erosion except where exposed on the upstream side of an obstacle or the lee side of a sharp break in slope.

The fines-free, crystal- and lithic-rich sheath around large clasts in the one-clast-thickness, lithic concentration zone is interpreted as a segregation feature, caused by the coarse clasts

acting as nuclei for bubbles which removed fines from the surrounding material (Wilson 1981). The presence of this sheath implies that while the larger lithics were being incorporated into the base of the flow, the gas velocity must have equalled or exceeded parameter U_{mp} (Wilson 1984), confirming that pore-fluid pressures must have been high and effectively equal to the load pressure.

Grainsize stratification. The grainsize stratification is interpreted to primarily reflect the changing thickness of the flow as it passed over fixed points on the ground surface. If the flow varied in thickness along its length, then stresses at a fixed point underneath the flow would have fluctuated (Wilson 1981). As the flow thickness increased, material at the base would have been compressed, increasing the pore-fluid pressures and promoting easier shearing, and vice versa. Changes in flow thickness are thus envisaged to have caused fluctuations in the amount and grainsize of material being deposited at the flow base. Under high shearing rates, as the flow thickness increased smaller amounts of finer-grained or no material were deposited, whereas as the flow thickness decreased greater amounts of coarser material were laid down. From this, each layer in the IVD is interpreted to represent the passage of a fluctuation in the flow thickness. The fluctuations may be considered on two scales; first, as separate pulses or batches of material and, second, as minor fluctuations (waves) on the surface of a continuous flow. If the scale of the grainsize fluctuations in the IVD is taken to reflect the scale of the flow thickness changes, then the IVD stratification implies that the flow was erupted as batches of material which by *ca.* 25 km from vent had coalesced into a single wavy flow and by *ca.* 40 km had formed into a single wave of material. The implications of this model on the eruption dynamics are considered in Wilson & Walker (1981).

Another possible interpretation is that these fluctuations in shear stress, which are thought to have generated the grainsize stratification, were due to turbulence within the flow body. While turbulence was probably widespread in the near-vent flow (see §6) and contributed to the grainsize variations in the IVD there, it is thought more likely that flow-thickness fluctuations generated the grainsize stratification elsewhere, for two reasons. First, where best exposed, the fine-scale stratification is plane parallel for tens of metres along the outcrop; it is considered unlikely that stress fluctuations due to turbulence could have acted uniformly over such distances. Second, the grainsize stratifications are no less numerous on the upstream side of obstacles than on the downstream side, where turbulence would, from the development of lee-side lenses, be expected to have been more severe.

Bedforms: topography-induced. These features are evidently related to the passage of the flow over obstacles. The low deposition angle (significantly less than the repose angle) of the lee-side beds is considered to be a result of the fluidization state of the material and the momentum with which the deposits were emplaced. The lee-side lenses are interpreted to form in vortices where the flow left the ground surface (Walker *et al.* 1981*b*). However, the distances to which lee-side lenses are found behind an obstruction are less than expected were the distance controlled by the time required for the flow to free flight back to the ground surface. The reaction of the flow to the landscape was apparently much faster than if gravity were the only force involved. It is suggested that, as would occur with a normal fluid, a low pressure zone formed on the lee side of the obstacles and the flow filled the vortex at a rate controlled both by gravity and the speed with which the flow could expand under the pressure gradient; field evidence then suggests that the latter process was extremely rapid.

Bedforms: self-induced. The self-induced bedforms appear to be controlled by the same processes as the topography-induced bedforms. However, in most cases, the lensoid wavelengths are

rather smaller (generally less than 10–15 m) than would be expected under a flow travelling at such high velocities. The erosive contacts between the lensoids show that erosion and deposition occurred concurrently at the base of the flow, and the wavelengths now seen are thus interpreted to represent those superimposed only during the last stages of deposition.

(ii) *The VPI*

In general, data from the VPI are consistent with the mechanisms proposed by Sparks (1976) to explain grainsize variations in layer 2 deposits. Layer 2a represents the fossil boundary layer to the valley pond, where grading is controlled by shearing, while grading in layer 2b is controlled by the buoyancy-induced movement of large clasts. In detail though, fluidization studies demonstrate that gas-flow processes exert an important control on the grading processes (see, for example, Wilson 1980).

Layer 2a. At many proximal exposures, the gradual reverse grading into the valley pond suggests that high shear-strain rates were present through much of the thickness of the unit, which is interpreted as being a feature of deposition from a very fast-moving flow. In very distal exposures the absence of layer 2a merely reflects the scarcity of coarse clasts, whose presence would make layer 2a visible.

At intermediate distances from vent, the presence or absence of layer 2a largely depends on the presence or absence of a very permeable layer underneath layer 2. Where the valley pond rests on the ground layer or FDI, layer 2a is often absent or poorly defined, whereas where it rests on fines-bearing jetted deposits, or a phreatoplinian ash, or the pre-eruption soil, layer 2a is often well marked. From the relationship between these two extremes (see, for example, figure 55, plate 8) it appears that the more permeable was the underlying layer, the higher were the shear-strain rates within it during the later stages of flow emplacement, and hence the poorer the development of layer 2a in the overlying VPI. Thus as for the IVD (§5(*b*) (i), above), it can be inferred that at least some of the lithic enrichment in layer 2a is the result of the incorporation of material from layer 1.

Layer 2b and the PCZ. The near-vent (out to *ca.* 20 km) type 1 sections appear to be genuine low-gas-velocity deposits, with no clear evidence for any grading other than that produced by shearing. Many distal valley ponds also appear to be of type 1; however, a thin 'scum' of PCZ material often betrays the presence of type 2 or type 3 grading, despite a general lack of segregation bodies in the underlying layer 2b (see §9(*b*)).

At intermediate distances (*ca.* 15–60 km) and, less often, closer to and further from vent, the VPI is of types 2 or 3, showing buoyancy-induced coarse-tail grading. From fluidization experiments (Wilson 1980, 1981), two kinds of PCZ were predicted to occur above flow types 2 and 3; both kinds are seen in the Taupo ignimbrite (Wilson 1981; Wilson & Wright 1985). Briefly, PCZ layers in type 2 sections merge gradually into the underlying part of layer 2b, are less-strongly bimodal and have a fine-grained matrix which is similar in nature to that in the rest of layer 2b. Those in type 3 sections are usually sharply demarcated, contain segregation bodies, are more-strongly bimodal and have a more pumiceous matrix than the underlying layer 2b. Thus, part at least of the fine/light-material-enriched segregation layer of the Taupo flow, whose presence is a corollary of the high gas flow rates, is represented by the matrix of the type 3 PCZ material. The PCZ layers which are too thick to have originated *in situ* are interpreted to have formed above the entire thickness of the moving flow and then been draped over the landscape in the wake of the flow (Wilson & Walker 1982).

The coarse-pumice-bearing, matrix-absent lenses at the top of some of the layer 2b sections

are not segregation bodies as they totally lack any matrix and occur above sections of all three fluidization types, and are not lee-side lenses as they occur on the level surface of the deposit. Similar features observed in the Mount St Helens ignimbrites have two origins. First, some of them represent levee and snout deposits which have been buried by a later flow unit; in such cases, the original flow-surface topography has often been flattened out to form a near-planar, sub-horizontal flow unit boundary, as seen in the Taupo VPI. Second, these bodies sometimes underlie secondary phreatic and reworked deposits, and appear to have been generated by strong winds winnowing the fines out of the pumice-rich top of the underlying flow unit. Both modes of origin seem possible in the Taupo ignimbrite.

Layer 2c. It is postulated that layer 2c represents another portion of the fine/light-material-enriched segregation layer of the Taupo flow, this explaining its abundance of pumice and fines, its lack of coarse lithics and low c.c.fs. The coarse-pumice-enriched material consists of a matrix which is common to both layer 2c varieties, plus a 'floating phase' of coarse ultra-light pumices which have been derived by flotation from layer 2b. The characteristics of the Taupo layer 2c closely resemble those of layer 2c deposits above other type 3 ignimbrites in New Zealand (Wilson 1981; Wilson & Wright 1985). The confinement of layer 2c to valleys is attributed to its fine-grained nature, which allowed it to drain downslope under the influence of gas-flow rates insufficient to mobilize the underlying material.

The natures of the coarse-pumice enriched layer 2c and the type-3 PCZ are often so close that their different positions in the ignimbrite are ascribed to purely local circumstances. Where slopes were gentle, the segregation layer seems to have remained *in situ* to form a type 3 PCZ; where the slopes were steeper, it apparently moved downslope to form layer 2c.

The scarcity of segregation bodies within layer 2c is a result of the origin of the layer itself. In fluidization experiments, the segregation layer at the top of the bed (which corresponds to layer 2c) is very depleted in crystals and lithics, and is sufficiently well sorted that a high proportion of its weight is supported by the gas flow (Wilson 1984). Any segregation bodies formed within it can be readily remixed and the layer can remain homogeneous even after undergoing strong fluidization. After the gas supply is turned off, segregation pipes in the lower part of the bed are truncated against the base of the segregation layer, or continue upwards only as thin, fines-depleted pumiceous pipes. Analogues to this are seen in the Taupo ignimbrite where segregation pipes in layer 2b often terminate at the base of layer 2c.

(*c*) *The distant facies*

The distant facies is interpreted as the deposit of the flow near its outer limits where, although its volume was reduced by deposition, its velocity remained high (figure 2) (Wilson & Walker 1982). It is envisaged that the flow volume was reduced by deposition such that what was body material nearer vent became mixed into the flow head, producing the mix of jetted deposit and IVD characteristics in the facies, and the strongly fluidized remnants of the flow were spread over the landscape. In lower-lying distal areas, it is thought that the lower velocity and greater bulk of the flow caused separate layers 1 and 2 to be generated to the outer limits of the flow. In its outermost reaches the flow had thus split into two fractions, a lower-volume, highly energetic part and a more bulky, slower-moving part in valleys and on low interfluves. The inliers of distant facies material reflect this process by occurring slightly closer to vent, as only the fastest moving parts of the flow climbed the highest hills.

6. Origins of the lateral variations

Lateral variations in the ignimbrite are examined from four perspectives. First, lateral variations in the development of the different facies and their variants (figure 5) are considered. Second, the lateral grainsize and compositional variations shown by the main facies are examined and, third, these data are used to infer the relationships between the head and body of the flow. Fourth, some of the distinct regional variations seen in the ignimbrite are discussed. Lateral variations in the grainsize and composition of layer 2 are broadly discussed by Walker & Wilson (1983), but are considered in detail here.

(*a*) *Lateral variations in the development of each facies*

(i) *From vent out to* 20–25 *km*

Out to 13–15 km from vent, jetted deposits are absent and layer 1 is represented only by the near-vent fines-bearing variety of the ground layer, which also persists out to 22 km. It seems that this close to vent the jetting process did not operate, and that the segregation process which generated the ground layer material was less efficient. Out to *ca.* 20 km, the IVD shows little or no compositional zonation, has low c.c.fs (figure 49) and $< 63\ \mu m / < 10\ \mu m$ ratios (figure 17). The IVD bedforms imply that the near-vent flow responded exceedingly rapidly to undulations in the ground surface, and P_m sizes and c.m.f. proportions in the IVD and adjacent VPI are similar (figures 39 and 41). From this evidence, the ignimbrite out to *ca.* 20 km is considered to have been deposited by the flow while it was still 'condensing' out from the collapsing eruption column. Theory suggests that during the transition from eruption column to pyroclastic flow, the material would be expanded compared with normal pyroclastic flow material (Sparks 1976; also see §9(*b*)) and highly turbulent, owing to the passage of huge quantities of gas and the kinetics of the forming flow (Sparks *et al.* 1978; Wilson 1980). The deposits are then interpreted to reflect the more dilute and turbulent nature of the near-vent flow.

First, however, the lack of near-vent jetted deposits is not simply explained. One possibility is that because of the extremely high flow velocity, jetted material could not move appreciably faster than the flow itself. Another possibility is that air taken into the flow merely served to inflate the mixture further, rather than to cause jetting. Both factors were probably important. At 13 km (figure 5), jetted deposits first appear, and beyond 16 km they become fully developed. Their changing characteristics may reflect the deflation or deceleration of the flow, or both. From 13 to 20 km, occasionally to 26 km, the jetted deposits are wholly fines-depleted and compositionally zoned (figure 13, example 2), and it is thought that the jetted material was winnowed by its passage through the air, to lose its fines and become segregated into a lithic-rich base and a pumiceous top. Beyond 16 km, increasing quantities of material were jetted with little modification from the flow head to generate fines-bearing jetted deposits, which in turn interacted with vegetation to generate FDI (§5(*a*)).

The efficiency of the segregation process which generated the ground layer can be considered (see, for example, Wilson 1984) as the degree to which a narrow grainsize-range, uniform-density fraction is separated out from a more poorly sorted, dominantly pumiceous material (the flow head). Thus the fines-bearing near-vent ground layer is interpreted as a product of less efficient segregation from the dilute turbulent flow; only the coarsest packets of segregated material were capable of sedimenting out this close to vent. Moving outwards, and especially beyond 20–30 km

from vent, the efficiency of the segregation process becomes better, as reflected by the lack of fines (figures 14 and 15), good sorting (figure 19*d*) and high c.c.fs (figure 25*b*) in the ground layer. A similar contrast in fines contents and sorting is seen between other near-vent lithic-rich breccias and their coeval ground layers (Wright & Walker 1977, 1981; Wright 1979; Druitt & Sparks 1982). It could be argued at Taupo that, as the outer limit of the fines-bearing ground layer is similar to that of the early ignimbrite flow units (Paper I, figure 7), fine material in the former was derived by erosion from the latter. However, a fines-bearing ground layer is found in places where the early flow units are absent, and a fines-free ground layer can be found overlying partly eroded early flow unit material.

The break in slope of the layer 1 L_m data occurs at *ca.* 20 km from vent. From comparisons with other ignimbrites, this point marks the outer limit of the Taupo 'lag-breccia deposit' (Wright & Walker 1977; Druitt & Sparks 1982). At Taupo, the lag deposit, normally confined to the immediate vicinity of the vent, has been pushed outwards by the immense violence of the flow to cover an area exceeding 1000 km^2.

Features seen in the near-vent IVD are also consistent with the more dilute nature of the flow. The lithic-rich lenses are interpreted to represent material which segregated out very inefficiently in response to the high gas flow rates associated with the deflation of batches of material moving at very high velocities. The absence of a significant compositional zonation in the IVD out to 20 km (figure 5) may be related to the turbulence in the flow; unlike in the IVD further from vent (§5(*b*)), any material eroded from layer 1 was completely incorporated into the flow, instead of being mixed into only the very base of the flow. The coarser-scale layering in the IVD persists out to *ca.* 25 km from vent, which point is thought to mark the coming together of the flow from a series of batches of material into a single wavy flow. This roughly coincides with the outer limit of the lag breccia deposit and is interpreted to indicate the distance at which the flow had essentially fully deflated from the dilute eruption column. It is thought that the nearer-vent flow was dilute enough that irregularities in the underlying ground surface could be accommodated by expansion or contraction at the base of the flow with little change in the flow density, as evidenced by the lack of lee-side lenses as far out as 18 km (figure 5). Once partially deflated to 'normal' densities (§9(*b*)) beyond 12–15 km, the flow could respond much less rapidly to changes in the ground surface, and lee-side lenses formed where the flow locally left the ground. The complex lensoid- and cross-bedding structures found from 9 to 21 km are interpreted as the results of the high energy turbulent depositional régime.

The reasons for the lack of fluidization-induced grading in many of the proximal VPI exposures are not clear. Presumably it is somehow related to the high velocities (cf. the prevalence of shearing-induced grading), or the expanded or turbulent nature of the flow, or both.

(ii) *Beyond* 20–25 *km from vent*

Beyond 20–25 km the flow is interpreted to have travelled as a single wavy mass, and from *ca.* 40 km as a single huge wave.

Jetted deposits are thickest between 20 and 40 km (figure 8) and the degree of upwards fines depletion and FDI development in layer 1 are greatest at these distances. It is thought that the intensity of jetting decreased further outwards from vent than this, and that the resulting smaller volumes of the individual jets reduced the scale and efficiency of mixing with vegetation, causing

the amounts of gas thus generated to decrease. Also, the flow probably cooled away from vent in response to the throughput of ingested air and thus less gas could be extracted from the vegetation before the jetted deposits were buried by the rest of the flow.

The ground layer was generated out to the distal limits of the flow, but is very patchy beyond 60–65 km because, it is thought, of the very low crystal-plus-lithic contents of the flow at these distances, this in turn being related to the nature of the flow there (§6(*b*)(i)).

The IVD shows a fine-scale stratification out to *ca.* 40 km but thereafter is essentially a single layer, this being interpreted to mark the final coming together of the flow as a single wave of material. The outwards decrease in IVD thickness is interpreted to be a complex function of three factors; first, the outwards thinning of the flow by radial spreading; second, the diminishing volume of the flow through deposition; and, third, the change from multiple batches of material nearer vent into a single wave in more distal areas. Because the relationships between flow thickness and volume and the resulting IVD thickness cannot be assessed, the importance of the first two factors in causing the general outwards exponential decrease in IVD thickness cannot be separated. However, it is thought that, coupled with the evidence from the grainsize stratification, the thicker, nearer-vent IVD reflects deposition from multiple batches of flow material (figure 56). The overall outwards decrease in IVD thickness cannot

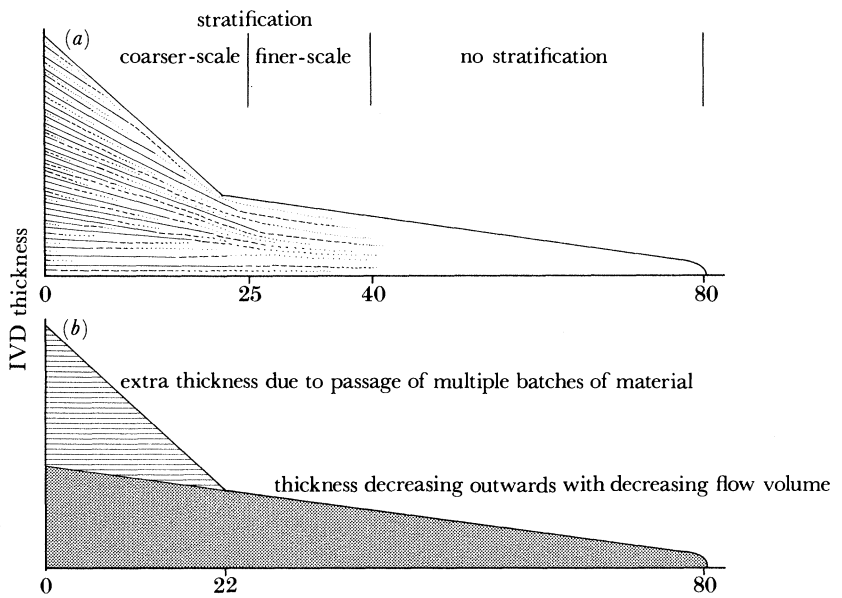

FIGURE 56. Semi-quantitative diagram to illustrate the origin of features in the IVD. (*a*) The stratification within the IVD persists to 25 km (coarse-scale) and 40 km (fine-scale) from vent. (*b*) The 25 km mark in part (*a*) roughly coincides with a break in the rate-of-change of IVD thickness at 22 km (figure 36 *a*). Hence the outwards-decreasing IVD thickness is considered to result from two processes: first, the passage of larger numbers of flow batches nearer vent and second, the diminishing volume of the flow due to both deposition and radial spreading. See text for further discussion.

solely be due to radial spreading of the flow (i.e. IVD thicknesses inversely proportional to distance from vent) as this predicts anomalously great IVD thicknesses in the outer reaches of the deposit. Similarly, a radial spreading model fitted to typical distal IVD thickness data significantly underestimates the observed near-vent IVD thicknesses.

The VPI is evenly developed throughout the ignimbrite, the areas and volumes of individual

valley ponds being functions of local factors rather than the distance from vent (Wilson & Walker 1982). Variations in the fluidization-induced grading styles in the VPI are more easily understood when lateral variations in some of the parameters are considered (see below).

(*b*) *Lateral variations of parameters within individual facies*

All parameters measured in the ignimbrite show great variations laterally within individual facies as well as lesser contrasts between the facies at any distance. The former are used here to model the emplacement history of the flow and to explain the lateral variations within the facies. The latter are used (Wilson & Walker 1982 and §7) to examine relationships between different facies produced at the same time or at the same distance from vent.

In this section, the lateral variations of parameters measured in the ignimbrite are interpreted in terms of changes in the composition or the kinetic behaviour of the flow (see table 2). Layer 2 is discussed first because it forms the bulk of the ignimbrite; variations in layer 1 are then compared with their equivalents in layer 2.

TABLE 2. DEPENDENCE OF LATERAL CHANGES OF VARIOUS PARAMETERS MEASURED IN THE IGNIMBRITE ON CHANGES IN EITHER THE COMPOSITION (C) OR THE KINETIC BEHAVIOUR (K) OF THE FLOW

	layer 2		layer 1	
parameter	IVD	VPI	jetted deposits	ground layer
thickness	K	K	K	K
L_m	K	K	K	K
P_m	K > C	C ≫ K	C ≈ K	—
c.m.f. content	C > K	C	C > K	K ≫ C
⩽ $\frac{1}{8}$ mm content	C ≫ K	C	C > K	K ≫ C
< 63 μm content	C ≫ K	C	—	—
< 63 μm/< 10 μm ratio	C	C	C > K	K ≫ C
M_z	C ≫ K	C	C ≳ K	K ≫ C
σ_I	C ≫ K	C	C ≳ K	K ≫ C
p.c.l.	C > K	C	C ≫ K	K
lithic-plus-crystal content	C	C	C > K	K
c.c.f.	C	C ≳ K	C ≳ K	K
crystal:lithic ratio	K	K	K	K
pumice bulk-density	C > K	C > K	C > K	K

(i) *Layer* 2

Parameters that vary with flow composition. Out to *ca.* 20 km from vent, the changes seen are consistent with the model presented above, from field evidence alone, for the initial deflation and 'coming together' of the flow from the collapsing eruption column. In the IVD there is no change in the ⩽ $\frac{1}{8}$ mm content (figure 42), a drop in the content of < 63 μm material (figure 43) and M_z and σ_I values (figure 45), and a rise in (< 63 μm)/(< 10 μm) ratios (figure 17), the contents of crystals plus lithics (figure 47) and c.c.fs (figure 49). In the VPI these changes are generally less well marked and any systematic variations are masked by scatter. This is because the relevant parameters are affected by the contents of coarse material (lithics in layer 2a, pumice in layer 2b) which blur the variations. Those parameters which are least affected (e.g. the c.c.f.) show closely similar variations in the IVD and VPI. It would be expected that as the flow deflated away from vent it would lose large amounts of fine, dominantly vitric material and become correspondingly enriched in crystals and lithics (Walker

1972; Sparks *et al.* 1978; Wilson 1980). However, while changes in (< 63 μm)/(< 10 μm) ratios, crystal-plus-lithic contents and c.c.fs are well marked, changes in ⩽ $\frac{1}{8}$ mm and < 63 μm contents are much smaller or absent. These features are interpreted as indicating that while large quantities of fine material were being lost (to generate the crystal and lithic enrichment), comparable quantities of fines were being generated by comminution to buffer the ⩽ $\frac{1}{8}$ mm content of the flow. The accompanying small drop in < 63 μm contents and significant rise in (< 63 μm)/(< 10 μm) ratios, coupled with limited data on comminution processes acting elsewhere in the flow (see later in this section), are then thought to imply that the comminution products were slightly depleted in < 63 μm material and strongly depleted in < 10 μm material with respect to the original eruptive mixture.

Theory suggests that the transition from dilute collapsing eruption column to fully formed pyroclastic flow occupies a few tens to hundreds of seconds (Sparks *et al.* 1978), while recent field data imply that this transition may be even more rapid (Druitt & Sparks 1982). Features seen in the Taupo ignimbrite suggest that the flow had become largely deflated by *ca.* 13 km and had fully deflated to its moving state by *ca.* 20 km from vent. Knowing that substantial portions of the flow were travelling at more than 200 m s^{-1} (see figure 2), the time scales indicated for these events (less than 60 and less than 100 seconds, respectively) are consistent with theory.

By extrapolation of parameters back towards vent, the nature of the eruption column material that formed the bulk of the flow can be estimated (figure 57). If the c.c.f. of the eruptive mix is assumed to be 1 (figure 49), then the rapid rise of c.c.fs to 2–4 by 20 km from vent implies the loss of 50–75 % by mass of vitric material. However, a crucial point is that this vitric material was in part redistributed *within* the flow (which was much thicker than the deposits which it

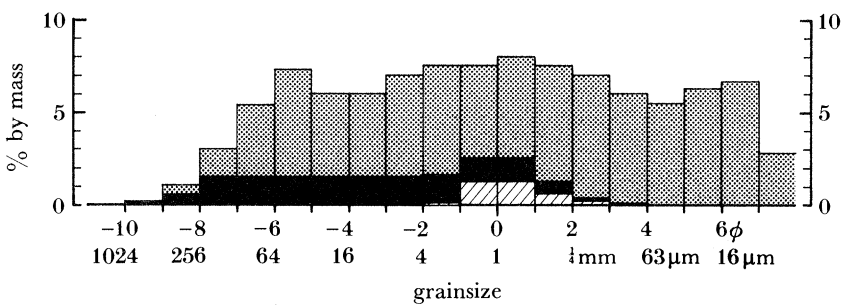

FIGURE 57. Histograms showing the inferred nature of the original eruptive mixture for the bulk of the Taupo ignimbrite; stipple, pumice and shards; solid black, lithics; diagonal hatching, crystals. (N.B. No allowance is made for the unusually coarse lithics present in the first-erupted material; see figure 9). From extrapolations of the near-vent data from layer 2, the following estimates are made for $D = 0$ km: < 1 mm content = 50–60 %, ⩽ $\frac{1}{8}$ mm content = 35–40 %, < 63 μm content = 20–25 %, (< 63 μm)/(< 10 μm) ratio = 4–5, $M_z \approx 0.0$, $\sigma_1 \approx 4.0$, crystal:lithic ratio ≈ 0.2, c.c.f. ≈ 1.0, lithic content ≈ 15 % (all percentages are by mass). The 0.01 percentile is assumed to be 1000 mm, which allows for coarse pumices in the PCZ and extrapolation to $D = 0$ km of the $D \geqslant 20$ km L_m data from layer 1.

These grainsize data are plotted on probability paper and a curve fitted to be most consistent with the above data. The curve has parameters $M_z = 0.0$, $\sigma_1 = 4.3$, < 1 mm content = 50 %, ⩽ $\frac{1}{8}$ mm content = 34.5 %, < 63 μm content = 21.5 % and < 10 μm content = 5 %. The percentage in each size fraction is then read off to construct the grainsize histogram. The crystal histogram is drawn by using unpublished relative-percentage data for the crystal contents in each of the 2 mm–63 μm size fractions, such that the total crystal content is 3.5 % by mass. Lithics are assumed to form 50 % of material in the ⩾ 256 mm fractions, and 50 % of the total crystal-plus-lithic content in the 1 mm–63 μm fractions (as is roughly so in most layer 2 samples); the remaining lithics are then evenly divided between the 128–2 mm fractions. The < 63 μm fraction is assumed to be vitric material.

laid down (Wilson & Walker 1982)), eventually reappearing as the distal ignimbrite, rather than being lost entirely to the overlying dilute cloud to form a layer 3 deposit (Sparks & Walker 1977).

Once the flow had deflated and coalesced away from vent it continued radially outwards for another 50–70 km as essentially a single mass of material. To model those parameters that are considered to reflect primarily the flow composition, the entire body of the flow at 20 km from vent, i.e. 25 km^3 or more of material (this being the approximate volume of ignimbrite beyond that distance), is modelled by a fluidized bed. In beds of ignimbrite materials fluidized in the laboratory at moderate to high gas velocities, segregation and grading processes produce distinctive structures and grainsize variations (Wilson 1980, 1984). Such a bed consists of three parts (figure 58, plate 8): a basal coarse/dense-material-enriched layer, which represents sedimented segregation bodies; an intermediate part in which dense and light constituents are normally and reversely graded, respectively, and which contains segregation bodies; and an upper fine/light-material-enriched segregation layer. This upper part consists of fine pumiceous material, which is carried to the bed surface by bubbles, but which is too coarse to be elutriated, together with variable amounts of coarse pumices that have sufficiently low densities to float in the layer. The fluidized bed thus shows predictable variations in its nature (figure 59). From

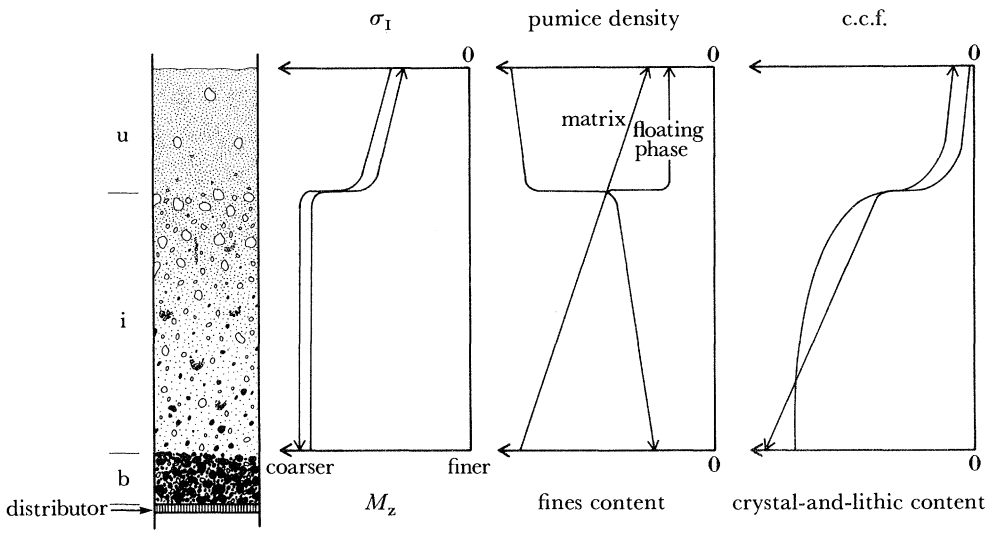

FIGURE 59. Schematic diagram of the fluidized system illustrated in figure 58, showing selected characteristics of the intermediate (i) and upper (u) portions of the bed which are predictable from experimental studies (Wilson 1984).

theoretical considerations (Wilson 1981), a rapidly moving pyroclastic flow can be modelled as a less-sheared upper part moving over a strongly sheared base; as such a flow moves, its slower base is left behind to form the deposit (figure 60). If this emplacement model is combined with the fluidized bed model described above, then lateral variations in layer 2 can be compared with predicted vertical variations in the fluidized bed.

Apart from the superficial absence of a basal segregation layer associated with layer 2 (considered later in § 7), the correspondence between the model and lateral variations in layer 2 is remarkably good. In particular, the greatly different nature of layer 2 from *ca.* 60 km outwards is explained; the ignimbrite in this outer area represents the fine/light-material-

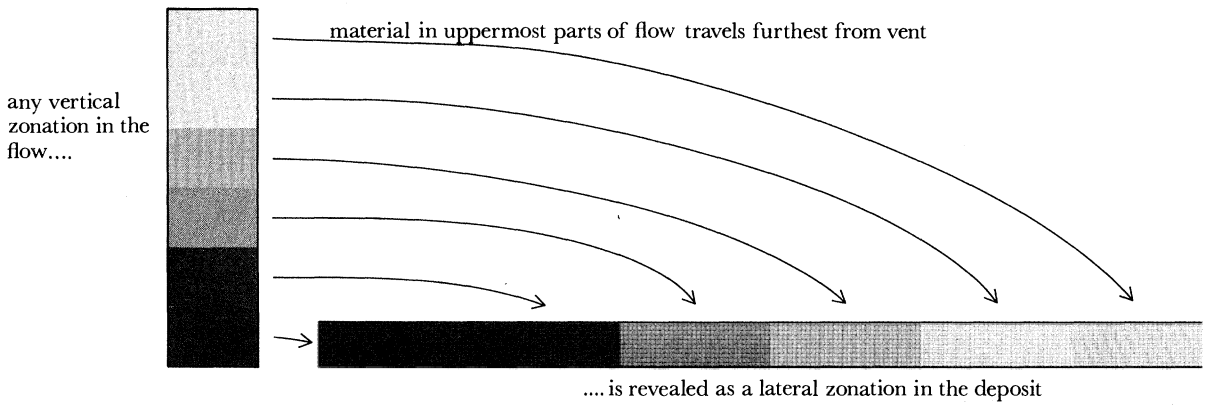

FIGURE 60. Schematic diagram illustrating results from an overall emplacement model for a rapidly moving pyroclastic flow.

enriched segregation layer from the top of the flow. The volume of this segregation layer, roughly 3–5 km^3, is significantly greater than that seen as either the type 3 PCZ matrix or layer 2c. The last two are thus considered to represent fluidization processes operating on a smaller, more local scale.

A test of the model can be based on the fact that segregation layers seen above laboratory fluidized beds (Wilson 1980, 1984) and found above type 3 flow units in other New Zealand ignimbrites (Wilson 1981) are visibly depleted in coarse lithics, which are too coarse and dense to be carried up by the gas flow, and intermediate-sized pumices, which are too coarse to be moved by the gas flow and too dense to float in the segregation layer. Data from layer 2b were used to minimize fluctuations caused by kinetic effects (IVD, layer 2a) or local fluidization (PCZ, layer 2c) in the plot of 8 mm pumice and 2 mm lithic contents against distance from vent in figure 61. The clearly defined and drastic decreases in the abundances of these components at 55–60 km from vent lend strong support to the model.

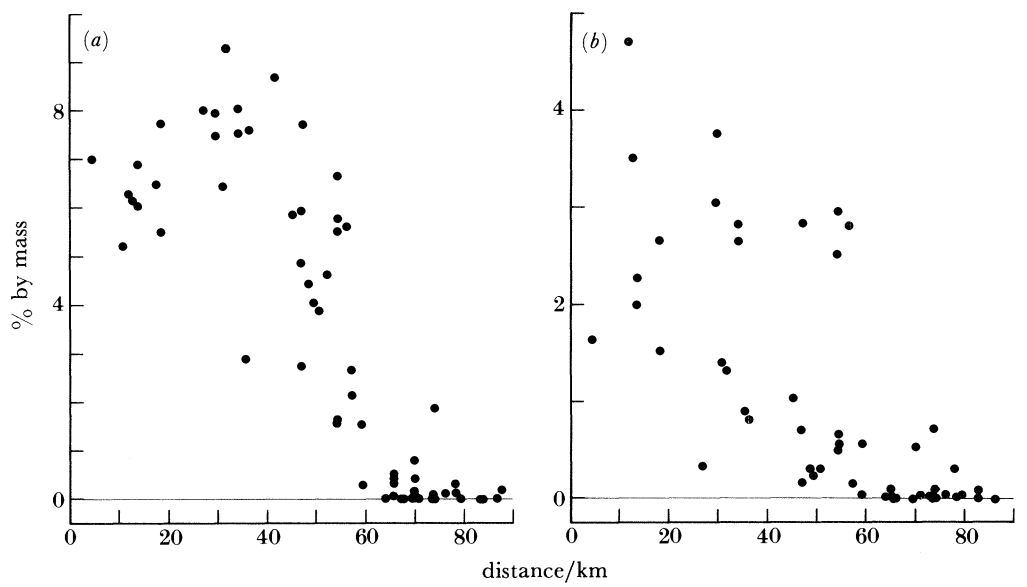

FIGURE 61. Contents of (*a*) pumice in the 8 mm and (*b*) lithics in the 2 mm sieve fractions of layer 2b (excluding the PCZ), against the distance from vent.

This model explains the following features of the grainsize and composition of layer 2. The generally high P_m values in the VPI out to *ca.* 60 km (figure 39) and the broad girdle of coarse-pumice outcrops (figure 40) are interpreted as representing the coarse-pumice-rich top of the intermediate part of the model fluidized bed. The stranded masses of PCZ material appear to represent portions of this pumiceous top which were deposited *en mass* over the landscape. If the flow body beyond 55–60 km from vent was a segregation layer, then the poor development of layer 2c at these distances is explained; the grainsize and compositional contrast between the flow itself and any segregation layer derived therefrom would probably be too small to be noticed in the field or detected by using sieve analyses, and would have easily been destroyed by bubbling-induced circulation within the flow.

The outwards increase in fine-material contents in layer 2 (figures 42 and 43) is interpreted to reflect the upwards movement of fines within the flow in response to fluidization. Note that the correspondence between model and deposit is closest for layer 2b; in the IVD, layers 2a and 2c and the PCZ, more-local factors such as shearing- and fluidization-induced grading blur the relationships. If more-specific parameters, such as the $\leqslant \frac{1}{8}$ mm content (figure 43) or the < 1 mm pumice content (figure 62) of layer 2b, are examined, then the discontinuity at 55–60 km from vent is most clearly displayed.

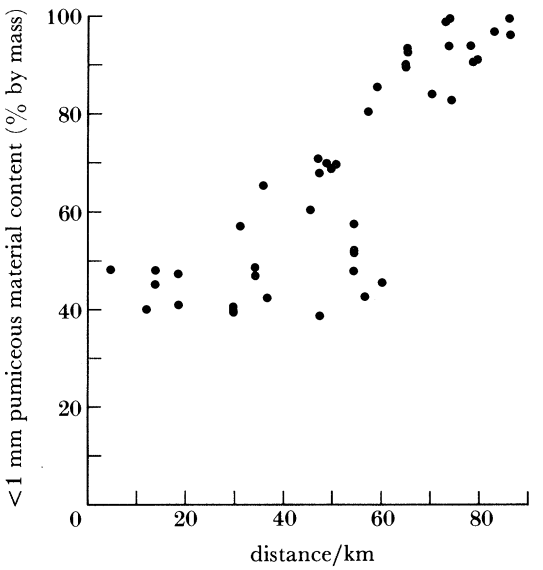

FIGURE 62. Content of < 1 mm pumiceous material in layer 2b (excluding the PCZ), against the distance from vent.

Variations in the $(< 63\ \mu m)/(< 10\ \mu m)$ ratio (figure 17) cannot easily be predicted. Whereas this ratio varies by more than 4 in the Taupo ignimbrite, other type 3 flow units show relatively little variation between layers 2a, 2b and 2c (Wilson 1981). The distal ignimbrite, often enriched in $< 10\ \mu m$ material, is interpreted from the model to represent material that was carried to the top of the flow, but the corresponding medium-scale fluidization structure seen at individual exposures (layer 2c) shows little significant enrichment of $< 10\ \mu m$ material over layer 2b. The reason for this discrepancy is not understood.

Four pieces of evidence are against the distal enrichment of fines being caused by the accumulation of comminution products. First, comminution products are apparently absent

from other deposits of types 2 and 3 (Wilson 1981). Second, if comminution processes were important, then evidence for them should be most obvious in the IVD, where shear-strain rates were probably highest during emplacement; however, if comminution products are present there, they are invisible, as the IVD and its adjacent VPI share similar < 63 μm contents and $(< 63$ μm$)/(< 10$ μm$)$ ratios. Third, studies from analogous industrial systems suggest that such parameters as the $(< 63$ μm$)/(< 10$ μm$)$ ratios of comminution products will stay uniform and cannot alone generate systematic variations with distance from vent (Wilson 1981). Fourth, had comminution been important in the flow, pumices in the most distal ignimbrite should be the densest, whereas the opposite is the case (figures 26 and 51).

Values of M_z and σ_I show similar variations in both of the main layer 2 facies. Layer 2b has fairly uniform M_z and σ_I values out to 55–60 km from vent (i.e. in the intermediate part of the model fluidized system), which drop abruptly thereafter (i.e. in the segregation layer), as expected from the model. The fine variety of layer 2c is always finer and better sorted than the bulk of layer 2, as predicted from the model. Layer 2a and the IVD show more gradual lateral variations; as these facies are deposited from the extreme base of the flow, some coarse material is absent owing to shearing-induced grading, and hence lateral variations of these parameters partially reflect kinetic effects (cf. with the next subsection).

The composition of layer 2 broadly follows the fluidization model, the crystal-plus-lithic content and c.c.fs increasing outwards as the flow deflated and lost fine vitric material (figures 47 and 49) and then declining sharply beyond 60 km. However, there is much scatter, which is attributed to two causes. First, the overall crystal-plus-lithic content are often affected by intermediate-scale fluidization processes operating at individual exposures (§9(*b*)). Second, many IVD and layer 2a samples have demonstrably incorporated crystals and lithics by erosion from layer 1. If these two processes are allowed for, then variations in the crystal and lithic contents in layer 2 are much closer to those predicted by the fluidized-bed model. For example, in the plot of layer 2b lithic contents against distance from vent in figure 63, there is again a sharp decrease at 55–60 km. Notice also that the minimum lithic content of layer 2b decreases outwards from *ca.* 20 km, again as predictable from the fluidized bed model.

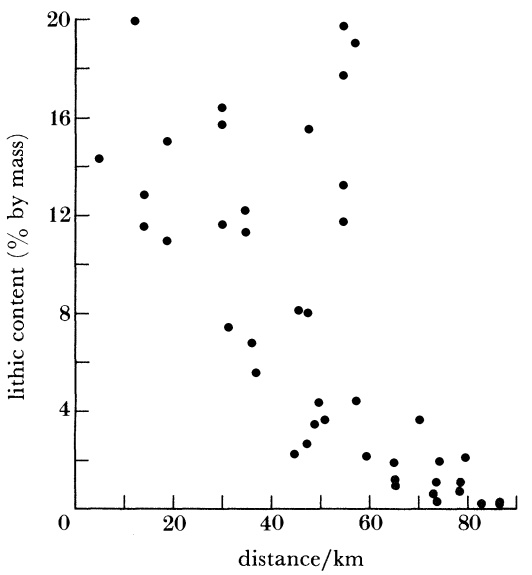

FIGURE 63. Content of lithics in layer 2b (excluding the PCZ), against the distance from vent.

Pumice bulk densities in layer 2 decrease outwards, as expected from the model, but there is no discontinuity at 55–60 km (figure 51). The absence of the discontinuity is attributed to large regional variations in pumice density within the individual facies (§8(*a*)) and to variations in pumice density within individual layers caused by local fluidization (Wilson 1981; Wilson & Wright 1985).

Parameters that vary with flow kinetics. Lateral variations in several layer 2 parameters are inferred to have been controlled or influenced by kinetic processes, such as shearing, fluidization or turbulence within the flow. Such processes act on whatever material is presented to them, with little regard for its composition.

As discussed above (§6(*a*)(ii)), the IVD thickness is thought to be controlled by several kinetic processes which affected the deposition of material from the flow. The VPI thickness is completely independent of the distance from vent (i.e. the flow composition) and is considered to be controlled by kinetic factors which determined the degree of drainage of material into valleys (Wilson & Walker 1982).

Although, as discussed above, the crystal-plus-lithic content of layer 2 reflects the flow composition, L_m variations (figure 37) are controlled largely by the flow kinetics, as the L_m sizes are independent of the absolute lithic abundance and are controlled by the ability of the flow to carry, or erode and incorporate, lithics of a given size. Whereas P_m data in the VPI reflect the flow composition, those from the IVD do not. In the proximal IVD and VPI, P_m sizes are fairly similar, this being interpreted as reflecting the turbulent conditions, coarse pumices being evenly partitioned between the two facies. Further from vent, the IVD was deposited from the coarse-pumice-depleted base of the flow, and changing P_m sizes in the flow were smoothed out by shearing to give a general outwards decrease (figure 39).

Variations in M_z and σ_I in the IVD are interpreted to result from the effects of kinetic processes, notably shearing, acting on the changing flow composition. Many of the M_z and σ_I variations in layer 2b result from changes in the contents of coarse ($\geqslant 4$ mm) pumices, which are depleted by shear-grading processes in the IVD. Thus lateral changes in the coarseness and sorting of the flow are only dimly reflected in the IVD (and layer 2a). However, the more gradual lateral changes in M_z and σ_I caused by the upward accumulation of fines within the flow are still clearly marked in the IVD and layer 2a.

Kinetic processes also influenced the composition of the IVD and layer 2a, via the erosion and incorporation of layer 1 material (principally the ground layer) into the base of layer 2. The effectiveness of this process varied with very local controls, discussed in §5(*b*).

Layer 2 crystal:lithic ratios (figure 50) show no simple changes in response to the changing flow composition with distance from vent. Under strong fluidization in the laboratory (Wilson 1984), crystals and lithics in the same size fraction tended to segregate out together, and this is reflected in the composition of segregation bodies in the ignimbrite (§9(*a*)). Thus the lateral changes in crystal:lithic ratios are here ascribed to the different grainsize distributions of the crystal and lithic populations (figure 64). As the flow moved laterally, the average grainsize of the deposited material decreased, and hence the relative proportion of crystals increased even though the absolute contents of crystals and lithics decreased drastically (figure 47).

(ii) *Layer* 1

Parameters that vary with flow composition. In the jetted deposits, P_m sizes (figure 12) would be expected to follow those of the VPI, but such is not the case. Near vent, both data sets are similar, but thereafter P_m sizes in the jetted deposits decrease steadily outwards, either because

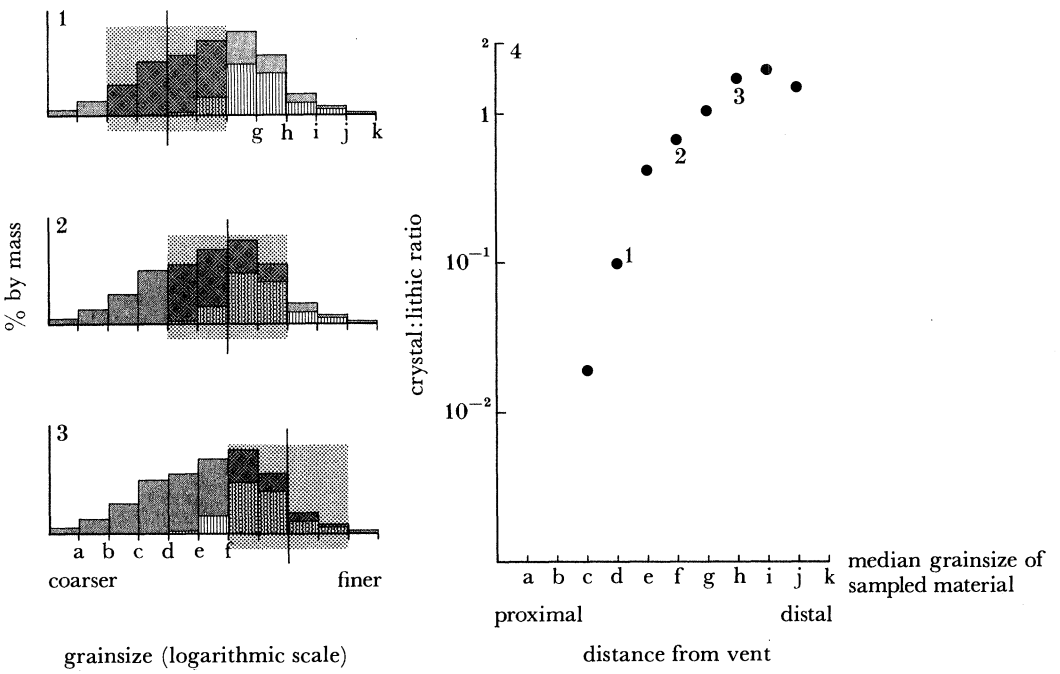

FIGURE 64. Semi-quantitative diagram illustrating how the different grainsize populations of crystals (vertical hatching) and lithics (shading) cause lateral variations in crystal:lithic ratios in the ignimbrite. In the ignimbrite, crystals have a narrower grainsize distribution (see figure 57) and so as the grainsize range (stipple) of material sampled from the flow becomes finer with increasing distances from vent (1–3) the crystal:lithic ratios increase (4; cf. figures 25 and 50).

large pumices in the flow head were broken up during emplacement or because the flow portion that generated the VPI was richer in coarse pumices than the flow head.

Once the effects of mixing with vegetation on the ground surface are allowed for, grainsize and compositional parameters in the jetted deposits broadly follow those in layer 2. The fines contents of the jetted deposits (figure 15) show lateral variations similar to those in layer 2, but the overall fines content of the former is lower because of fines losses during emplacement (figure 16).

Close to vent, the jetted and layer 2 deposits share similar ($< 63\,\mu m$)/($< 10\,\mu m$) ratios (figure 17), but beyond *ca.* 40 km they diverge. This is attributed to changes in the intensity of fluidization undergone by the jetted material. Nearer to vent, the fluidization intensity was such that $< 63\,\mu m$ and $< 10\,\mu m$ material was removed fairly evenly (for comparison, note the low ($< 63\,\mu m$)/($< 10\,\mu m$) ratio in the near-vent ground layer sample). As the fluidization strength waned with distance from vent, the finest material was preferentially removed and hence the ($< 63\,\mu m$)/($< 10\,\mu m$) ratios of distal jetted deposits remain high despite the increasing absolute contents of $< 63\,\mu m$ material.

From *ca.* 20 km outwards, M_z and σ_I in the jetted deposits (excluding FDI, whose grainsize characteristics more reflect processes operating outside the flow head) change by 4–5 and *ca.* 1 ϕ, respectively (figure 20); changes broadly comparable to those in layer 2b. However, the jetted deposits show no clear discontinuity at 55–60 km, and the most-distal jetted deposits are 1.5–2 ϕ coarser and 0.7–1.0 ϕ more poorly sorted than layer 2. The preferred explanation for this is that the overall nature of the flow-head material changed laterally, roughly synchronously

with, though to a lesser extent than, the flow body (cf. §7), and that turbulence served to keep the head well mixed. Thus instead of the jetted material segregating out to form separate, individually better-sorted facies, it was remixed by turbulence to retain its poor sorting.

In their crystal-plus-lithic contents and c.c.fs (figures 21 and 24), the jetted deposits follow similar trends to layer 2, but generally have higher crystal-plus-lithic contents and c.c.fs at any given distance, attributed to the strong fluidization during their emplacement. Pumice bulk-density data in the jetted deposits show similar trends to those in layer 2; in the former, an overall decrease is seen with increasing distance from vent (figure 26), but there are large local variations, attributed to regional factors (§8(*a*)) and fluidization processes.

Parameters that vary with flow kinetics. The thickness of the jetted deposits, beyond *ca.* 30 km from vent, decreases steadily (figure 8), a feature interpreted as reflecting the gradually diminishing intensity of the jetting process in response to the slowing (and cooling?) of the flow. In the jetted deposits, L_m sizes (figure 9*a*), like those in layer 2 and the ground layer, appear to have been controlled by the gradual depletion of large lithics through deposition, and by the diminishing ability of the flow to erode and incorporate large lithics. Again, as with layer 2 and the ground layer, crystal:lithic ratios in the jetted deposits (figure 25*a*) increase gradually away from vent in response to the decreasing mean grainsize sampled by the material (figure 64). Other parameters in the jetted deposits, although largely controlled by the flow composition (see above), are also affected by the turbulence or strong fluidization, or both, at the flow front or on the ground surface, these being the P_m, M_z and σ_I data, the contents of crystals plus lithics and the c.c.fs.

The ground layer differs from the jetted deposits in that it represents only a selected fraction of the head material. Thus any control exerted by the flow-head composition on parameters measured in the ground layer is at least strongly subdued by the kinetic processes (segregation and sedimentation) that generated the ground layer (Walker *et al.* 1981*a*). The kinetic processes are in turn related, via the amount of air ingestion, to the gradually outwards-decreasing velocity (and temperature?) of the flow. The L_m sizes, fines contents, and M_z and σ_I data (figures 9, 14, 15 and 19) are partly influenced by the flow composition (for example, if the flow only contains < 5 cm lithics, then larger lithics will not occur in the ground layer), but are mainly controlled by the strength of the fluidization. The crystal-plus-lithic contents, c.c.fs, crystal:lithic ratios and pumice bulk-densities (figures 21, 24, 25 and 26) are strongly controlled by the efficiency or strength of the fluidization. However, the most efficient fluidization, as reflected in low σ_I values and high crystal-plus-lithic contents, occurred beyond *ca.* 20–30 km from vent, whereas the strongest fluidization, as reflected by M_z values, occurred nearest to vent.

An important point is that all the ground layer parameters discussed above are essentially independent of the absolute abundance of any particular component. However, other parameters may show a close relationship to the flow composition. For example, were it feasible to measure the volume of the ground layer against the distance from vent, then it should vary in tune with the flow composition, this being seen qualitatively in the poorer development and lesser thickness of the ground layer in the outer reaches of the ignimbrite.

7. Relationship between the head and body of the flow

From the discussion in the previous section, layer 1 evidently shows some features in common with and others differing from layer 2. This is used here to provide information about the relationships between the head and body of the flow.

First, consider the jetted deposits. If the effects of interaction with surface vegetation are allowed for, then the parameters in which the jetted and layer 2 deposits are most similar and different are those which are related more to the flow composition and kinetics, respectively. The broad similarity of the variations in fines contents and c.c.fs suggests that material was supplied from the flow body to the head (Wilson 1980, figure 6), to be mixed in and then jetted. The supply rate can be examined by following how closely the variations in composition-dependent parameters match each other in the jetted deposits and layer 2b. For example, take the 8 mm pumice, 2 mm lithic and total-lithic contents which were used (figures 61 and 63) to mark the point where the composition of layer 2b changed as the segregation layer above the flow began to be deposited. Data for these components in the jetted deposits are plotted in figure 65; the first two decrease abruptly at 55–60 km, whereas no discontinuity is evident in the total lithic content. The 8 mm pumice and 2 mm lithic data change at roughly the same distance in layer 1 as in layer 2, implying that material was being moved forward relatively rapidly from the flow body into the head. The gradual decline in total lithic content suggests that an initially lithic-richer batch of material at the flow front (see figures 63 and 65*c*) became gradually lithic-depleted by deposition and by dilution by lithic-poorer body material which was mixed in before jetting. From the contrasts in grainsize and composition between the jetted deposits and layer 2 (figures 16 and 22), the jetted material must have spent relatively little time in the flow head, being carried forward from the flow body, mixed in and then jetted rapidly, losing only moderate amounts of fines (figure 16) and becoming mildly enriched in crystals and lithics (figure 22).

Second, consider the ground layer, which contains lithics almost an order of magnitude coarser than those in layer 2 near vent, but which in distal areas has essentially identical L_m sizes (figure 10). To model these changes, it is inferred that the first-erupted flow material was not only richer in lithics (see above) but contained a significantly coarser lithic population than the succeeding bulk of the eruptive material (figure 57). This coarser-lithic population was depleted by sedimentation and diluted by new material brought into the flow head, causing the L_m sizes and total lithic contents in layer 1 and 2 to converge with increasing distances from vent.

Earlier, in presenting the fluidized-bed model for the flow (§6 (*b*) (i)), the superficial absence of a coarse/dense-material-enriched segregation layer associated with layer 2 was noted. It now seems from the fluidized-bed model that the finer-grained top of the ground layer is that segregation deposit, that its deposition must have continued in the flow for some distance back from the flow front, and hence that the portion of the flow from which the ground layer was deposited must have been appreciably larger than that involved in the jetting process. Deposition of the ground layer is thus considered to have complemented the generation of such features as the PCZ and segregation layer at the top of the flow, the last being seen as stranded PCZ units and the distal layer 2 deposits, respectively. The actual contact between layers 1 and 2 was evidently a zone of very strong shearing, so it is envisaged that the deposition of

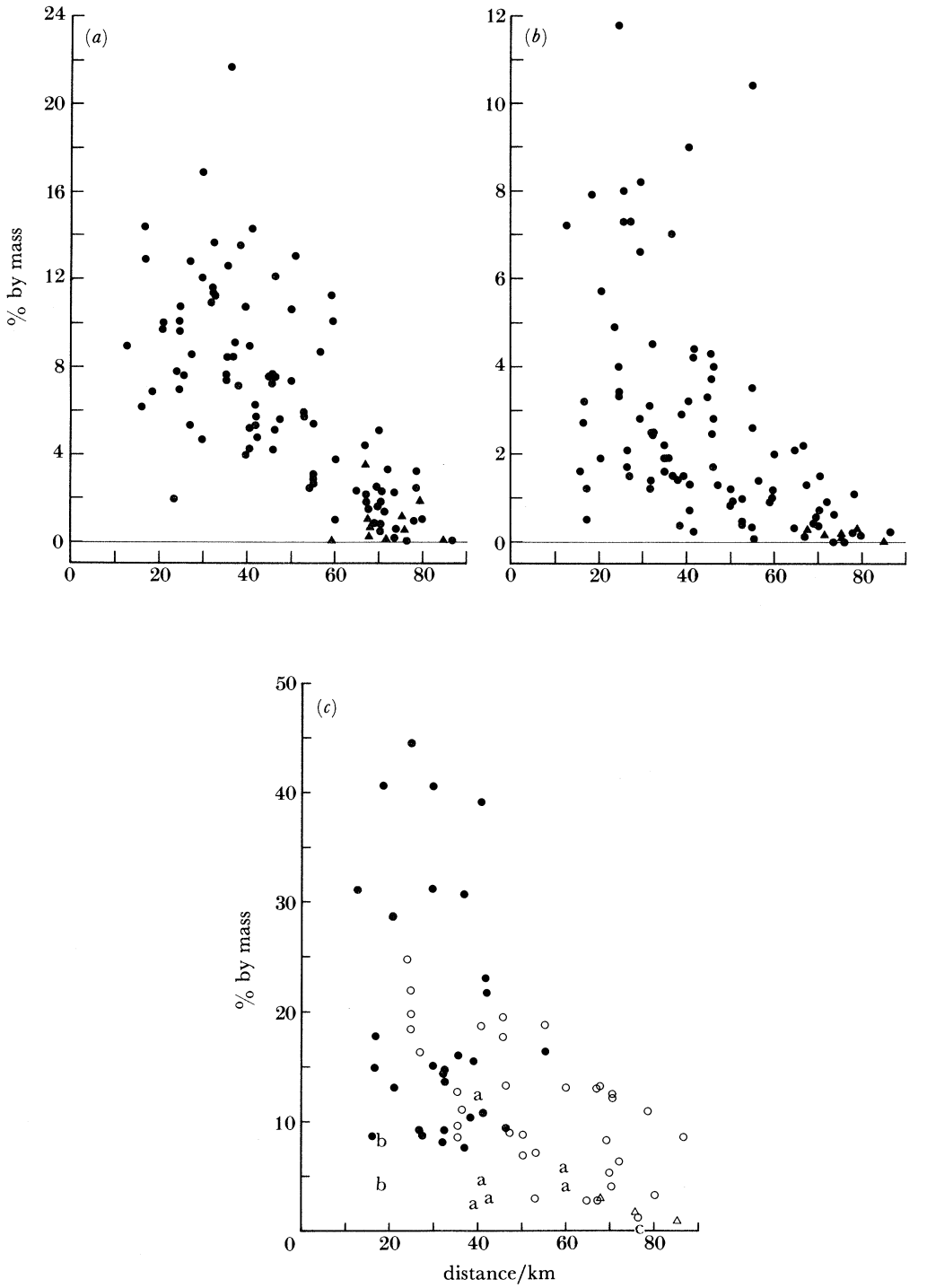

FIGURE 65. Contents of (*a*) pumices and (*b*) lithics in the 8 mm and 2 mm sieve fractions, respectively, and (*c*) the lithic contents in the jetted deposits (circles) and distant facies (triangles), against the distance from vent. Symbols in (*c*) are as in figure 14.

the lowest part of layer 2 represents the point at which formation of the ground layer ceased; only rarely have segregation pods been preserved sedimenting out within the base of layer 2.

From these inferences, a dynamic model is presented for the front parts of the flow (figure 66), in which the front-most part of the flow is involved in the jetting process, and a larger proportion of the flow is strongly fluidized by heated, ingested air. In this fluidized zone, coarse/dense constituents segregate out and sediment to generate the ground layer, while fine/light material is carried upwards, by the gas flow or buoyancy effects, or both, and rearwards, by air friction or by moving down the slope at the rear of the flow front; see Benjamin (1968) and Simpson & Britter (1979). The finest fractions are preferentially elutriated into the dilute cloud, but the remaining material accumulates as a coarse-pumice-enriched top plus segregation layer above the flow.

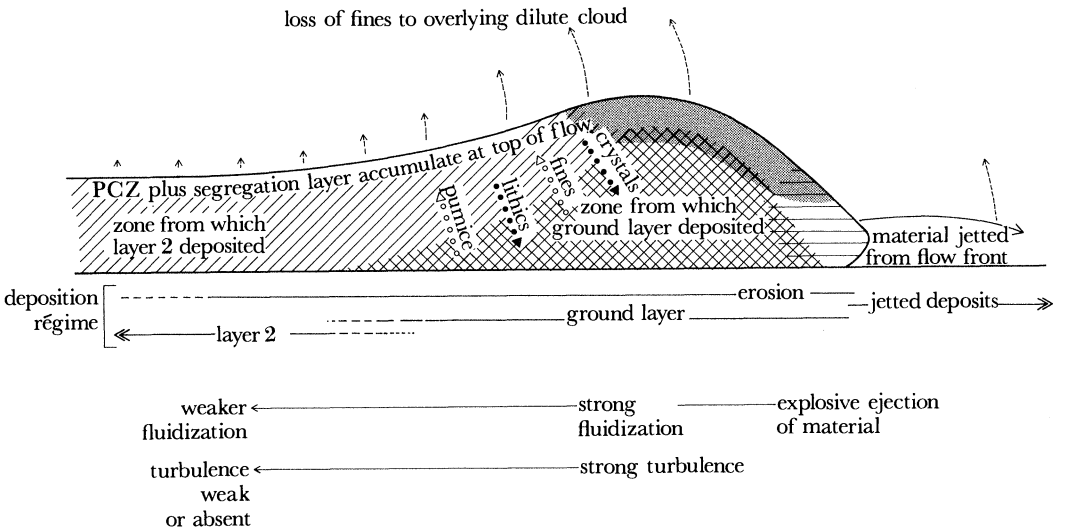

FIGURE 66. Schematic diagram illustrating the processes inferred to have operated at the front of the Taupo flow. The zones involved in jetting (horizontal hatching), segregation and sedimentation to generate the ground layer (cross hatching), and the generation of layer 2 (diagonal hatching) are indicated. The stippled zone at the top of the flow represents the area where mixing and air drag would have been most strongly developed; these processes are thought to be important in moving material which has been carried upwards within the flow head back towards the rear of the flow. The dotted arrows within the flow represent the overall transfer of fine/light components upwards and rearwards (eventually to form the distal ignimbrite) and of coarse/dense components downwards (to be preferentially deposited in the ground layer and proximal ignimbrite). The dashed arrows above the flow represent very fine material elutriated from the flow, which mixes with the atmosphere, rises to form a dilute ash cloud and its eventually deposited as a layer 3 co-ignimbrite ash. The various depositional, fluidization and flow régimes are tentatively indicated below the diagram. See text for further discussion.

It is envisaged that, as the flow travels, material from the flow body is cycled through the more strongly fluidized front of the flow and operated on, although except in the outermost reaches of the flow (where the distant facies was generated) only a portion of the flow was strongly fluidized at any one time. This would then explain how a dynamic pyroclastic flow can generate deposits that closely follow predictions made from a static fluidized bed. The term flow head is used to denote the region of strong fluidization at the front of the flow (Wilson 1980), in or from which were generated the layer 1 deposits, but what is now apparent is that the layer 2 facies, although deposited from the less strongly fluidized body of the flow, have also been influenced by fluidization processes in the head.

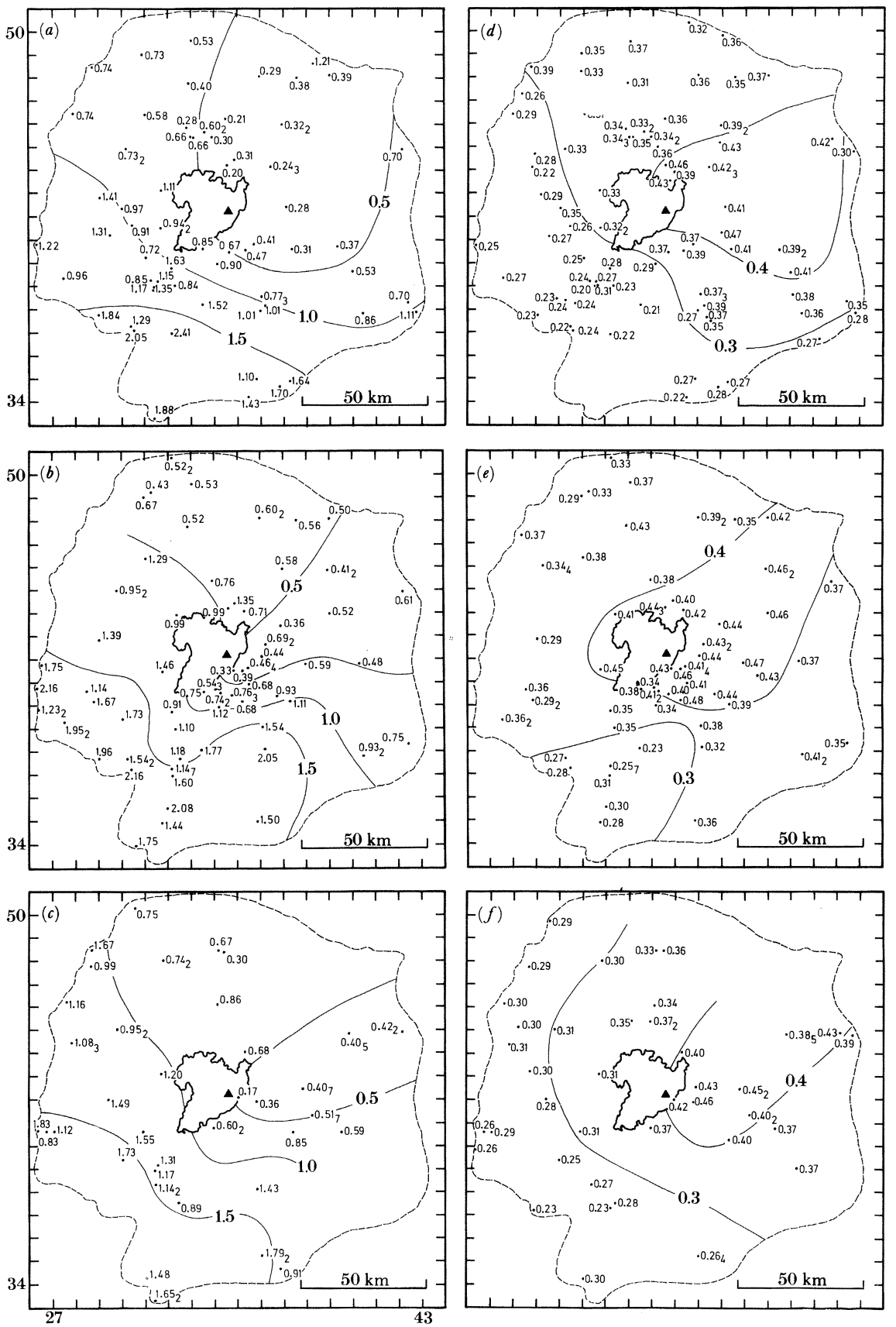

FIGURE 67. Maps of crystal:lithic ratios in (*a*) the jetted deposits, excluding FDI, (*b*) the IVD and (*c*) the VPI; and pumice bulk-densities (in g cm^{-3}) in (*d*) the jetted deposits, excluding FDI, (*e*) the IVD and (*f*) the VPI. The suffix for each data point indicates the number of samples, one by default.

The presence of stranded PCZ material as close to vent as *ca.* 13 km implies that the initial 'differentiation' of the flow must have occurred that soon, and the reasonable conclusion is that this was induced by gases expelled during the deflation of the flow away from the collapsing eruption column. It is envisaged that as the flow moved further away from vent, gases supplied by air ingestion became dominant in producing strong fluidization at the front of the flow.

8. Regional variations in the ignimbrite

Two kinds of regional variation occur in the ignimbrite, the first related to overall variations in some of the grainsize and compositional parameters and the second to differences seen in the ignimbrite at high altitudes.

(*a*) *Variations in the nature of the ignimbrite about the vent*

Although all the parameters measured in the ignimbrite show some scatter in values, the crystal:lithic ratios (figures 25 and 50) and pumice bulk-densities (figures 26 and 51) are particularly noticeable in this regard. If both parameters are plotted as maps (figure 67), then this scatter is evidently in part due to distinctive regional variations. The portion of the flow that went to the north and northeast of vent contained lower crystal:lithic ratios and higher density pumice than the portion that went to the south and southwest, for reasons which are unclear.

Four other regional asymmetries are also apparent in the ignimbrite. First, the parent flow travelled unequal distances in different directions about the vent, and the furthest-travel distances do not coincide with the easiest routes (figure 1). The inference that the volume of material available controlled the distance reached by the flow (Wilson & Walker 1981) implies that either the volume of material erupted varied in different directions, or that where the flow reached to smaller distances it laid down a shorter but slightly thicker deposit. Second, obvious asymmetries are seen in the L_m sizes in areas immediately around Lake Taupo (figures 11 and 38) as a result of the coarser-lithic-bearing front part of the flow being trapped in remnants of the pre-eruption Lake Taupo (Paper I, §3). Third, heat alteration colours in layer 2 are better developed in two broad areas east, south and west of vent (figure 28) and, fourth, the very largest pumices in layer 2b are found only to the east of vent (figure 38), both features having unknown causes.

(*b*) *Variations in the ignimbrite at high altitudes*

In areas to the east and south of vent, the ignimbrite covers large areas above the modern tree line. There the ignimbrite has characteristics which differ from those at lower altitudes in the same region and at the same distance from vent (Wilson 1981). The jetted deposits and layer 2 tend to be richer in fines and pumice (see, for example, figures 15 and 21), to have high crystal:lithic ratios (see, for example, figure 25) and to contain lower-density pumice (see, for example, figure 26). The ground layer is very well sorted, has high crystal-plus-lithic contents and high crystal:lithic ratios. These trends seen at high altitudes are similar to those seen within the respective deposits as the distance from source increases. Thus from the fluidized-bed model for the flow (§6 (*b*) (i)), it is postulated that the ignimbrite at high altitudes was deposited from the upper parts of the flow which, being less affected by ground friction, were more mobile and thus able to climb the highest mountains. Jetted deposit and layer 2

grainsizes and compositions thus reflect the finer and more pumiceous nature of the upper part of the flow, while the nature of the ground layer is interpreted as a result of the more efficient segregation in the head as the flow slowed in response to the heights climbed.

9. Fluidization processes in the ignimbrite

Fluidization is inferred to have played a major role in generating the facies and structures in the ignimbrite. These effects are examined on three scales. *Small-scale structures*: the individual segregation bodies, such as pods and pipes, seen in the ignimbrite at any exposure; *medium-scale structures*: the fluidization-induced grading processes seen when a single ignimbrite flow unit is examined at a given exposure; *large-scale structures*, which only become evident when an appreciable extent or the whole of an ignimbrite is mapped.

(*a*) *Small-scale structures*

In fluidization experiments (Wilson 1980, 1984), two types of primary segregation structures are seen; coarse/dense-material-enriched pipes and pods, and an upper fine/light-material-enriched segregation layer (sedimentation of the pipes and pods then generates a secondary segregation layer at the base of the bed (Wilson 1980, figure 4)). In this section, structures of the first type are discussed; the upper segregation layer has only been recognized forming intermediate- or large-scale structures.

In the ignimbrite, abundant counterparts to experimental segregation bodies are seen. Two distinct morphological types occur: pods, forming lenses, crescent shapes or irregular masses from *ca.* 1 to 40 cm across, and pipes, forming sub-vertical features from a few millimetres to 40 cm wide and up to tens of metres high. In three dimensions, the pipes are cylindrical in form, or are elongated to form channels. By analogy with experimental observations, pods and pipes are interpreted to form within 'fluid' and 'stiff' matrices, respectively, i.e. the former are features preserved from the moving flow and the latter were formed within more rigid parts of the moving flow or after the flow had come to rest.

In addition, from published fluidization studies (reviewed in Wilson 1981), it can be predicted that large clasts in strongly fluidized systems will act as nuclei for bubbling and hence create segregation bodies around them. This is seen in the ignimbrite where large lithics and pumices in type-3 sections are often coated in a thin fines-free sheath of crystals and lithics. Most carbon fragments also show this feature; however, instead of merely concentrating a pre-existing gas flow, the carbon itself has produced the gas.

All the above segregation structures were generated while the flow was still moving or had just come to rest. Their distribution within the ignimbrite is described in the relevant field descriptions. Other secondary segregation structures are very common where water gained access to the still-hot ignimbrite (Paper I, §5). Several segregation bodies in the ignimbrite were sampled, along with their host material, to examine the processes involved during segregation (sample and locality details are in Wilson (1981)). Data from these samples lead to the following conclusions:

First, all the segregation bodies are fines-depleted with respect to their hosts (figure 68). In most cases, only fine material ($\leqslant \frac{1}{8}$ mm) has been lost.

Second, all the segregation bodies are enriched in crystals and lithics with respect to their hosts (figure 68), the degree of enrichment being greatest in the largest segregation bodies.

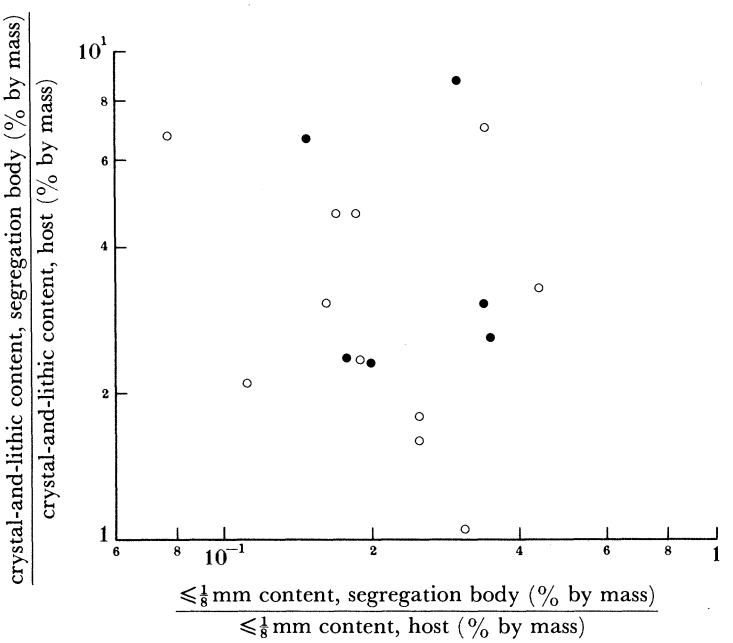

FIGURE 68. Comparison of the relative degrees of fines depletion and crystal-plus-lithic enrichment in small-scale segregation bodies relative to their hosts: •, segregation bodies associated with carbonized vegetation; ○, segregation bodies found independently of carbonized vegetation.

Experimental observations (Wilson 1984) suggest that crystals and lithics would segregate out evenly; this is tested by plotting the relative amounts of crystal- and lithic-enrichment in the segregation bodies (figure 69). In segregation bodies generated *in situ* (above and around carbonized vegetation), crystals and lithics are equally enriched relative to the host. In segregation bodies found independently of carbonized vegetation, contamination by material

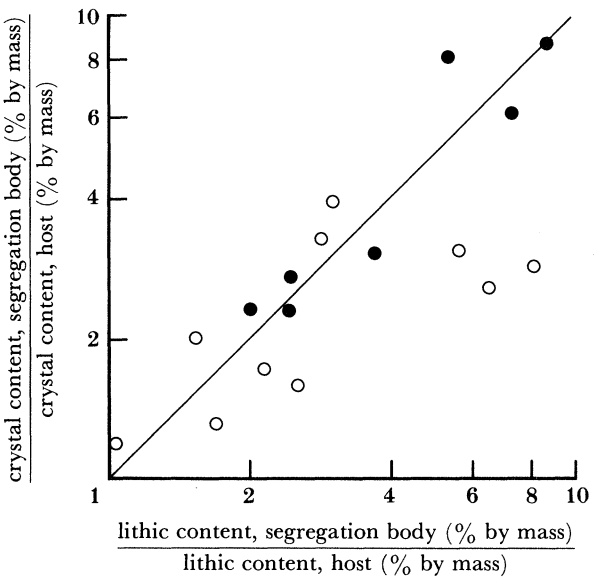

FIGURE 69. Comparison of the relative degrees of crystal and lithic enrichment in segregation bodies relative to their hosts. Symbols are as in figure 68.

with a different crystal:lithic ratio appears to have occurred, though possibly the gas velocities were high enough to alter the crystal:lithic ratio (see figure 64).

Third, the segregation bodies are always coarser than their hosts, usually by about 1.5ϕ (figure 70*a*) and, with one exception, have very uniform σ_I values between 1.5 and 2.1 (figure 70*b*). Essentially identical relationships were reported by Walker (1971).

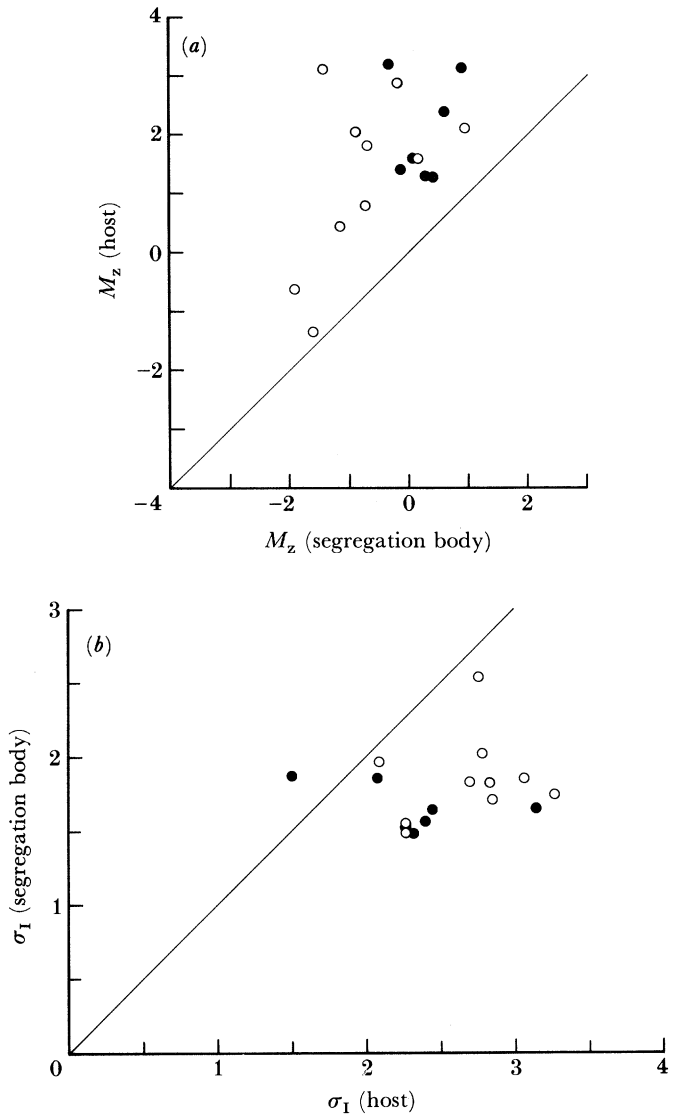

FIGURE 70. Comparison of (*a*) M_z and (*b*) σ_I data from segregation bodies and their hosts. Symbols are as in figure 68.

The relationships between the segregation bodies and their hosts are very similar to those between the ground layer and the least fines-depleted jetted deposits at the same distance from vent (see, for example, Walker 1971). The ground layer and segregation bodies are both fines depleted, crystal- and lithic-enriched, and have M_z about 1.5 ϕ coarser than their known or inferred hosts, though in segregation bodies the amounts of crystal and lithic enrichment were

seemingly limited by the size of the structures and the lower inferred gas velocities. In general, the larger the segregation body, the more closely its nature approaches that of the ground layer at the same distance from vent.

(*b*) *Medium-scale structures*

Medium-scale structures are very common in the ignimbrite and appear in three situations.

First, on the upvent side of many obstacles the ignimbrite contains a greater abundance of pipes and pods which are, from their distribution, evidently generated by transient violent degassing as the flow impacted into the obstacle.

Second, local gas sources may generate fluidization structures (especially within layer 2) that are superimposed on the overall fluidization grading of the deposit (see below). For example, where carbonized vegetation is locally abundant, large patches of fines-depleted material occur around and above the carbon, and an upper segregation layer may sometimes be preserved. Where the hot ignimbrite was flooded by water, large patches of the deposit are shot through with pipes and the host material is rather fines-depleted and friable.

Third, and most important, are those fluidization structures generated by residual gas flow rates inherited from the moving flow, forming the three types of fluidization grading proposed by Wilson (1980); these are discussed in Wilson (1981) and Wilson & Wright (1985) and only summarized here. In this ignimbrite, sections of all three fluidization types are present; all the jetted deposits are of type 3, while the VPI can be of types 1, 2 or 3, with the particular types occurring at particular ranges from vent (figure 5).

Type 1 sections occur in the VPI in many proximal (less than 20 km) and distal (more than 60 km) localities. In the proximal sections, the absence of fluidization-induced grading is though to be related to the turbulent, expanded state or high velocities of the flow, or both. In the distal sections, the absence of grading is interpreted to be a result of the relatively good sorting of the flow (figure 45). In laboratory experiments, material with $\sigma_I \lesssim 1.5$ could undergo strong fluidization and yet leave little trace of the former presence of high gas velocities. This is because material of these sorting characteristics has a high proportion of its weight supported by the gas flow at high gas velocities (Wilson 1984, figure 11); as a result, the material is very 'fluid' and any segregation bodies can be remixed into the material. The distal layer 2 is in itself thought to be a vast segregation layer derived from the whole flow, and hence the frequent absence of segregation structures, including layer 2c, is interpreted to be a direct result of the sorting characteristics of the material and does not at all reflect on the strength of the fluidization within it.

Sections of types 2 and 3 are widespread in the VPI (figure 5). In layer 2b, a downward enrichment in lithics is often poorly developed, but an upward enrichment in pumice is ubiquitous, at its extreme forming the PCZ. Two types of PCZ are recognized (§5(*b*)(ii)), one associated with type 2 sections and produced by pumice rising through a non-bubbling matrix, the other with type 3 sections where the ascent of pumice accompanied and was greatly accelerated by bubbling. Layer 2c only occurs above type 3 sections and is the natural analogue to the upper fine/light-material-enriched segregation layer observed in the laboratory.

As first noted by Sparks (1976), the density of the pumice clasts that can be demonstrated to have floated can be used to place constraints on the degree of expansion and overall density of the flow. Pumice clast-density data were obtained for coarse pumices in type 2 and type 3 PCZ units and layer 2c in the Taupo and several other New Zealand ignimbrites (Wilson 1981).

The matrix around the pumices was taken to be represented by the < 2 mm fraction of the relevant samples. Results are listed in table 3; from these, it is concluded that the expansion of the sample matrices, expressed as

$$\frac{(\rho_{\text{matrix}})_{\text{at rest, lightly packed}}}{(\rho_{\text{matrix}})_{\text{during emplacement}}} - 1.0 \times 100\,\%,$$

where ρ is the density, did not exceed 155 % over the lightly compacted state. These maximum expansion (i.e. minimum density) data represent absolute limits for the relevant portions of the deposit, as the matrix forms only part of the deposits (roughly 45–95 % by volume) and

TABLE 3. ESTIMATES OF THE MAXIMUM DEGREE OF EXPANSION OF A MOVING PYROCLASTIC FLOW, DERIVED FROM PUMICE DENSITY DATA

(The pumice density data are from the densest clasts which can be inferred to have floated in the unit. Matrix (< 2 mm material) densities are given for the (column A) loosest-packed and (B) lightly compacted states; columns C and D give the respective maximum degrees of expansion in the moving flow (i.e. where the matrix and floating-pumice densities are the same). For the Earthquake Flat and Rotoiti Breccias and the Waimihia ignimbrite, the type 3 PCZ and layer 2c samples are from the same locality in each deposit. Sample and locality details are in Wilson (1981).)

deposit	unit	pumice density g cm^{-3}	matrix density g cm^{-3} A	matrix density g cm^{-3} B	maximum expansion of matrix (% by vol.) C	maximum expansion of matrix (% by vol.) D
Taupo ignimbrite	type 3 PCZ	0.36	0.65	0.80	81	122
	type 3 PCZ	0.31	0.52	0.66	70	113
	type 3 PCZ	0.29	—	0.72	—	148
	type 3 PCZ	0.38	0.63	0.82	68	119
	type 3 PCZ	0.33	0.60	0.84	82	155
	layer 2c	0.37	0.62	0.75	68	103
	layer 2c	0.26	0.46	0.59	77	127
Earthquake Flat Breccia	type 3 PCZ	0.89	—	1.34	—	51
	layer 2c	0.74	1.07	1.24	45	68
Rotoiti Breccia	type 3 PCZ	0.89	—	1.32	—	48
	layer 2c	0.72	0.87	1.08	21	50
Waimihia ignimbrite	type 3 PCZ	0.60	1.00	1.24	67	107
	layer 2c	0.55	0.88	1.18	60	115

is fine-grained and of low density, so that the amount of expansion per unit gas flow is maximized (Wilson 1984). From this, it is concluded that the overall expansion of the moving-flow material over its at-rest, lightly compacted state (i.e. the ignimbrite) probably never exceeded *ca.* 100 % by volume (see also p. 75, below).

(*c*) *Large-scale structures*

Four fluidization-induced features are developed on such a large scale that they are recognized only by mapping the whole ignimbrite.

First, the relative proportions and the degrees of development of several of the facies or variants within the ignimbrite reflect the nature, extent or strength of fluidization within the flow (§6(*a*)).

Second, the nature and composition of the proximal deposits record the deflation and coalescence of the relatively dilute eruption column mixture into the relatively dense pyroclastic flow, with the attendant loss of fines and enrichment in crystals and lithics (§6(*a*)(i)).

Third, lateral variations in grainsize and composition shown by some of the facies in the ignimbrite are related to the overall degree of fluidization within the flow beyond *ca.* 20 km from vent; either directly, like the contents of fines, crystals and lithics in the jetted deposits and layer 2, or indirectly, like the crystal:lithic ratios in the ground layer (§6(*b*)).

Fourth, some regional variations in the ignimbrite reflect differences in the fluidization intensity about the vent. Most clearly defined of these is the outcrop area of FDI, which coincides with the area where large amounts of fresh vegetation were overridden by the flow (Walker *et al.* 1980*a*).

10. Discussion and conclusions

The Taupo ignimbrite represents the end product of a single vent-generated flow, and provides a direct analogue for single flow unit ignimbrites, or individual flow units within compound deposits (Wright 1981).

(*a*) *Distribution and palaeovelocities*

On an overall scale, the ignimbrite is a type example of deposits termed low-aspect-ratio ignimbrites, which are characterized by being extremely widespread for a given volume of material (Walker *et al.* 1980*b*). Height-climbed data suggest that the flow probably exceeded 250–300 m s^{-1} near vent, which are the highest velocities yet inferred for a pyroclastic flow, although theory suggests that this may not be unusual (Sparks *et al.* 1978). Estimates of absolute-minima velocities of 60–160 m s^{-1} are inferred from several other ignimbrites (see, for example, Yokoyama 1974; Sparks 1976; Francis & Baker 1977; Miller & Smith 1977; Barberi *et al.* 1978; Okada & Yokoyama 1982), and the 1980 Mount St Helens blast was observed to propagate at velocities locally exceeding 150 m s^{-1} (Moore & Sisson 1981).

Field evidence implies that on hilly interfluves the flow moved at high velocities right to its distal limits, and terminated only where it ran out of material. This in turn implies that the energy-line concept for predicting distances travelled by pyroclastic flows and surges (Malin & Sheridan 1982) cannot be applied in this and analogous examples because the range of the flow is controlled by its volume, not its velocity.

The violence of the Taupo flow is attributed to the extremely high inferred magma eruption rate of *ca.* 3×10^7 m^3 s^{-1} (Wilson & Walker 1981). This rate is one to two orders of magnitude above those inferred for comparable or larger ignimbrite-producing eruptions (see, for example, Curtis 1968; Wilson 1978, Ninkovich *et al.* 1978; Ledbetter & Sparks 1979; Rampino & Self 1982), but these represent longer sustained events. To illustrate this, the overall magma eruption rate during the ignimbrite-generating phase of the 1883 Krakatau eruption was *ca.* 3×10^5 m^3 s^{-1} (Self & Rampino 1981), but during four major ignimbrite-generating pulses the eruption rate probably approached 10^7 m^3 s^{-1} for a few tens of seconds (S. Self, personal communication). Taupo-like events (in terms of eruption rates) may well prove to be not unusual, the problem being that when of small volume the products are so widespread that they have little chance of preservation, and when of large volume the violently emplaced deposits may be masked by earlier or later material, or both. For example, a flow unit within a large *ca.* 20000 year old ignimbrite in New Zealand (Self 1983) is relatively widespread (its parent flow surmounted barriers more than 600 m high) but forms only one flow unit within a thick, compound, high-aspect ratio deposit in areas close to vent (author's unpublished data).

(*b*) *Origins of the facies*

Facies developed in the ignimbrite are related to the Sparks *et al.* (1973) ignimbrite layering scheme, as modified by Wilson & Walker (1982) and in this paper (figure 71). The three-layer terminology of Sparks *et al.* (1973) is retained (cf. Fisher 1979), and interpreted genetically (Wilson & Walker 1982) as *layer 1*: deposits resulting from processes operating within or in advance of the flow head; *layer 2*: deposits of the flow body and tail; *layer 3*: deposit of the dilute ash cloud overlying the pyroclastic flow proper (Sparks & Walker 1977).

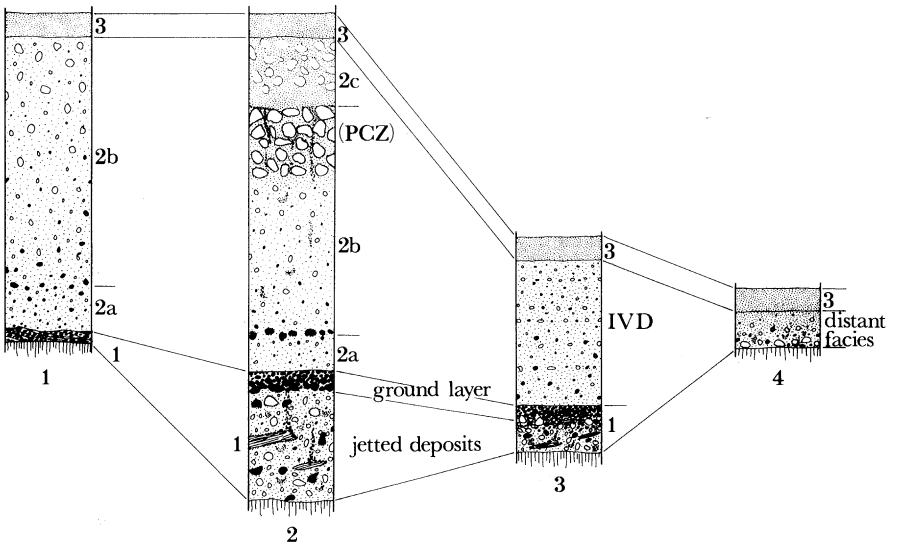

FIGURE 71. Schematic diagram showing relationships between the layering scheme of Sparks *et al.* (1973) (column 1 and some idealized typical stratigraphic columns from the Taupo ignimbrite: 2, type-3 VPI; 3, IVD; 4, the distant facies.

At Taupo, the layer 1 deposits are demonstrably derived from the same flow as layer 2 (see, for example, figure 67) and cannot represent a separate vent-derived deposit (cf. layer a of Fisher (1979); Froggatt (1981)). No evidence is seen of ash-cloud surges (layer c of Fisher (1979)) above the ignimbrite; however, they may be masked by secondary phreatic deposits.

(*c*) *Lateral variations in facies development*

Lateral variations in facies development relate primarily to differences between the nearer-vent (less than 20–25 km) and more distal depositional régimes.

In proximal areas, features in layers 1 and 2 suggest that they were deposited from a turbulent, more dilute flow that was still in the processes of deflating and coalescing from the collapsing eruption column. At all exposures, the flow generated separate layers 1 and 2, but until beyond 12–13 km was unable to generate jetted deposits, and was dilute enough to hug the ground surface very effectively and generate dune-like bedforms on level ground. Beyond 12–13 km, not only do jetted deposits appear, but also the 'conventional' fines-free ground layer, a compositionally-zoned IVD containing lee-side lenses and a VPI showing fluidization-induced grading structures. The 12–13 km mark is the crucial boundary between what is in effect a laterally moving eruption column nearer vent and a dense pyroclastic flow beyond, although the deflation process continued as far out as 20–25 km as marked by the outer limits

of the fines-bearing ground layer, an IVD which contains lithic-rich lenses and lacks lee-side lenses and a compositional zonation, and type 1 sections in the VPI (figure 5).

Two features seen in the near-vent Taupo ignimbrite have been recorded from other deposits. First, fines-bearing lithic-rich lag-breccias or lag-fall deposits have been documented as an extremely near-vent facies (Wright & Walker 1977, 1981; Wright 1979; Druitt & Sparks 1982). Second, large-scale dune-like bedforms with associated lee-side lenses occur in the proximal veneer deposits of the May 1980 ignimbrite at Mount St Helens (T. C. Moyer, personal communication; author's own observations).

The characteristics of layers 1 and 2 beyond 12–13 km from vent are, after allowing for the generation of unusual facies due to the extreme violence of the flow, typical of other ignimbrites. The proximal Taupo ignimbrite thus shows what depositional and grainsize characteristics would result if pyroclastic flows were dilute and turbulent, and demonstrates that most ignimbrites yet documented in adequate enough detail were deposited by dense pyroclastic flows (see also §10(*f*)(iii)).

(*d*) *Lateral variations of parameters*

All the facies in the Taupo ignimbrite show great lateral variations in grainsize and compositions, which exceed those in any documented ignimbrites (see, for example, Williams 1942; Kuno *et al.* 1964; Fisher 1966; Yokoyama 1974; Sparks 1975; Wright 1981).

The lateral variations in layer 2, which forms the bulk of the ignimbrite, are primarily modelled by considering the flow by *ca.* 20 km from vent to consist of a gigantic fluidized bed (figure 59) which is moved sideways and has material removed from its base to generate layer 2 (figure 60). After allowing for the effects of local processes such as shearing-induced grading, the erosion and incorporation of layer 1 material, and fluidization grading, this model closely accounts for all of the lateral variations in the nature of layer 2. In particular, the fine-grained pumiceous nature of layer 2 beyond *ca.* 60 km from vent is explained by its being the deposit of a fine/light-material-enriched segregation layer developed above the moving flow.

There are two extreme interpretations of how this model was represented in the actual flow: first, that at *ca.* 20 km from vent the flow was fully layered, as in the model system, and, second, that the zonation in the flow was gradually developed by air ingestion fluidization during emplacement (figure 66). Evidence for the former includes the presence of stranded PCZ material at *ca.* 13 km from vent and the abruptness of the changes in grainsize and composition in layer 2b at 55–60 km. Evidence for the latter includes the interpretation of the ground layer as a segregation deposit formed complementary to the upward movement of pumice in the flow, and the gradual nature of the changes seen in the ignimbrite at high altitudes. From this it is concluded that at least some zonation had been induced in the flow by *ca.* 13 km from vent, but that much of the zonation was gradually generated as the flow was moving (figure 66).

In layer 1, the jetted deposits largely follow layer 2 in their lateral changes, but differ in some respects. The parameters in which the jetted deposits closely mimic the changes in layer 2 are those most dependent on the flow composition; conversely, where the two layers differ, the relevant parameters are controlled by kinetic processes related to the flow régime or fluidization (§10(*f*)(i)). Thus the jetted deposits become much richer in fines and pumice outwards, and show sharp changes in composition, but not sorting, at 55–60 km from vent. Lateral variations in the ground layer are strongly controlled by fluidization processes and only dimly reflect the flow composition.

From the interrelationships between layers 1 and 2 it is inferred that the front part of the flow was erupted with a higher proportion of very coarse lithics and a higher total lithic content than the bulk of the flow. As the flow travelled, this coarser, lithic-richer material was depleted by deposition and diluted by other material moving in from the flow behind until, in the outer reaches of the flow (70–80 km), the flow head contained only slightly more, and coarser, lithics than the body (figure 10 and cf. figures 63 and 65).

(*e*) *Regional variations*

Part of the scatter in lateral variations of some parameters is attributable to regional differences in the nature of the flow; it was erupted with a higher crystal:lithic ratio and denser pumice to the north and northeast than to the south and southwest (figure 67). These variations are similar in the jetted deposits, IVD and layer 2b, demonstrating that these facies must have been derived from the one flow, and that the jetted deposits cannot represent an earlier vent-generated flow unit (cf. Froggatt 1981). Heat alteration colours (figure 28) and the largest pumices in layer 2 (figure 40) are also asymmetrically distributed. Similar relationships in maximum pumice sizes are recorded in some Japanese ignimbrites (Kuno *et al.* 1964; Yokoyama 1974), for reasons which are similarly uncertain.

Variations in the range of the Taupo flow are largely attributed to either differences in the amounts erupted or variations in the average thicknesses of the deposits in different directions. This is in contrast to most other documented flows, whose ranges were determined by their kinetic energy, which flowed the furthest down the easiest pathway (e.g. Katmai: (Curtis 1968)).

Changes in the ignimbrite at high altitudes are explained by supposing that the upper, more fines- and pumice-rich part of the flow (which travelled further from vent) was more mobile and preferentially climbed the mountains. Similar features are seen in the Campanian ignimbrite (Barberi *et al.* 1978).

(*f*) *Fluidization processes*

(i) *Fluidization structures*

The recognition of fluidization-induced structures in the ignimbrite allows direct comparisons to be made with results from laboratory experiments. First, it can be predicted that the sorting parameters in any ignimbrite material undergoing strong (type 3) fluidization will try to attain values ($\sigma_I < 1.5$) at which a high proportion of the material weight is supported by the gas flow (Wilson 1984, figure 11). Facies in the Taupo ignimbrite which have undergone strong fluidization follow this prediction quite closely; the ground layer and distal layer 2 deposits approach or reach this level of good sorting (figures 19 and 45), while the matrix of layer 2c and segregation bodies in the ignimbrite approach but do not quite reach it (figures 45 and 70). Laboratory experiments thus fairly closely predict the sorting parameters of natural fluidized systems despite the gross differences in ambient conditions.

Second, it appears from the laboratory experiments that the density contrasts between crystals and lithics are less important than grainsize differences in promoting their segregation, at least in poorly sorted samples ($\sigma_I > 1.5$). In the ignimbrite this relationship holds, provided that differences in the overall grainsize distributions of the crystals and lithics are taken into account. For example, small-scale segregation bodies, especially those demonstrably formed *in situ*, have generally similar crystal:lithic ratios to their hosts (figure 69), whereas this does not

hold for the ground layer, which is richer in lithics owing to the very strong fluidization during its genesis (figure 64).

Third, an upper fine/light-material-enriched segregation layer above type 3 deposits, which was predicted from experimental studies (Wilson 1980), is recognized in the field and termed layer 2c. Its characteristics conform to predictions from the laboratory experiments; it is sharply demarcated from layer 2b, very pumice rich, and generally free of internal small-scale fluidization structures. The presence of coarse floating-phase pumices, although making the overall sorting much poorer, does not induce strong segregation, probably because the pumices were neutrally or positively buoyant and easily moved around in response to gas flow processes.

(ii) *Gas sources*

Some inferences can be made of the relative importance of various gas sources (Wilson 1980) in the fluidization history of the Taupo flow.

Gases trapped during flow formation. The inference that the flow must have become partially zoned with respect to grainsize and composition by *ca.* 13 km from vent implies that high gas flow rates associated with the transition from eruption column to pyroclastic flow were responsible for this.

Air ingested at the flow front is interpreted to have been directly responsible for the generation of the jetted deposits and ground layer and, by inference, much of the large-scale fluidization grading within the flow that generated such features as the distal fines- and pumice-rich ignimbrite.

Gases supplied by carbonized vegetation were demonstrably responsible for the generation of all but a small amount of FDI from the jetted deposits, and also for producing local fines-depleted patches in layer 2. Many small-scale segregation structures in the ignimbrite were generated after emplacement by gases from included logs and branches.

Gases supplied by ground- and surface-water were responsible for secondary fluidization effects where the hot ignimbrite was flooded by water; they do not appear to have significantly influenced the primary emplacement behaviour of the flow.

Gases supplied by fragmentation of clasts do not appear to have been significant, as data from deposits of the most strongly sheared parts of the flow suggest that relatively little comminution occurred (§6(*b*)(i)).

Gases supplied by exsolution from juvenile clasts were suggested as being potentially important in pyroclastic flows (Sparks 1978). However, two facts suggest that this contribution was insignificant here. First, the fluidization history of the ignimbrite is explicable if the gases concerned were solely supplied by other sources. Second, Sparks's (1978) analysis predicts that, all other conditions being equal, the thicker the deposit the higher the maximum gas flow rate at the top of the unit; this does not hold, as the palaeo-fluidization states of the VPI sections are unrelated to their thicknesses. New data obtained by R. S. J. Sparks (personal communication) suggests that pumice degassing may occur much more rapidly than suggested in Sparks (1978) and hence exsolved gases would contribute mainly to gas flow rates in the collapsing eruption column.

It thus appears that the most important gas source in the ignimbrite was air ingested by the moving flow.

Several authors (e.g. Anderson & Flett 1903; Lacroix 1904; Fenner 1923; Reynolds 1954; McTaggart 1960) have suggested that pyroclastic flows owe their great mobility to fluidization.

At Taupo, this suggestion, is, to a first approximation, incorrect in that it can be inferred that the strongly fluidized nature of the flow (due largely to air ingestion) and its remarkable mobility are both products of its high emplacement velocities, which in turn are attributed to an extreme eruption rate (Wilson & Walker 1981). Lesser effects of fluidization on the mobility of the flow might be seen in the late-stage drainage of material down slopes or valleys after the main emplacement event, but this is of minor importance in this case.

(iii) *Density and degree of expansion of the flow*

Two opposing opinions have arisen on the nature of pyroclastic flows. Some consider the distribution characteristics of ignimbrites and the apparent ability of pyroclastic flows to cross high mountain ranges to indicate that the flows are very thick and dilute, and cross the ranges by flooding over them (see, for example Ono 1965; Aramaki & Ui 1966; Yokoyama 1974; Suzuki & Ui 1982). Others, from the similarity of ignimbrites to other sedimentary high-particle-concentration deposits, consider them to be relatively dense and little expanded, and relate their distribution to high velocities imparted at source (see, for example, Sparks 1976; Francis & Baker 1977; Miller & Smith 1977). The importance of using the densities of pumice clasts that had demonstrably floated towards the top of an ignimbrite flow unit as indicators of the minimum density (i.e. maximum expansion) of the parent flow was recognized by Sparks (1976). However, a major problem is that such features could conceivably be generated by residual gas flow rates after the (possibly highly expanded) flow had come to rest. More recent data help resolve this problem.

First, laboratory data suggest that even at very high gas velocities ignimbrite materials are not highly expanded because of severe channelling, this process being controlled by the poor sorting of the samples (Wilson 1984).

Second, the recognition of fluidization-induced flow types and facies, notably layer 2c, enable those portions of the ignimbrite that were most strongly fluidized during emplacement to be identified (Wilson 1980; Wilson & Walker 1982; this paper).

Third, it can be inferred that some features, such as the stranded type-3 PCZ material and distal ($\geqslant$ 60 km) layer 2 deposits, were generated by processes acting on the thickness of the whole flow (Wilson & Walker 1982; this paper).

These data mean that pumice density data can be confidently used, knowing that the resulting deductions regarding the flow densities apply, at least in the third case above, to the active pyroclastic flow.

The data in table 3 show that beyond 20 km from vent the Taupo flow material was probably not more than *ca.* 50% expanded over its loose-packed, non-fluidized condition, i.e. *ca.* 100% expanded over its final compacted state, and had a bulk-density of *ca.* 0.3–0.6 g cm^{-3} (compared with 0.6–1.2 g cm^{-3} for the lightly packed bulk-density of the ignimbrite). Note however that these data cannot necessarily be used to infer the thickness of the parent flow from thickness measurements on the ignimbrite. At Taupo the parent flow was demonstrably much thicker than the deposits which is laid down (Wilson & Walker 1982) so, for example, a 100 m thick flow might leave behind a 10 m thick layer 2 deposit which would then deflate to form at least 5 m of ignimbrite. Two further points can be made from table 3. First, there are no systematic differences between data from, for example, layer 2c and the distal layer 2 deposits, suggesting that inferences about flow expansion derived from measurements on *in situ* fluidization structures do reflect the fluidization state of the flow as a whole. Second, limited

data from other New Zealand ignimbrites show that the strongly fluidized Taupo flow was the most highly expanded and thus the Taupo data appear to form one extreme for other ignimbrite-producing pyroclastic flows. These inferences strongly imply that the relatively dense and poorly expanded pyroclastic flow model (Sparks 1976) is the correct one for ignimbrites.

(*g*) *Depositional models and flow régimes*

Two contrasting depositional models have been presented for pyroclastic flows, one invoking layer-by-layer deposition (Fisher 1966, 1979), the other considering an ignimbrite to represent merely the flow that has come to rest (Sparks 1976). The Taupo ignimbrite shows features both compatible and incompatible with both models (Wilson & Walker 1982) and in doing so reconciles them. The thickness and disposition of the ignimbrite demonstrate that it was emplaced by a relatively dense flow whose thickness was of the order 10–100 times that of the IVD (Wilson 1981), consistent with the Fisher model. However, structures in the VPI are only consistent with their final emplacement as flows little thicker (because of fluidization expansion) than the modern deposit, as in the Sparks model. It is thus concluded that the more violently emplaced a flow is, and the lower the aspect ratio of its deposit, the closer it will follow the Fisher model (i.e. tend towards being entirely an IVD plus any layer 1 deposits) and the less violently emplaced, the closer it will follow the Sparks model. From this it follows that the thickness of the parent flow cannot be simply related to the thickness of the ignimbrite; only the density of the former can be limited from pumice density data.

Turbulence, analogous to the high Reynolds number instability in normal fluids, is often assumed to be present in pyroclastic flows, but more recent work suggests that it may not be present (Sparks 1976; Wright & Walker 1977, 1981). In the Taupo flow, four main kinds of turbulence are thought to have been of importance in influencing the deposition and characteristics of the ignimbrite.

First, in laboratory experiments, the turbulence induced by strong fluidization tends to remix the samples because of the presence of bubbling (Wilson 1984). However, with poorly sorted materials ($\sigma_I > 1.5$), the segregation accompanying bubbling dominates such that bubbling-induced turbulence is incapable of completely remixing the material. In the Taupo flow this kind of turbulence is inferred to have been strongest in the flow head, accompanying air ingestion. The presence of the ground layer demonstrates that this turbulence did not wholly remix the head, but the poorer sorting of the jetted deposits compared to layer 2 (§7) indicates that turbulence succeeded in preventing complete segregation of the head material. In the distal better sorted deposits, bubbling-induced turbulence was probably important in type 1 VPI sections by mixing in segregation bodies (§10(*a*)).

Second, the irregular nature of the ground surface traversed by the flow has induced turbulence, most notably in the jetted deposits, where very efficient mixing with vegetation occurred, and in the lee-side structures seen in the IVD.

Third, high shear-strain rates at the base of and below the flow body produced another kind of turbulence which resulted in the erosion and incorporation of material from layer 1 and underlying deposits into the base of layer 2. This mixing appears to have occurred regardless of the overall flow régime at the base of layer 2, and its efficiency depends largely on the nature of the substrate (§5(*b*)).

Fourth, substitution of plausible values for relevant parameters in the Reynolds number equation (see Sparks 1976, p. 177) suggests that turbulence due to an overall kinetic instability

would have been widespread in the Taupo flow. Indeed, the kinetic model adopted for the Taupo flow (figure 66) is based on laboratory studies of high Reynolds number gravity flows (see Wilson 1980). However, the fact that the overall grainsize and compositional variations in the ignimbrite beyond *ca.* 20 km from vent are closely matched by the fluidized-bed model suggests that strong high-Reynolds-number turbulence may have been absent or was ineffective in the flow body. Two reasons are inferred for this; first, the fluidization grading would have introduced a large, stable density gradient within the flow, which would have strongly suppressed mixing on a whole-flow scale and, second, the high solids concentration of the flow would have tended to dampen out any disturbances small enough not to be influenced by the density gradient. On the other hand, the contrasting nature of layer 2 at exposures less than and greater than *ca.* 13 km from vent suggests that strong turbulence of this kind was present near vent. Closer to vent than *ca.* 13 km, the more expanded nature of the flow, coupled with the nature of the transition from eruption column to pyroclastic flow, kept the flow turbulent and almost completely mixed (except for material deposited as the ground layer). Once the flow had partly deflated, become less expanded and contained a stable density gradient, large-scale turbulent mixing induced by kinetic instability is though to have been suppressed in the flow body. In this case, the clear demarcation between the near-vent and remaining deposits suggests that these relationships may hold for other ignimbrites, and that the deposits of fully turbulent pyroclastic flows will only be found in the immediate vicinity of the vent.

(*h*) *The anarchy of ignimbrites*

The work on the Taupo ignimbrite shows that the rapid eruption of n km^3 of pyroclastic material, of composition x% pumice, y% crystals and z% lithics, yields many different rock types of greatly differing appearance, and grainsize and compositional characteristics. In theory the whole suite of deposits generated by a single pyroclastic flow could be studied, and their volumes and compositions recombined to yield an estimate of the original nature of the erupted material at any point, but in practice it is doubtful if this can ever be done.

In the Taupo ignimbrite, a first approach to estimating the nature of the originally erupted material is made by extrapolating some parameters in the near-source deposits back towards the vent (figure 57). From this and the nature of the processes involved in generating the various facies in the ignimbrite it is evident that the grainsize and composition of any part of the deposit are not simply related to the values of these parameters in either the parent flow or the original eruptive mixture (see, for example, Wilson & Walker 1982, figure 7). Similarly, the mechanical processes involved in generating the facies in the ignimbrite are such that the thickness of any facies at any point is not simply related to the thickness of the parent flow, although the fluidization state of the flow may be inferred.

In short, this work illustrates what may be termed the anarchy of ignimbrites, namely that the deposits seen at any given exposure bear no simple relationship to the thickness, grainsize distribution or composition of the parent flow. Only detailed work, covering a fair extent or the whole of an ignimbrite will begin to define its characteristics adequately, and hence allow some inferences to be made about the nature of the parent flow. Whether the great variations shown by the Taupo ignimbrite are unusual, or are eventually revealed to be commonplace, is something that will only be demonstrated with much more detailed work.

This study was initiated and largely supervised by G. P. L. Walker and I am greatly indebted to him for his help, encouragement and support in this work. For their help at various stages and in various ways I am grateful to many, particularly J. H. Dare, A. M. C. Davis, J. H. Latter, M. O'Grady, R. J. Pike, D. L. Pryor, S. Self, I. E. M. Smith, R. S. J. Sparks, J. Sutton, J. V. Watson, T. H. Wilson and J. V. Wright. R. S. J. Sparks is thanked for his encouragement and careful and critical reviews of the manuscript. The use of facilities at the U.S. Geological Survey at Menlo Park, California and the assistance of R. Kadish in the early stages of preparation of this paper are gratefully acknowledged. Generous financial support for this work came from the N.E.R.C. (research studentship) and the Royal Society (Mr and Mrs John Jaffé Donation Research Fellowship).

References

Anderson, T. & Flett, J. S. 1903 Report on the eruptions of the Soufrière in St Vincent, and on a visit to Montagne Pelée in Martinique. *Phil. Trans. R. Soc. Lond.* A **200**, 353–553.

Aramaki, S. & Ui, T. 1966 The Aira and Ata pyroclastic flows and related calderas and depressions in southern Kyushu, Japan. *Bull. volcanol.* **29**, 29–47.

Bagnold, R. A. 1954 Experiments on a gravity-free dispersion of large solid spheres in a Newtonian fluid under shear. *Proc. R. Soc. Lond.* A **225**, 49–63.

Barberi, F., Innocenti, F., Lirer, L., Munno, R., Pescatore, T. & Santacroce, R. 1978 The Campanian Ignimbrite: a major prehistoric eruption in the Neapolitan area (Italy). *Bull. volcanol.* **41**, 10–31.

Benjamin, T. B. 1968 Gravity currents and related phenomena. *J. Fluid Mech.* **31**, 209–248.

Curtis, G. H. 1968 The stratigraphy of the ejecta from the 1912 eruption of Mount Katmai and Novarupta, Alaska. In *Studies in volcanology* (ed. R. R. Coats, R. L. Hay & C. A. Anderson), *Geological Soc. Am. Mem.* **116**, 153–210.

Druitt, T. H. & Sparks, R. S. J. 1982 A proximal ignimbrite breccia facies on Santorini, Greece. *J. Volcanol. geotherm. Res.* **13**, 147–171.

Fenner, C. N. 1923 The origin and mode of emplacement of the great tuff deposit in the Valley of Ten Thousand Smokes. *Natn. geog. Soc. Contrib. Tech. Pap. Katmai Ser.*, **I**.

Fisher, R. V. 1966 Mechanism of deposition from pyroclastic flows. *Am. J. Sci.* **264**, 350–363.

Fisher, R. V. 1979 Models for pyroclastic surges and pyroclastic flows. *J. Volcanol. geotherm. Res.* **6**, 305–318.

Folk, R. L. & Ward, W. C. 1957 Brazos River bar, a study in the significance of grain-size parameters. *J. sediment. Petrol.* **27**, 3–26.

Francis, P. W. & Baker, M. C. W. 1977 Mobility of pyroclastic flows. *Nature, Lond.* **270**, 164–165.

Froggatt, P. C. 1981 Stratigraphy and nature of Taupo Pumice Formation. *N.Z. Jl Geol. Geophys.* **24**, 231–248.

Inman, D. L. 1952 Measures for describing the size distribution of sediments. *J. sediment. Petrol.* **22**, 125–145.

Kuno, H., Ishikawa, T., Katsui, Y., Yagi, K., Yamasaki, M. & Taneda, S. 1964 Sorting of pumice and lithic fragments as a key to eruptive and emplacement mechanisms. *Jap. J. Geol. Geogr.* **35**, 223–238.

Lacroix, A. 1904 *La Montagne Pelée et ses eruptions*. France: Paris, Masson et Cie.

Ledbetter, M. T. & Sparks, R. S. J. 1979 Duration of large magnitude explosive eruptions deduced from graded bedding in deep sea ash layers. *Geology* **7**, 240–244.

McTaggart, K. C. 1960 The mobility of nuées ardentes. *Am. J. Sci.* **258**, 369–382.

Malin, M. C. & Sheridan, M. F. 1982 Computer-assisted mapping of pyroclastic surges. *Science, N.Y.* **217**, 637–640.

Miller, T. P. & Smith, R. L. 1977 Spectacular mobility of ash flows around Aniakchak and Fisher calderas, Alaska. *Geology* **5**, 173–176.

Moore, J. G. & Sisson, T. W. 1981 Deposits and effects of the May 18 pyroclastic surge. In *The 1980 eruptions of Mount St Helens, Washington* (ed. P. W. Lipman & D. R. Mullineaux), *U.S. geol. Surv. Prof. Pap.* **1250**, 421–438.

Ninkovich, D., Sparks, R. S. J. & Ledbetter, M. T. 1978 The exceptional magnitude and intensity of the Toba Eruption, Sumatra: an example of the use of deep-sea tephra layers as a geological tool. *Bull. volcanol.* **41**, 286–298.

Okada, H. & Yokoyama, S. 1982 Discovery and significance of Osumi pumice fall and Ito pyroclastic flow deposits within Onami-Ike Crater, Kirishima Volcano. *Bull. volcanol. Soc. Jap.* **27**, 67–69.

Ono, K. 1965 Geology of the eastern part of Aso Caldera, central Kyushu, southwestern Japan. *J. geol. Soc. Jap.* **71**, 541–553.

Rampino, M. R. & Self, S. 1982 Historic eruptions of Tambora (1815), Krakatau (1883), and Agung (1963), their stratosphere aerosols, and climatic impact. *Quat. Res.* **18**, 127–143.

Reynolds, D. L. 1954 Fluidization as a geological process, and its bearing on the problem of intrusive granites. *Am. J. Sci.* **252**, 577–614.

Self, S. 1983 Large scale phreatomagmatic silicic volcanism: a case study from New Zealand. *J. Volcanol. geotherm. Res.* **17**, 433–469.

Self, S. & Rampino, M. R. 1981 The 1883 eruption of Krakatau. *Nature, Lond.* **294**, 699–704.
Simpson, J. E. & Britter, R. E. 1979 The dynamics of the head of a gravity current advancing over a horizontal surface. *J. Fluid Mech.* **94**, 477–495.
Sparks, R. S. J. 1975 Stratigraphy and geology of the ignimbrites of Vulsini Volcano, central Italy. *Geol. Rdsch.* **64**, 497–523.
Sparks, R. S. J. 1976 Grain size variations in ignimbrites and implications for the transport of pyroclastic flows. *Sedimentology* **23**, 147–188.
Sparks, R. S. J. 1978 Gas release rates from pyroclastic flows: an assessment of the role of fluidization in their emplacement. *Bull. volcanol.* **41**, 1–9.
Sparks, R. S. J., Self, S. & Walker, G. P. L. 1973 Products of ignimbrite eruptions. *Geology* **1**, 115–118.
Sparks, R. S. J. & Walker, G. P. L. 1973 The ground surge deposit: a third type of pyroclastic rock. *Nature (phys. Sci.), Lond.* **241**, 62–64.
Sparks, R. S. J. & Walker, G. P. L. 1977 The significance of vitric-enriched airfall ashes associated with crystal-enriched ignimbrites. *J. Volcanol. geotherm. Res.* **2**, 329–341.
Sparks, R. S. J., Wilson, L. & Hulme, G. 1978 Theoretical modelling of the generation, movement and emplacement of pyroclastic flows by column collapse. *J. geophys. Res.* **83**, 1727–1739.
Suzuki, K. & Ui, T. 1982 Grain orientation and depositional ramps as flow direction indicators of a large-scale pyroclastic flow deposit in Japan. *Geology* **10**, 429–432.
Walker, G. P. L. 1971 Grain size characteristics of pyroclastic deposits. *J. Geol.* **79**, 696–714.
Walker, G. P. L. 1972 Crystal concentration in ignimbrites. *Contr. Miner. Petr.* **36**, 135–146.
Walker, G. P. L., Heming, R. F. & Wilson, C. J. N. 1980*b* Low-aspect ratio ignimbrites. *Nature, Lond.* **283**, 286–287.
Walker, G. P. L., Self, S. & Froggatt, P. C. 1981*a* The ground layer of the Taupo ignimbrite: a striking example of sedimentation from a pyroclastic flow. *J. Volcanol. geotherm. Res.* **10**, 1–11.
Walker, G. P. L. & Wilson, C. J. N. 1983 Lateral variations in the Taupo ignimbrite. *J. Volcanol. geotherm. Res.* **18**, 117–133.
Walker, G. P. L., Wilson, C. J. N. & Froggatt, P. C. 1980*a* Fines-depleted ignimbrite in New Zealand – the product of a turbulent pyroclastic flow. *Geology* **8**, 245–249.
Walker, G. P. L., Wilson, C. J. N. & Froggatt, P. C. 1981*b* An ignimbrite veneer deposit: the trail-marker of a pyroclastic flow. *J. Volcanol. geotherm. Res.* **9**, 409–421.
Williams, H. 1942 The geology of Crater Lake National Park, Oregon, with a reconnaisance of the Cascade Range southward to Mount Shasta. *Carnegie Instn Wash. Publ.* **540**.
Wilson, C. J. N. 1980 The role of fluidization in the emplacement of pyroclastic flows: an experimental approach. *J. Volcanol. geotherm. Res.* **8**, 231–249.
Wilson, C. J. N. 1981 Studies on the origins and emplacement of pyroclastic flows. Ph.D. thesis, Imperial College, London University.
Wilson, C. J. N. 1984 The role of fluidization in the emplacement of pyroclastic flows, 2: Experimental results and their interpretation. *J. Volcanol. geotherm. Res.* **20**, 55–84.
Wilson, C. J. N. & Walker, G. P. L. 1981 Violence in pyroclastic flow eruptions. In *Tephra studies* (ed. S. Self & R. S. J. Sparks), pp. 441–448. Holland: Dordrecht, D. Reidel.
Wilson, C. J. N. & Walker, G. P. L. 1982 Ignimbrite depositional facies: the anatomy of a pyroclastic flow. *J. Geol. Soc. Lond.* **139**, 581–592.
Wilson, C. J. N. & Walker, G. P. L. 1985 The Taupo eruption, New Zealand. I. General aspects. *Phil. Trans. R. Soc. Lond.* A **314**, 199–228. (Paper I.)
Wilson, C. J. N., Walker, G. P. L. & Self, S. 1985 The concept of flow units in ignimbrites. (In preparation.)
Wilson, C. J. N. & Wright, J. V. 1985 The role of fluidization in the emplacement of pyroclastic flows. 3: Fluidization-grading processes in ignimbrites. (In preparation.)
Wilson, L. 1978 Energetics of the Minoan Eruption. In *Thera and the Aegean World*, vol. 1, pp. 221–228. London: Thera and the Aegean World.
Wright, J. V. 1979 Formation, transport and deposition of ignimbrites and welded tuffs. Ph.D. thesis, Imperial College, London University.
Wright, J. V. 1981 The Rio Caliente Ignimbrite: analysis of a compound intraplinian ignimbrite from a major late Quaternary Mexican eruption. *Bull. volcanol.* **44**, 189–212.
Wright, J. V. & Walker, G. P. L. 1977 The ignimbrite source problem: significance of a co-ignimbrite lag-fall deposit. *Geology* **5**, 729–732.
Wright, J. V. & Walker, G. P. L. 1981 Eruption, transport and deposition of an ignimbrite: a case study from Mexico. *J. Volcanol. geotherm. Res.* **9**, 111–131.
Yokoyama, S. 1974 Mode of movement and emplacement of Ito pyroclastic flow from Aira Caldera, Japan. *Tokyo Kyoiku Daigaku Sci. Rep.* C **12**, 17–62.

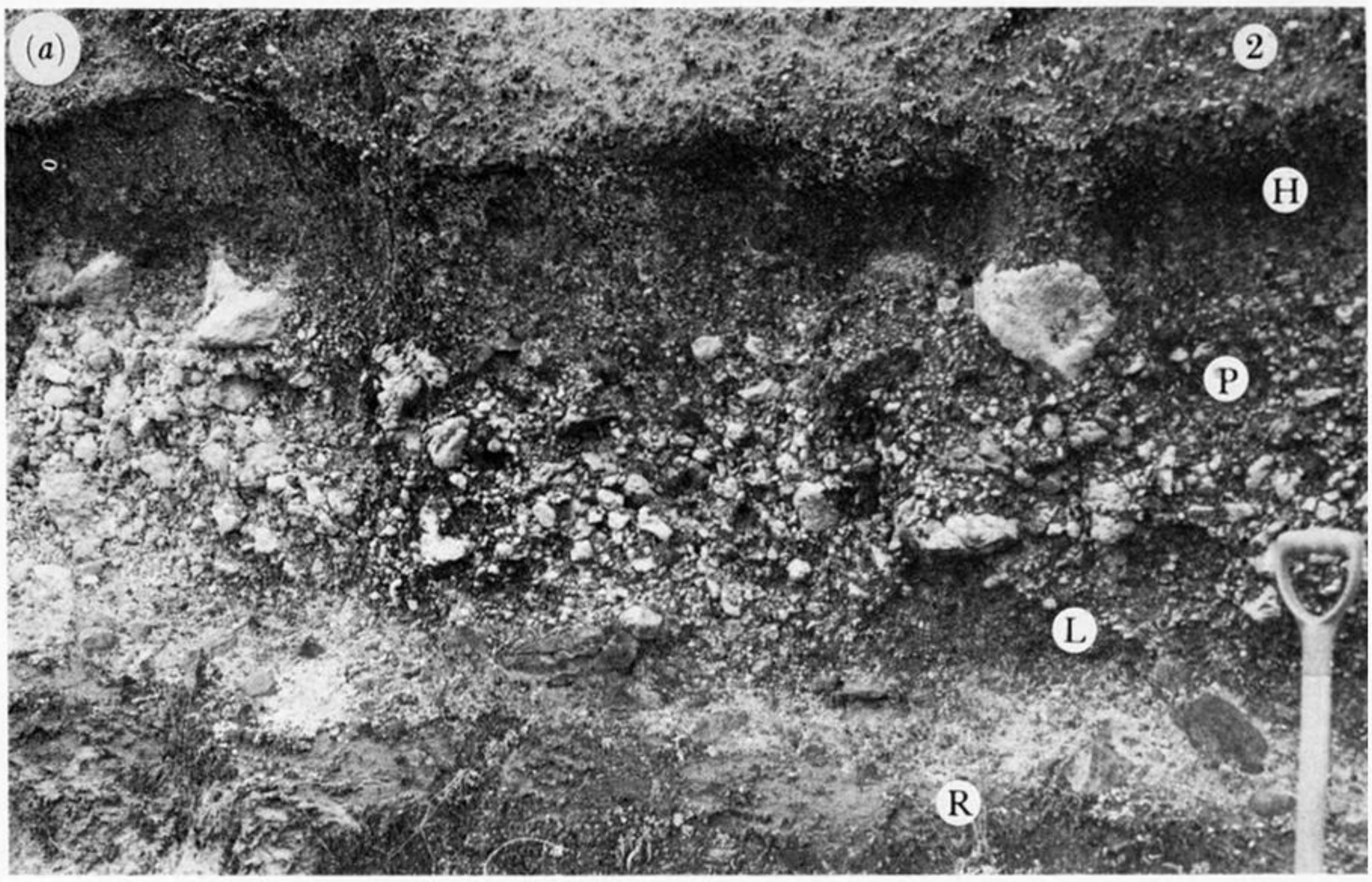

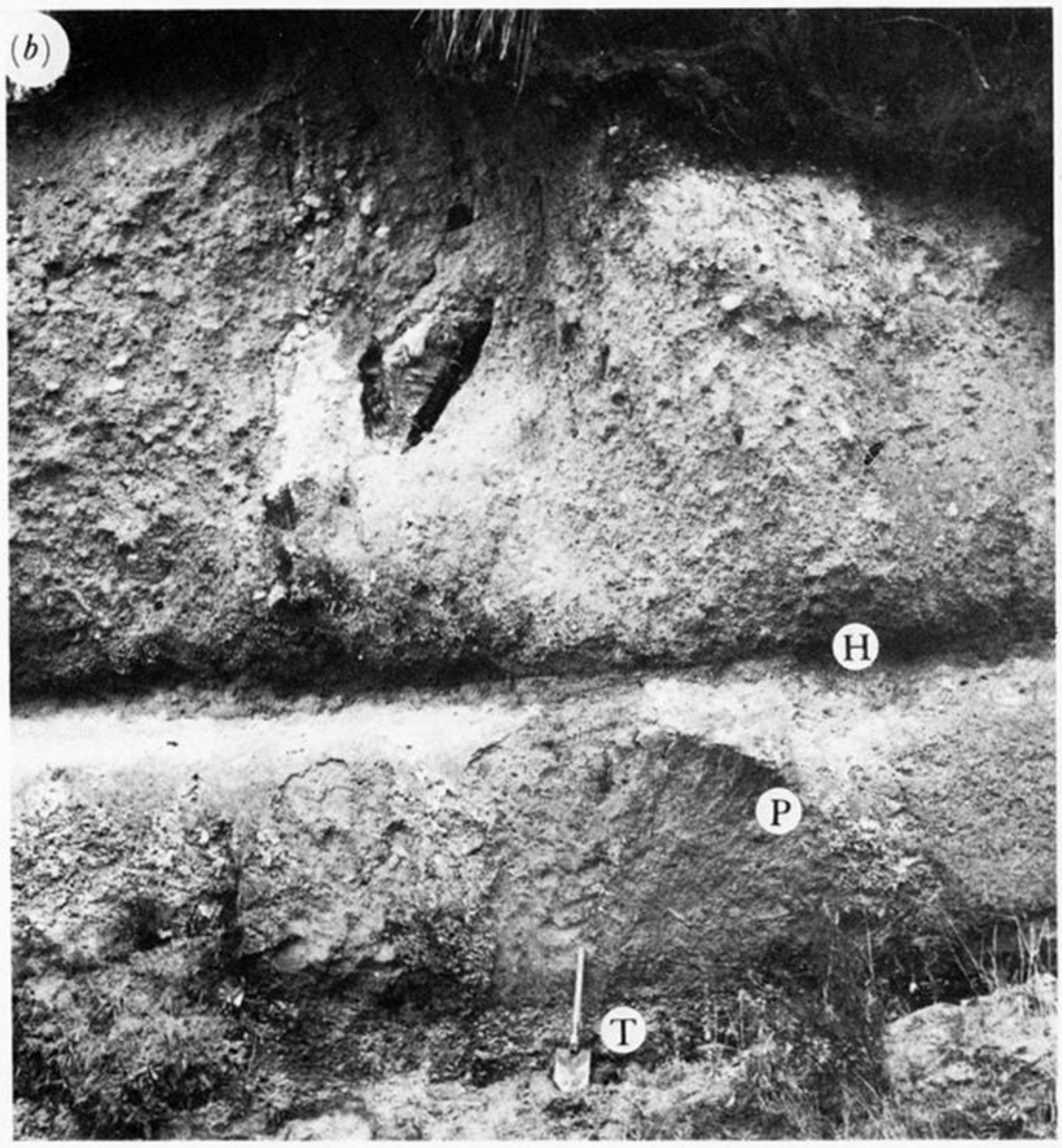

FIGURE 4. Layer 1(P) (excluding FDI, which is illustrated in Walker *et al.* 1980*a*). (*a*) Near-vent, wholly fines-depleted, compositionally zoned layer 1(P): R, Rotongaio phreatoplinian ash; L, lithic-rich base; P, pumice-rich top; H, layer 1(H); 2, layer 2 (veneer deposit). Locality at 3488 4078, 14 km from vent. (*b*) To the east of vent where layer 1(P) overlies thick co-eruptive airfall deposits: T, Taupo plinian pumice: P, layer 1(P): H, layer 1(H). Locality at 3971 4053, 49 km from vent. (*c*) A distal exposure at the base of a *ca.* 40 m thick valley pond where layer 1(P) is thin and layer 1(H) absent. Locality at 3681 3464, 72 km from vent. (*d*) At high altitudes, where variety a of layer 1(P) occurs, overlain by a poorly preserved layer 2 (veneer deposit). Locality at 3357 3820, 38 km from vent. (*e*) Layer 1(P), variety b, overlain by a thin layer 1(H) and layer 2: S, underlying soil. Locality at 3356 4061, 18 km from vent.

4(*d*)

4(*e*)

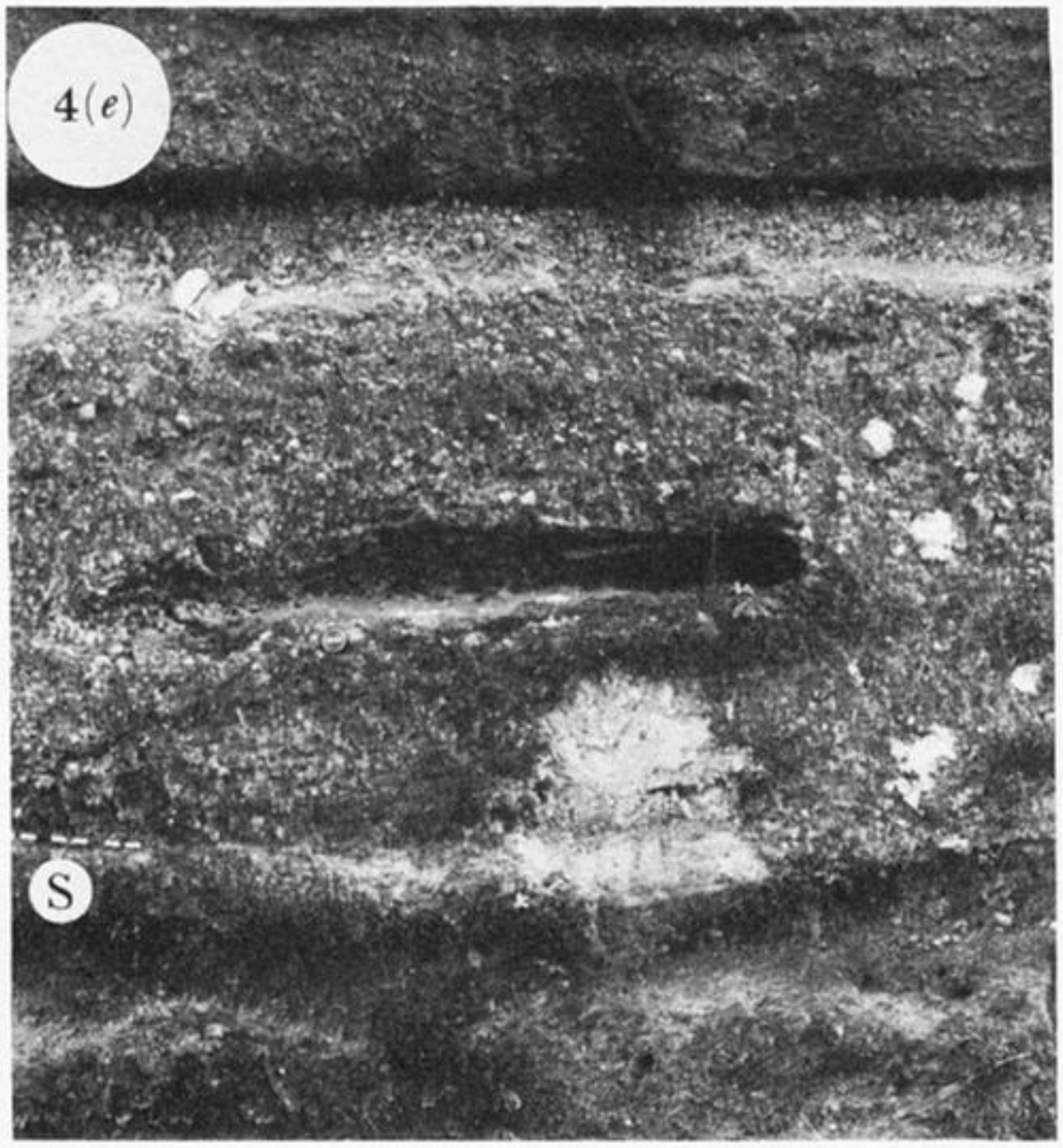

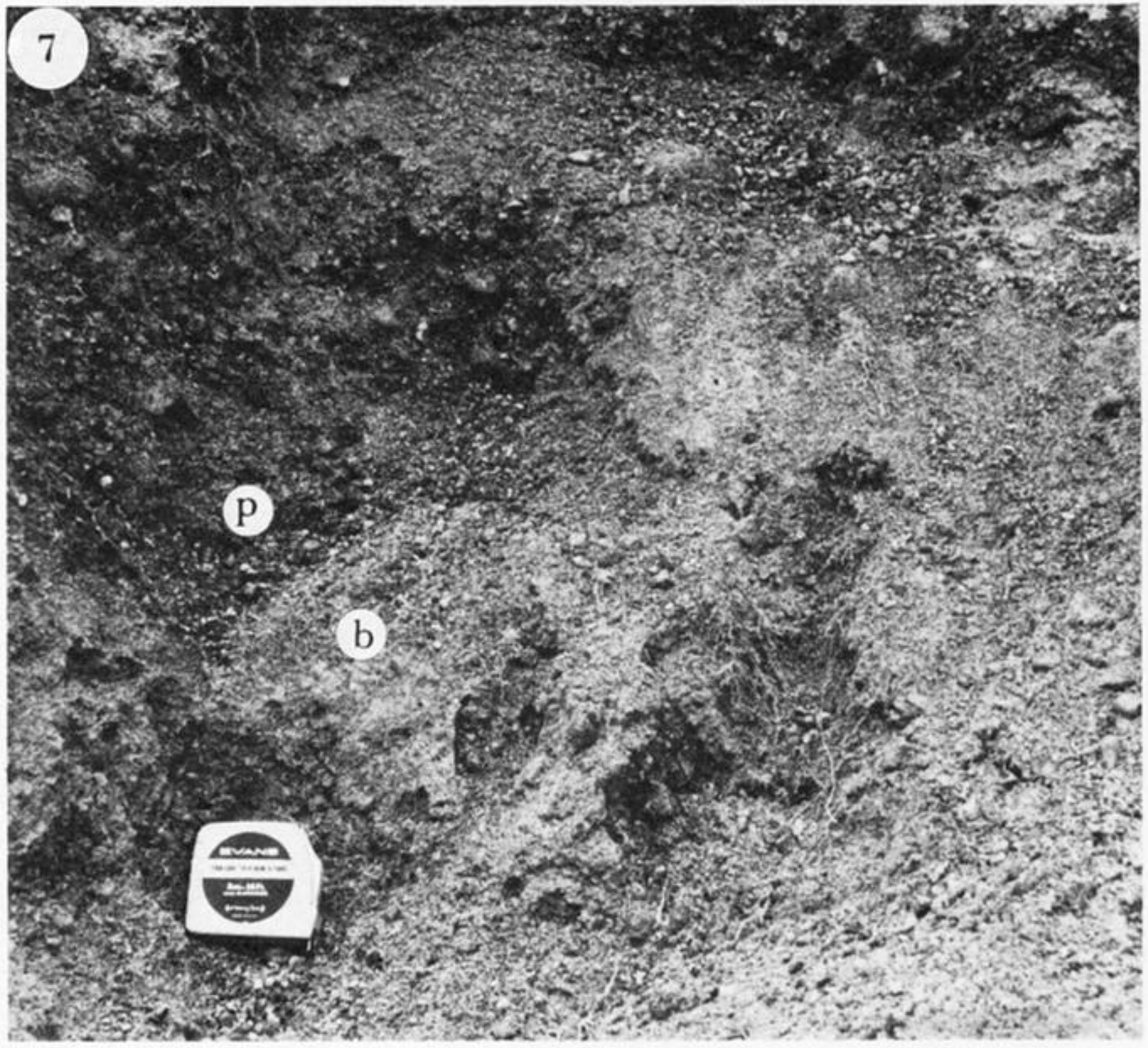

FIGURE 7. The matrix of the near-vent layer 1(H), showing the fines-bearing (b) and fines-poor (p) 'phases'. Locality at 3493 4353, 12 km from vent.

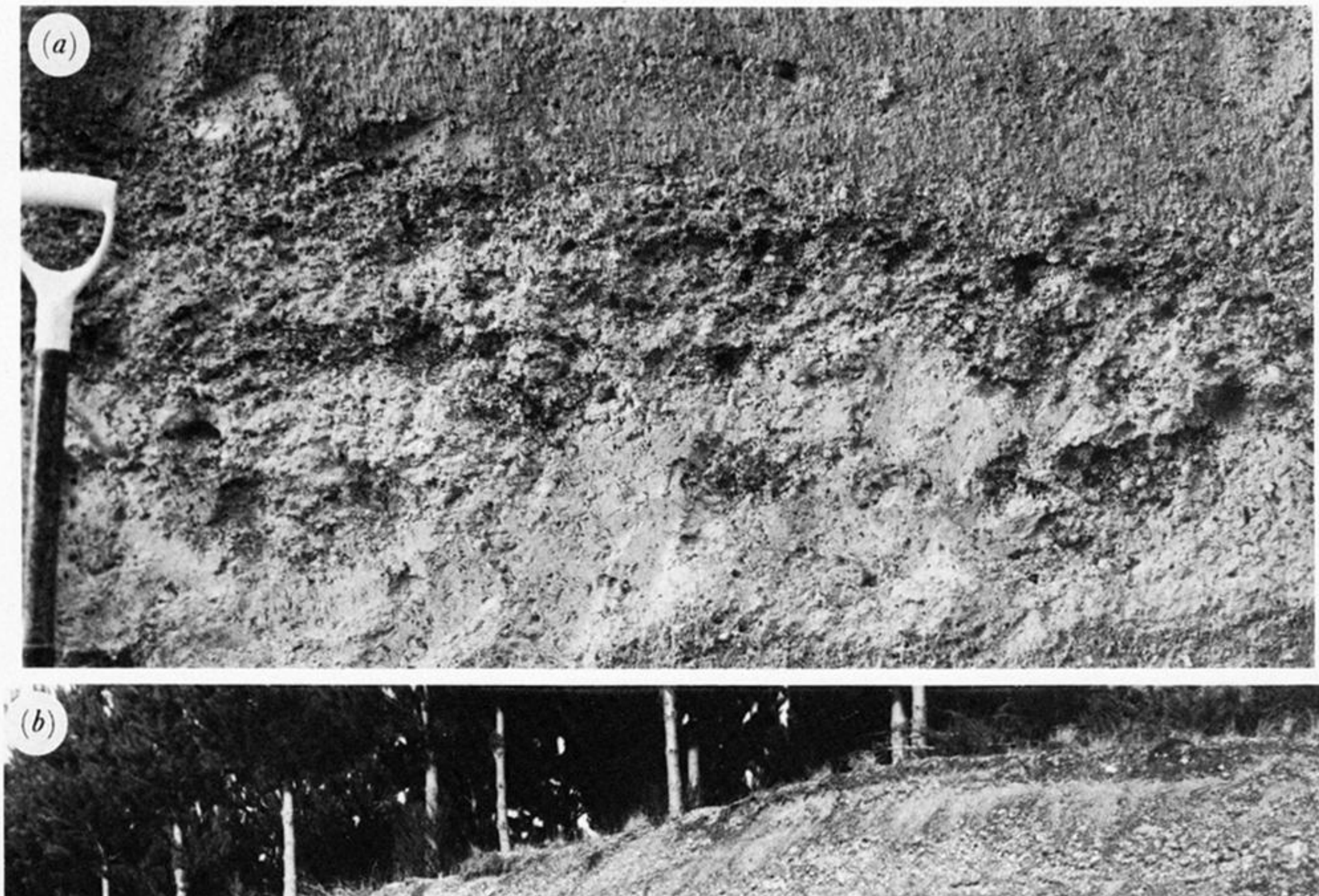

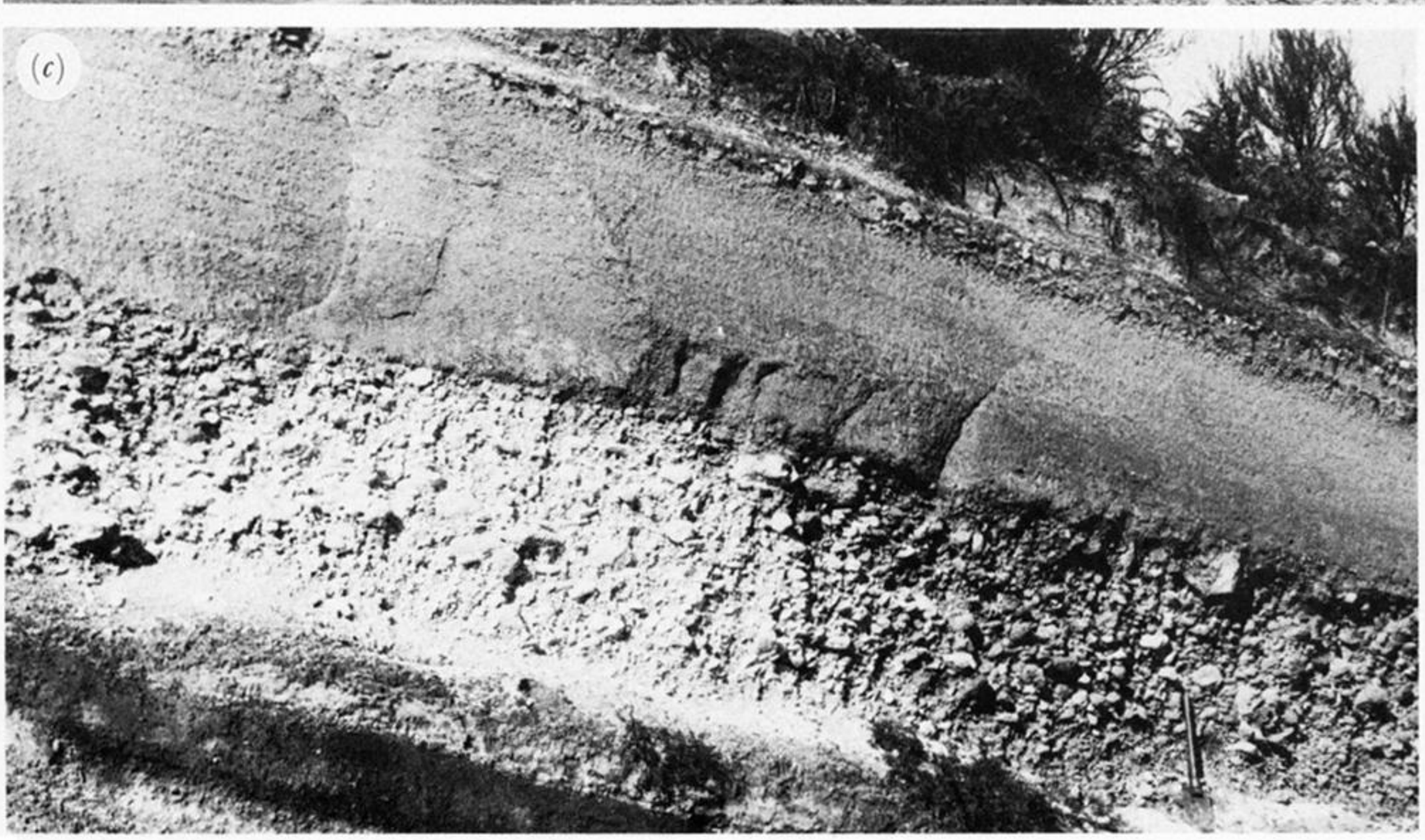

FIGURE 29 (*a*)–(*c*). Structures in the IVD (see text for discussion). (*a*) Detail of a lithic-rich lens within the IVD at the locality illustrated in (*e*). (*b*) Coarse-scale stratification. The flow travelled from left to right, closely parallel to the length of the exposure. Locality at **3619 4113**, 17 km from vent. (*c*) Fine-scale stratification in the IVD overlying coarse FDI. Locality at **3478 4050**, 16 km from vent. (*d*) Lee-side structure in the near-vent IVD where lee-side lenses are absent (cf. Walker *et al.*. 1981 *b*, figure 6 (*b*)). The IVD overlies the Rotongaio phreatoplinian ash (R). The flow travelled from left to right, closely parallel to the length of the exposure. Locality at **3547 4163**, 10 km from vent. (*e*) Partial cross-section through a dune-like structure in the IVD, developed on a flat underlying surface. The flow travelled from left to right at a shallow angle to the length of the exposure. Locality at **3460 4120**, 9 km from vent. (*f*) Low-angle foreset bedding in the IVD developed on a flat underlying surface. The flow travelled from left to right, roughly parallel to the length of the exposure. Locality. T3489 4122, 10 km from vent.


29(d)
R


(e)

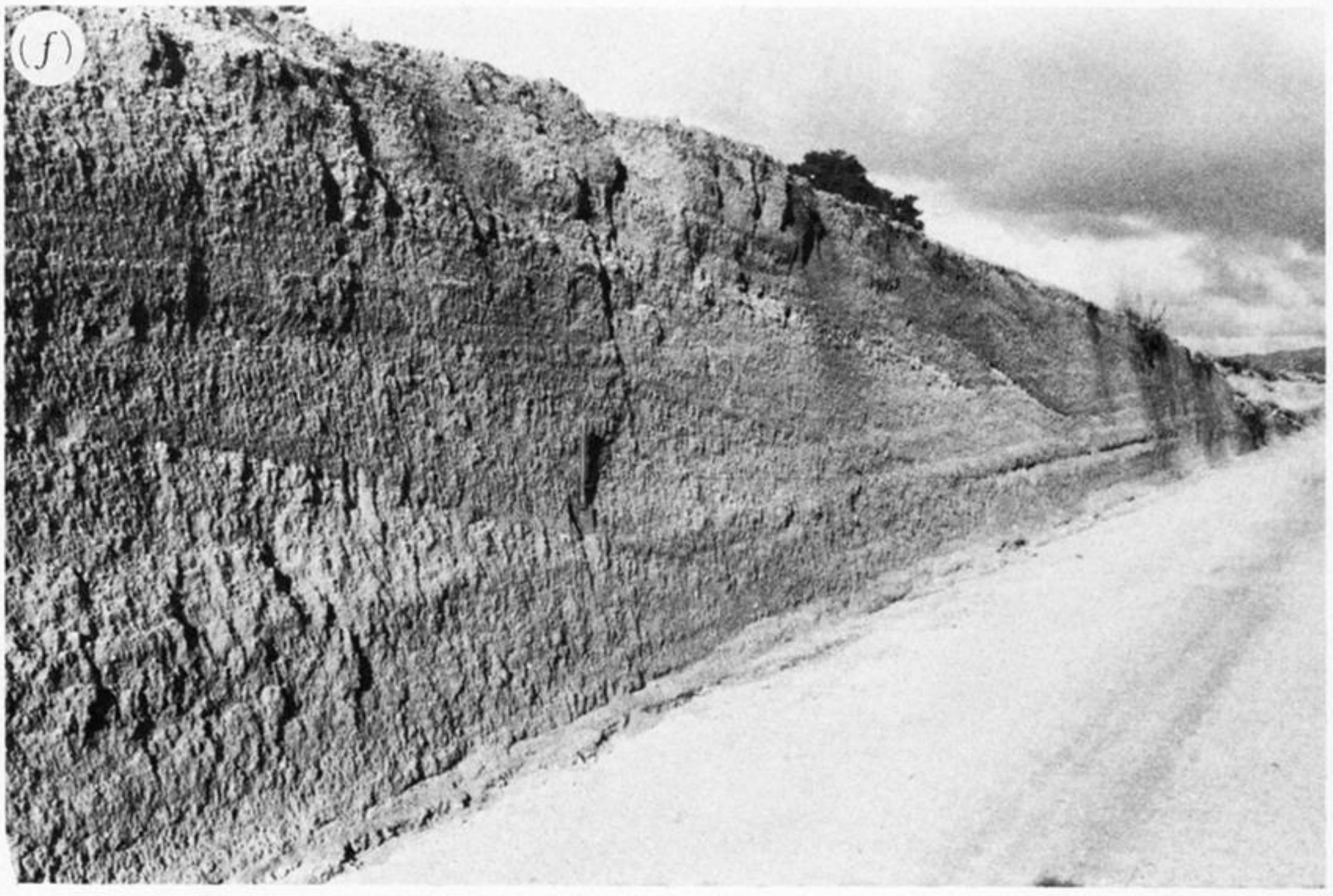
(f)

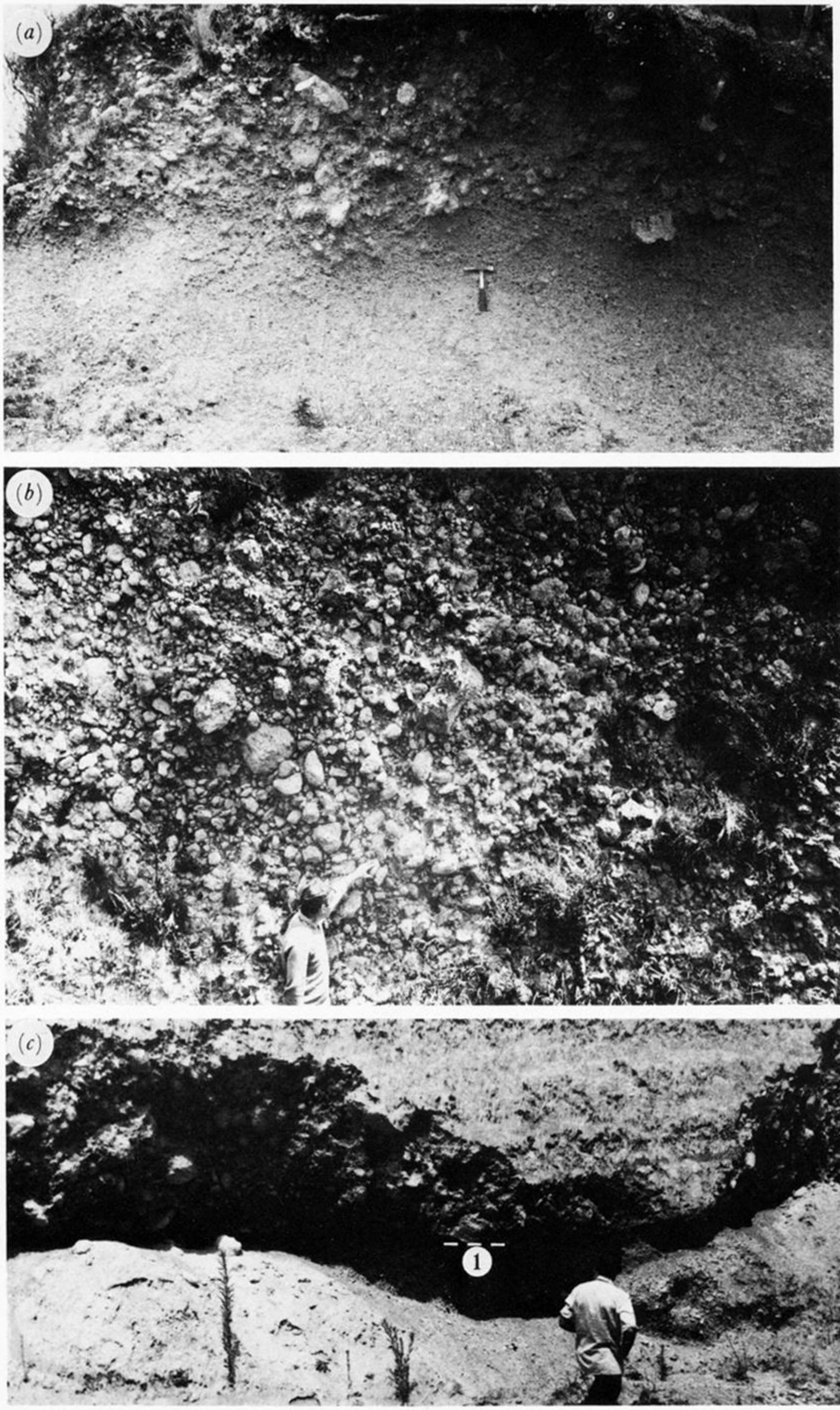

FIGURE 32. Pumice grading in the VPI (see text for discussion). (*a*) View of a type-3 VPI section showing an upper, clearly demarcated PCZ. Locality at 3843 4292, 36 km from vent. (*b*) Detail of coarse partially clast-supported PCZ. Locality at 3838 4139, 35 km from vent. (*c*) Base of a coarse PCZ unit which directly overlies layer 1(1) with only a poorly developed layer 2a intervening. Locality at 3454 4626, 37 km from vent.

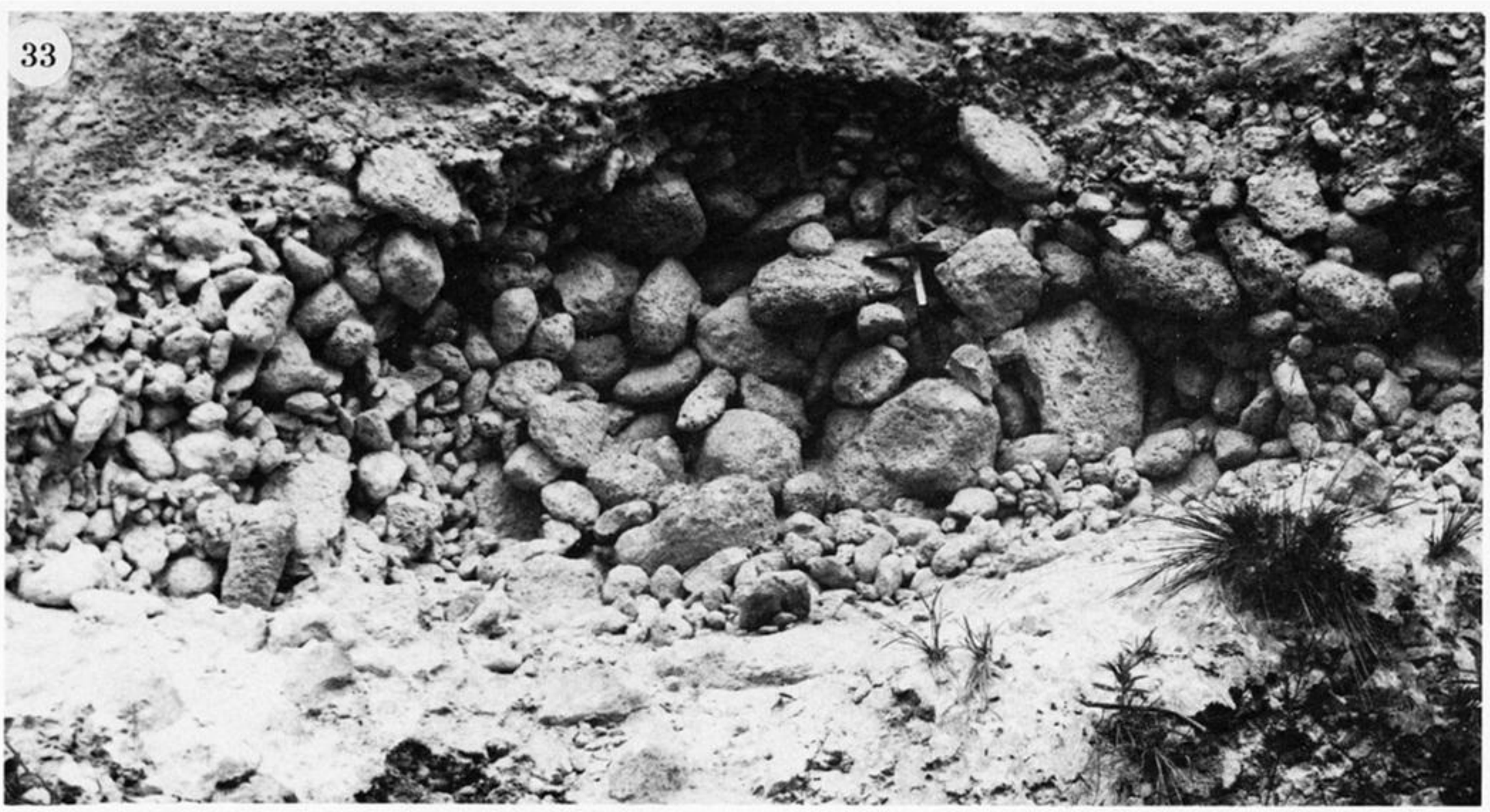

FIGURE 33. Pumiceous, matrix-absent lens in the VPI (see §4 (*b*) (i)). Locality at 3998 3991, 54 km from vent.

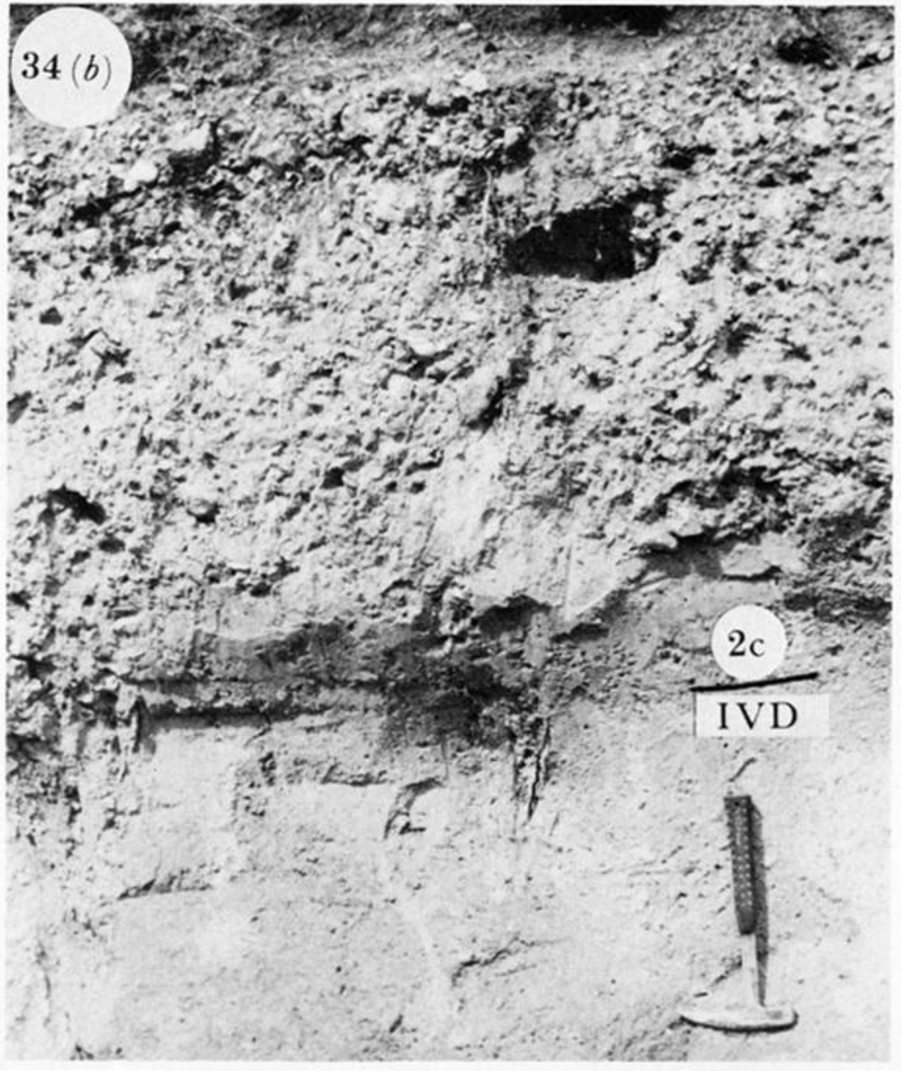

FIGURE 34. (*a*) Fine-grained layer 2c overlying a coarse, type 3 VPI unit, the latter passing laterally into a stratified IVD. Locality at 3612 4080, 19 km from vent. (*b*) Layer 2c, coarse-pumice-rich and strongly bimodal in its upper part, overlying the IVD; the boundary between them is fixed from the truncation of segregation pipes in the lower unit (see figure 35). Locality at 3243 3767, 46 km from vent.

FIGURE 52. The distant facies overlying the Taupo plinian pumice (T). The tape case is 5 cm square. Locality at 4143 4672, 75 km from vent.

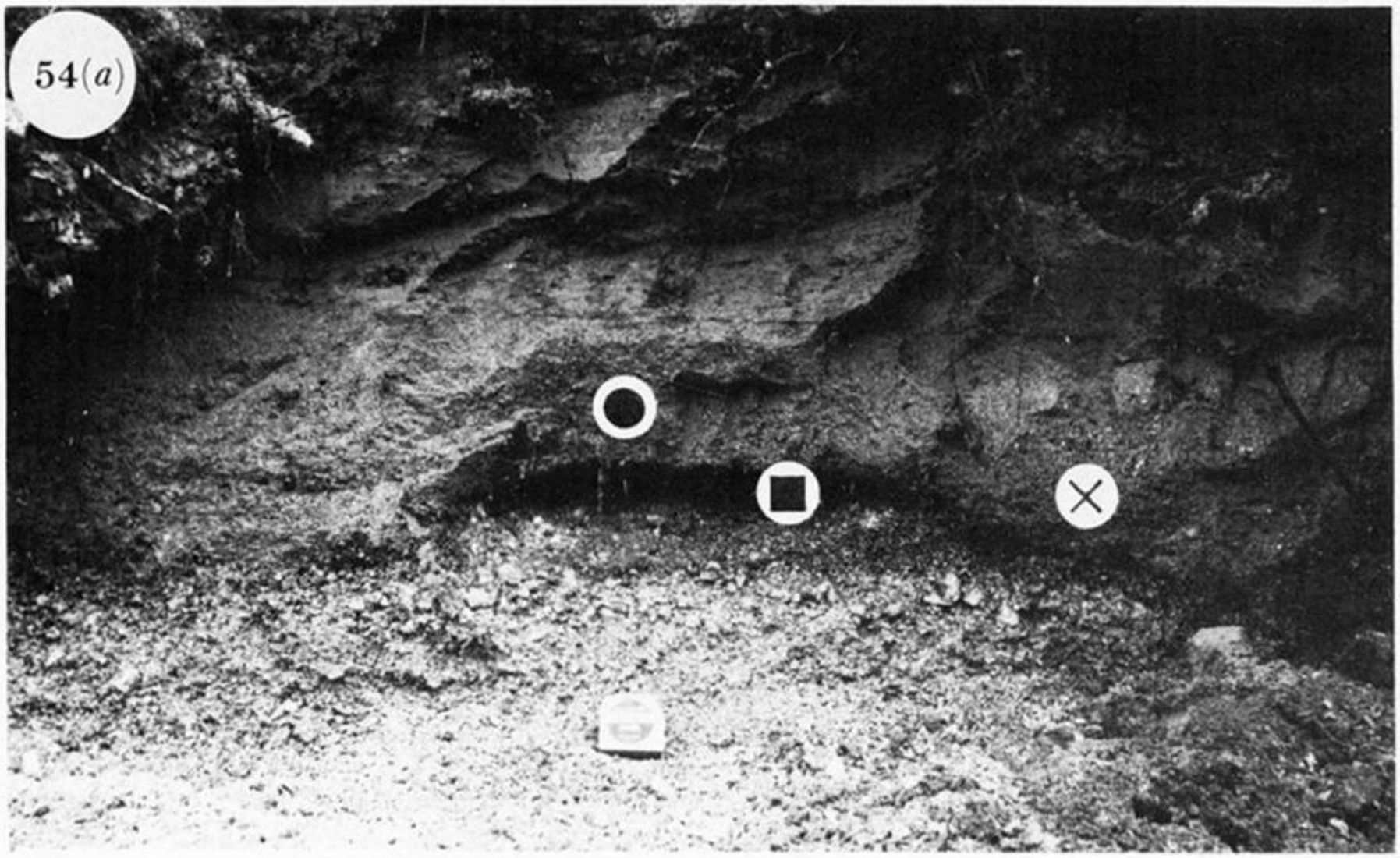

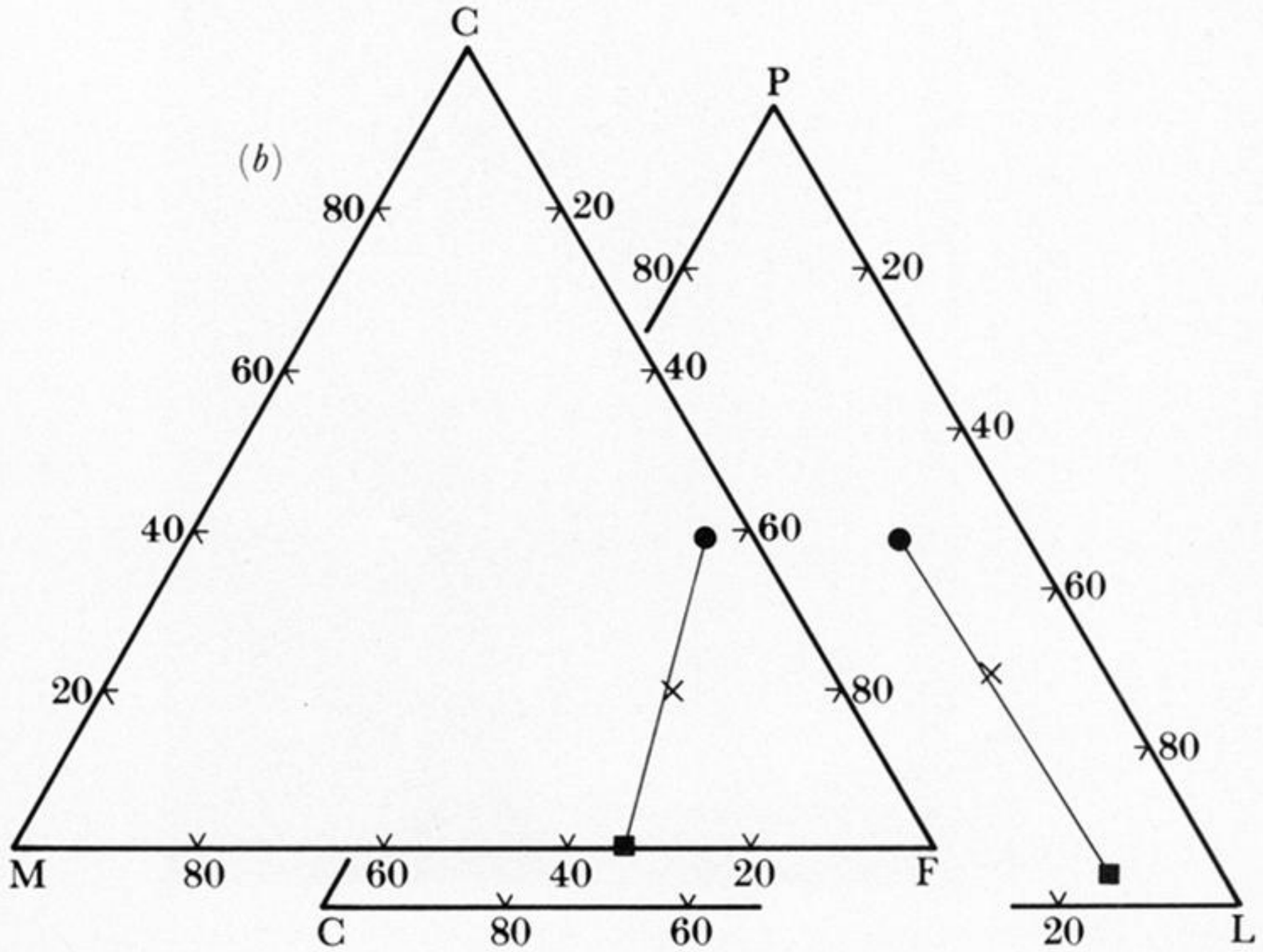

FIGURE 54. Erosion of layer 1 to produce a compositional zonation in the IVD. (*a*) Photograph of the IVD which has partly eroded the ground layer and underlying Taupo plinian pumice; symbols represent where the samples shown in (*b*) were collected. (*b*) C.m.f. and p.c.l. data (% by mass) from the IVD (●), ground layer (■), and the mixed material between the two (×). Locality at 3697 4346, 24 km from vent.

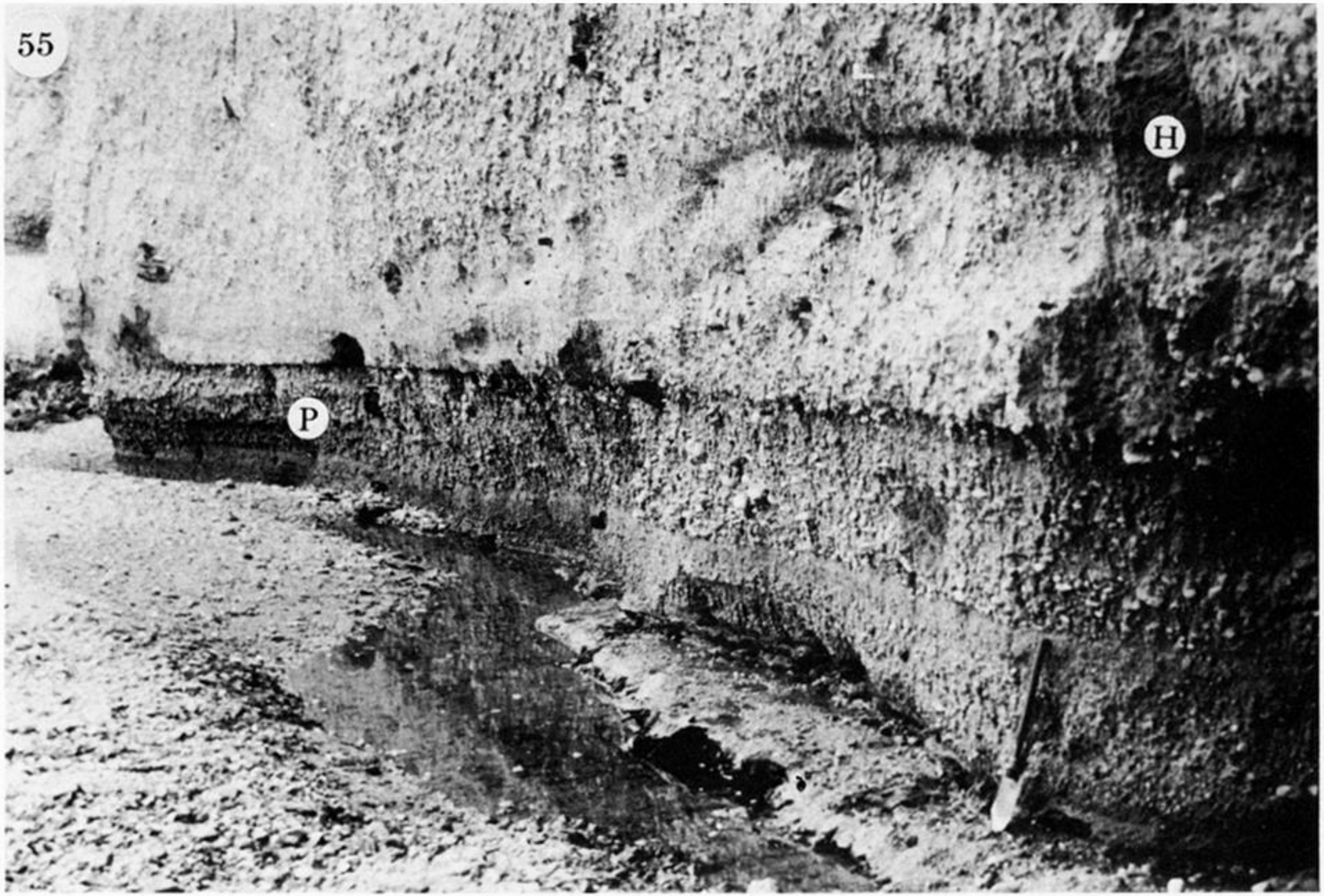

FIGURE 55. Role of a basal permeable layer in controlling the development of layer 2a. On the right, the VPI overlies a thin ground layer (H) with a poorly developed layer 2a; on the left, the ground layer has been removed and a clearly developed layer 2a overlies fines-bearing jetted deposits (P). The shovel rests on the pre-eruption palaeosol. Locality at 3612 3867, 35 km from vent.

FIGURE 58. Fluidized ignimbrite sample (Wilson 1980, figure 4), showing the basal (b), intermediate (i) and upper (u) portions of the bed (see text for discussion). Scale bar is 25 cm.

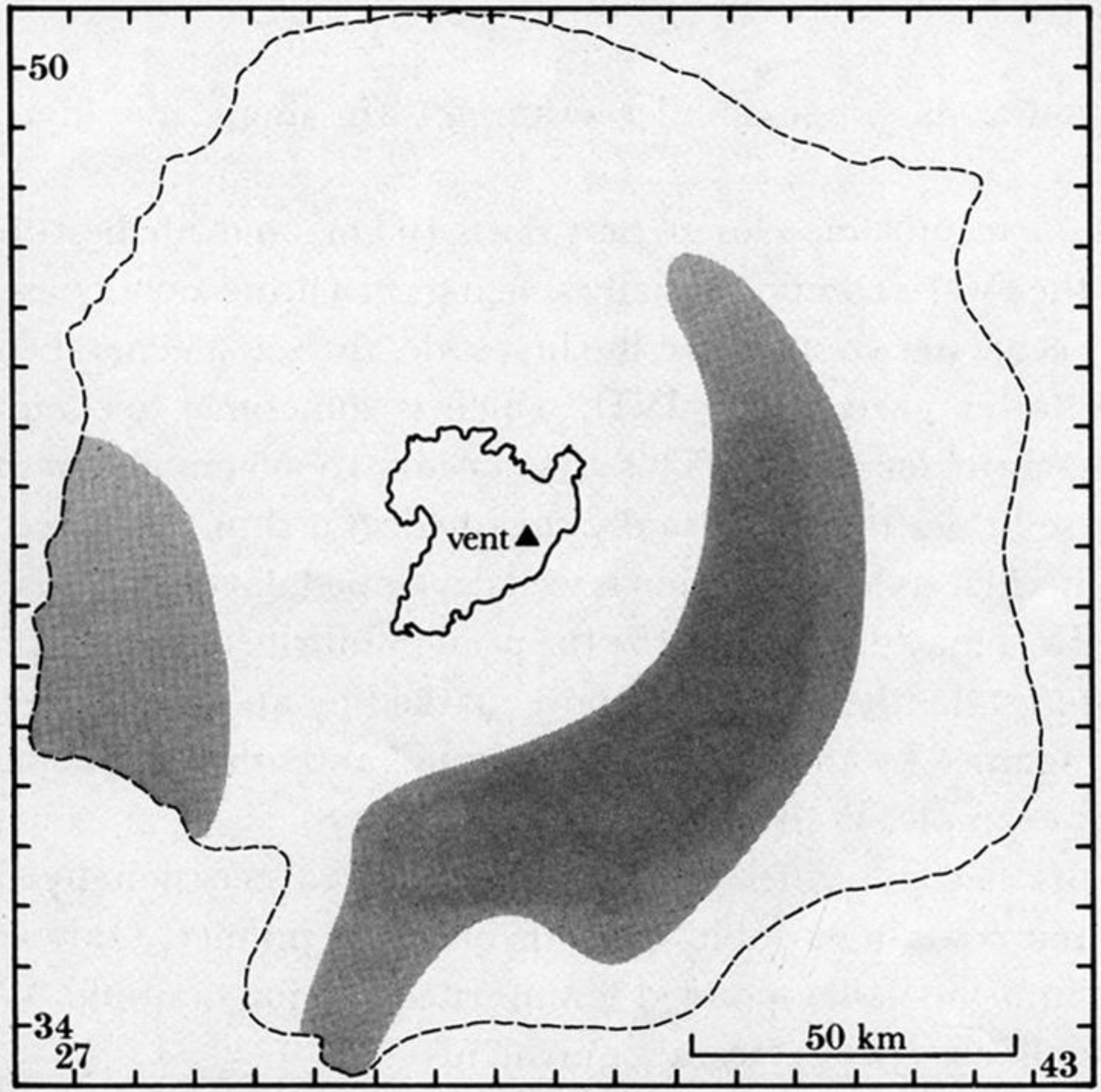

FIGURE 28. Map showing areas (shaded) where thermal alteration colours are best developed in layer 2 deposits.

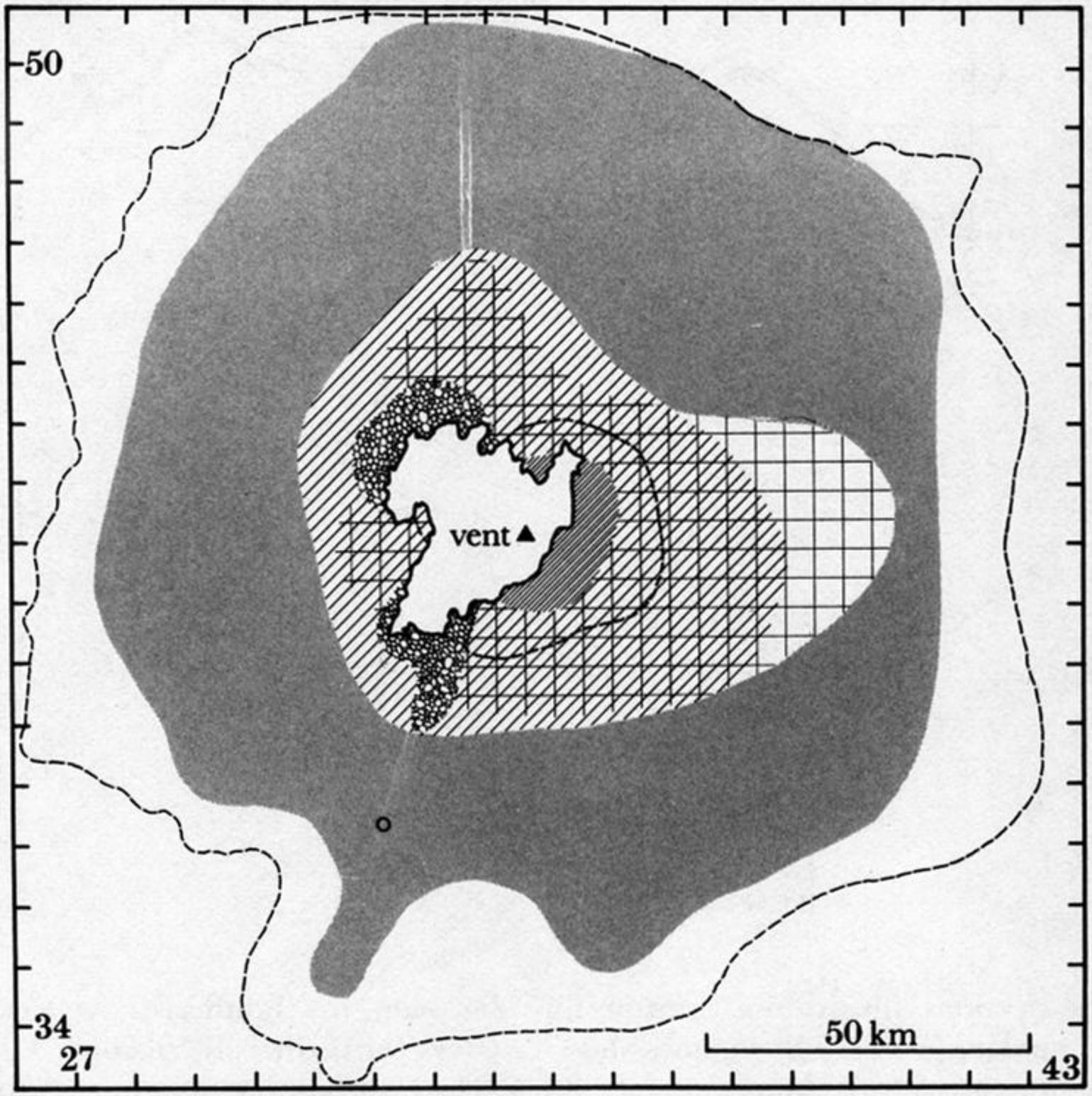

FIGURE 30. Map of the outcrop areas of effectively continuous IVD (shading) and the structures within it. The diagonal hatching denotes where a grainsize stratification occurs; within this area, the dashed line marks the outer limit of the coarser, nearer-vent style (§4 (*b*) (i)) and the denser hatching is where lee-side lenses are absent from the downstream side of obstacles. The cross hatching denotes areas where lee-side lenses are common. The open circle marks an isolated outcrop where the IVD is grainsize stratified (Walker *et al.* 1981 *b*, figure 3*c*). The bubble ornamentation denotes where the IVD is vesicular and contains tree moulds (see Paper I, §3).

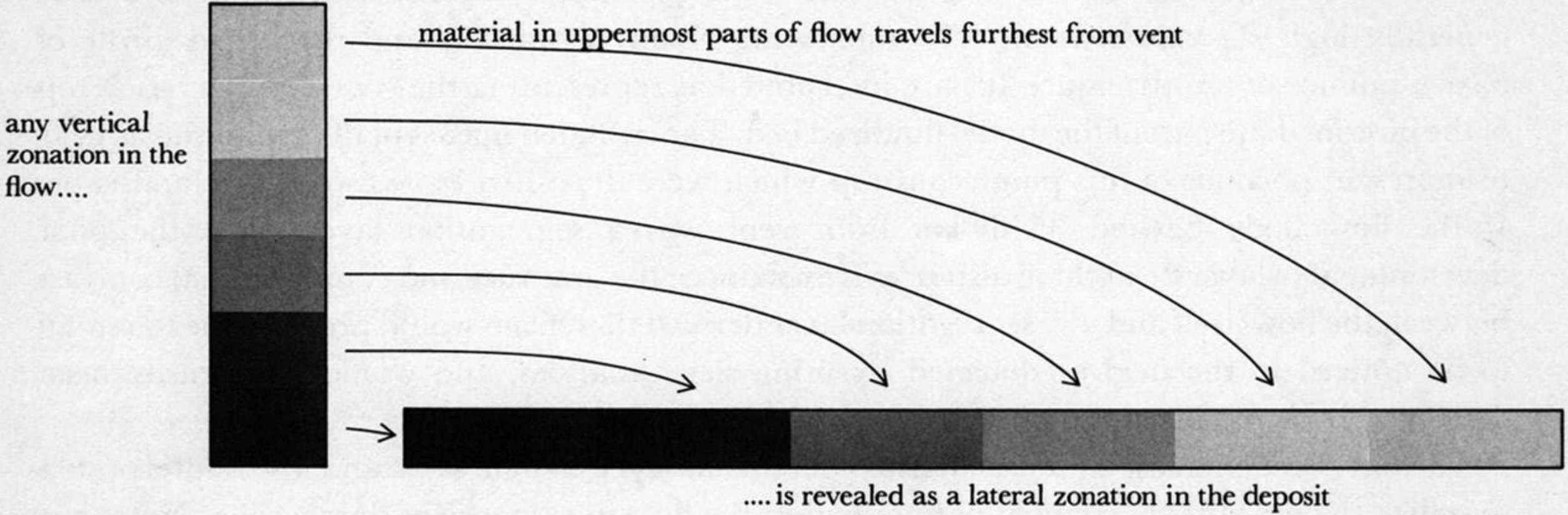

FIGURE 60. Schematic diagram illustrating results from an overall emplacement model for a rapidly moving pyroclastic flow.